Identification of novel microRNA targets and tumor suppressive functions of *miR-203* in murine skin

by

KENT AUGUSTUS RIEMONDY JR.

B.S., University of Utah, Salt Lake City, Utah 2007

A thesis submitted to the
Faculty of the Graduate School of the
University of Colorado in partial fulfillment
of the requirement for the degree of Doctor of Philosophy
Department of Molecular, Cellular, and Developmental Biology
2015

This thesis entitled:
Identification of novel microRNA targets and tumor suppressive functions of miR-203 in murine skin
written by Kent Augustus Riemondy Jr.
has been approved by
the Department of Molecular, Cellular and Developmental Biology

_____

Dr. Kevin Jones, Ph.D.

(Chair)

_____

Dr. Rui Yi, Ph.D.

Date_____

The final copy of this thesis has been examined by the signatories, and we find that both the content and the form meet acceptable presentation standards of scholarly work in the above mentioned discipline.

ABSTRACT

Riemondy, Kent Augustus, Jr. (Ph.D Molecular, Cellular and Developmental Biology)

Identification of novel microRNA targets and tumor suppressive functions of *miR-203* in murine skin

Thesis directed by Associate Professor Dr. Rui Yi

miRNAs are small non-coding RNAs, approximately 22 nucleotide in length, that mediate post-transcriptional repression of target mRNAs. Since their discovery in mammals in the early 2000s, miRNAs have been intensely studied and determined to be an important mechanism to regulate gene expression in diverse biological processes. In human cancers, miRNAs are known to act as tumor suppressors or oncogenes and are being actively explored as a possible mechanism for therapeutic intervention. In the mouse, multistage skin carcinogenesis is a well-established model for studying tumor development however the functions of miRNAs in this model are poorly understood.

The *Ras* oncogene was the first discovered oncogene in human cancers, and in mouse models of skin cancer it is required for tumor development. In order to elucidate the mechanisms by which oncogenic *Ras* initiates tumorigenesis in the skin, I conducted genome-wide profiling experiments to define the mRNA and miRNA landscape regulated by oncogenic *Ras.* From these datasets I identified a microRNA, *miR-203*, that is strongly suppressed by oncogenic *Ras.* Furthermore, I demonstrate that *miR-203* is commonly silenced in mouse models of Squamous Cell Carcinoma

(SCC), and in human skin SCC samples, strongly suggesting that *miR-203* may act to suppress SCC tumor development.

miR-203 is a broadly conserved miRNA that accounts for ~25% of the miRNA found in the epidermis of the skin. This miRNA was previously shown to promote keratinocyte differentiation by antagonizing epidermal cell proliferation, yet it's requirement for epidermal development and in skin cancer prior to this work were unknown. To address these important questions, a conditional *miR-203* knockout mouse model was generated. I showed that loss of *miR-203* perturbs epidermal embryonic development and enhances keratinocyte self-renewal. I next conducted mouse skin chemical carcinogenesis studies to analyze the functions of *miR-203* in skin cancer and demonstrated that loss of *miR-203* sensitizes skin to chemical carcinogenesis, resulting in enhanced tumor burden. Lastly, to identify the molecular mechanisms by which *miR-203* restricts tumorigenesis, I utilized genome-wide techniques to detect *miR-203* targets in keratinocytes. Ago2-HITS-CLIP, which identifies direct miRNA/mRNA interactions, was combined with genome-wide expression profiling to identify high confidence *miR-203* targets. From these studies novel *miR-203* targets that are involved in the regulation of *Ras/MAPK* signaling and cell division were identified. Collectively, these studies provide insight into the mechanisms and functions of *miR- 203* in the skin.

DEDICATION

This thesis is dedicated to the memory of Nicholas Fletcher, Kevin Landolt, and Lori Greiner.

ACKNOWLEDGEMENTS

This thesis would not have been possible without the support of the many friends, family, and coworkers that have helped me through the past six years.

I would like to thank my advisor and mentor Dr. Rui Yi. Rui's patience with me over the years has been immense and is certainly a trait that I now strive to incorporate into my own life. Even during the most trying times of this thesis work Rui has supported me and helped me to find successful solutions to the problems that I faced. Rui's motivation and enthusiasm for new ideas and methods has also allowed me to explore very diverse techniques and fields of research and consequently greatly aided my development as a scientist. I would also like to thank my thesis committee for providing me guidance during my thesis work. Thank you for taking the time to share your expertise and guidance. I would also like to thank all of the members of the Yi lab for providing critical advice, help with experiments, and emotional support especially when none of my experiments were working.

Friends and family have provided a much needed network of support during my thesis. I cannot thank them enough for dragging me out of the lab and reminding me of the world outside of my work. I especially want to thank my parents for their unwavering support of my work, even when I couldn't explain to them what I was doing or why it was important. Lastly, I want to thank my partner Michelle for always being there for me. I look forward to our life together.

TABLE OF CONTENTS

LIST OF TABLES

LIST OF FIGURES

CHAPTER 1

INTRODUCTION

microRNAs (miRNA) are ~22 nucleotide non-coding RNAs that negatively regulate gene expression. Since the initial discovery of the *C. elegans* miRNA, lin-4 in 1993, thousands of miRNAs have been identified by computational analyses and small-RNA cloning techniques (Lee et al., 1993; Lim et al., 2003). Important roles for miRNA mediated gene regulation have been revealed in virtually every biological system examined; including developmental processes, homeostatic mechanisms, stress responses, and disease states (Sun and Lai, 2013). Our present-day understanding of miRNA networks indicates that miRNA activity is likely a crucial regulatory mechanism in most gene regulatory networks that operate in mammalian cells.

MAMMALIAN SKIN AS A MODEL SYSTEM TO STUDY THE MIRNA PATHWAY

The skin serves an ancient role as the critical first barrier between the environment and the organism. The skin provides an elastic waterproof barrier to the environment but also provides essential roles in defense from pathogens and thermoregulation, as well as sociological functions such as providing organismal identity. The skin is composed of the squamous stratified interfollicular epidermis and associated appendages such as hair follicles, sweat glands, and sebaceous glands embedded within the collagenous dermis, which provides structure and subcutaneous fat deposits (Blanpain and Fuchs, 2006). Many different cell types are responsible for

constructing the diverse regions of the skin, including the keratinocytes of the epidermis, which form the cornified envelope in the stratum corneum, the hair follicle stem cells, which fuel the production of the differentiated lineages of the hair follicle, as well as critical fibroblast, immune cells, and dendritic cell populations.

Mammalian skin is a traditional model for studying developmental and cell biological processes, as well as responses to stress from environmental factors or disease states (Blanpain and Fuchs, 2009). Complex and integrated regulatory networks orchestrate self-renewal and differentiation of stem/progenitor cell populations as they are specified into the numerous cell types of the epidermis and hair follicle. Embryonic development of mouse epidermis begins around embryonic day (E) 9, when ectodermal progenitors transition to epidermal progenitors and begin to express the intermediate filament heterodimers Keratin 5 (*K5*) and Keratin 14 (*K14*) (Byrne et al., 1994). As embryonic development progresses into E14, progenitor cell proliferation undergoes a transition from symmetric cell division along the basement membrane, to occasional asymmetric division (Lechler and Fuchs, 2005). One daughter cell maintains a progenitor identity while the progeny detach from the basement membrane and initiate the early stages of epidermal differentiation marked by replacement of *K5/K14* with expression of the differentiation associated keratins, Keratin 1 (*K1*) and Keratin 10 (*K10*). Around E17.5 the initial wave of differentiation of the suprabasal layers reaches completion with the construction of a waterproof barrier known as the stratum corneum. The cornified keratinocyte of the stratum corneum is an enucleated cell composed primarily of a crosslinked protein and lipid membrane that functions to restrict fluid loss and protect again harmful infectious agents and noxious chemicals (Koster and Roop,

2007). The cornified envelope is continually shed and must be replaced through the proliferation and differentiation of epidermal progenitors. Upon the completion of epidermal development the interfollicular epidermis remains a static structure that maintains homeostasis by continual self-renewal of epidermal progenitors throughout the lifetime of the organism (Clayton et al., 2007). The differentiation of the basal epidermal progenitors provides a constant supply of suprabasal keratinocytes to maintain the waterproof stratum corneum.

Hair follicle morphogenesis begins during embryogenesis around embryonic day 14 through reciprocal interactions of mesenchymal dermal cell populations and epithelial progenitor cells (Sennett and Rendl, 2012). Activation of the β-catenin/Wnt signaling pathway is one of the earliest known signals for specifying the epidermal progenitors towards a hair follicle fate and initiating hair follicle morphogenesis (Huelsken et al., 2001). Subsequent to specification, the hair follicle progenitors undergo rapid proliferation, cytoskeletal reorganization, and migration into the dermis, coordinated by multiple signaling pathways. During this period of downward growth and movement, hair follicle stem cells (HFSCs) are specified, of which a subset then further differentiate to form the complex hair follicle structure. After initial morphogenesis, the HFSCs are maintained in the specialized stem cell niche known as the bulge (Cotsarelis et al., 1990). Throughout the adult's lifetime the hair follicle dynamically cycles between states of growth (anagen), destruction (catagen) and rest (telogen), which results in the continual maintenance of a hair coat for the lifetime of the animal (Schneider et al., 2009).

The diverse cellular processes that drive epidermal and hair follicle development and homeostasis provide a wealth of processes amendable to study in the skin. By using skin as a model system the transcriptional and post-transcriptional regulators, such as miRNA, that orchestrate such processes as cell adhesion and migration during keratinocyte differentiation and hair follicle morphogenesis, stem cell maintenance and specification during hair follicle cycling, and the regulation of cellular proliferation and cell cycle-exit during epidermal stratification can be defined. Additionally, the skin is a well-established model to study stress responses and how theses processes, when dysfunctional, can contribute to diseases, such as skin cancer and inflammatory skin disorders.

MECHANISMS OF MIRNA BIOGENESIS AND TARGETING

Canonical miRNAs are encoded in genes found in diverse genomic locations including introns of protein coding genes, in intergeneic regions, or from other non-coding RNAs such as tRNAs (Berezikov, 2011). Typically *RNA-Pol II* transcribes a primary miRNA precursor, which can vary in length of a few hundred to many thousands of nucleotides in length (Figure 1) (Lee et al., 2004). The primary transcript is next processed by the microprocessor complex composed of *Dgcr8* and *Drosha* (Kim, 2005). The RNAse-III domain of *Drosha* cleaves the microRNA hairpin recognized by *Dgcr8* from the primary transcript resulting in an dsRNA hairpin of 50-75 nucleotides, with a 5' terminal mono-phosphate, 3' terminal hydroxyl and a 2 nucleotide 3' overhanging single stranded portion (Lee et al., 2003; Yeom et al., 2006). Exportin 5, a member of the *Ras* small GTPase family, interactions with the pre-miRNA stem and the 2 nucleotide 3'

overhang, and exports the precursor miRNA into the cytoplasm (Yi, 2003).

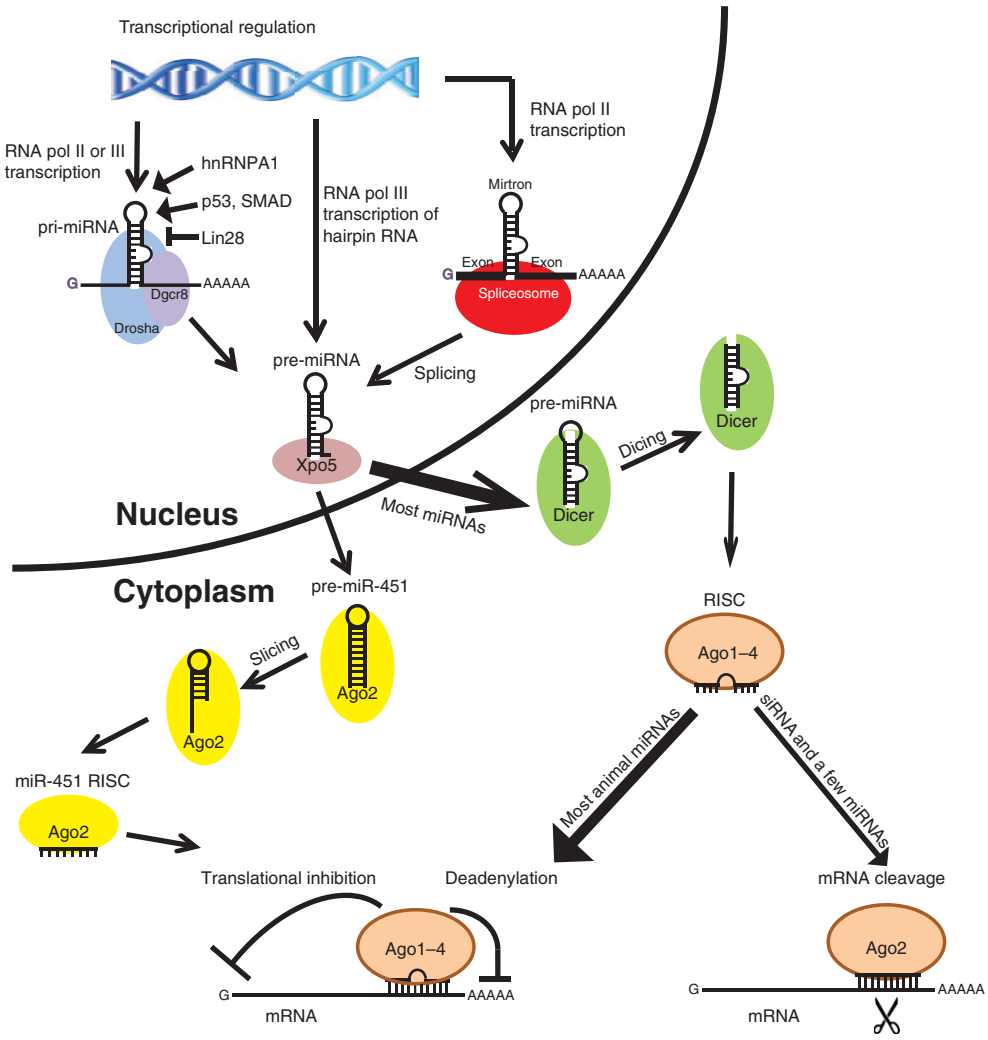

Figure 1. Schematic of the miRNA biogenesis machinery. Reproduced/Adapted with permission from the Journal of Cell Science (Yi and Fuchs, 2011)

Once in the cytoplasm, *Dicer* recognizes the precursor miRNA and using the RNase-III domain cleaves the terminal loop of the hairpin, producing a double-stranded RNA duplex with 2 nucleotide 3' overhangs on each end (Bernstein et al., 2001). After cleavage, one strand of the duplex is loaded into an *Argonaute* protein (one of four present in mammals). The strand selection process is mediated in part by the

thermodynamic stability of the end of the RNA duplex (Schwarz et al., 2003). The 5' end of the least stable terminal 2 nucleotide overhang is preferentially selected and loaded into an *Argonaute (AGO)* protein. The complex of single stranded mature miRNA with *Ago* forms the RNA Induced Silencing Complex (RISC) that functions to suppress targeted transcripts stability and translation (Ha and Kim, 2014). An additional protein, *TNRC6* (*TNRC6A*, *TNRC6B* or *TNRC6C* in mice and humans), is also recruited to the RISC and contributes to transcript destabilization, through providing interactions with the Poly-A-binding protein and the *CCR4/NOT1* deadenylase complex (Chekulaeva et al., 2011; Djuranovic et al., 2012).

The principles of miRNA targeting have been extensively investigated through a combination of genome-wide, computational, and structural studies. miRNAs target 3'UTRs through the use of a sequence motif known as the seed sequence (Lewis et al., 2003). This sequence is the 5' region of the miRNA from nucleotide position 2 to 7-9 . This region is the most conserved region of the mature miRNA sequence and the most effective sequence motif for influencing transcript stability in genome-wide studies. However, genome-wide studies that have investigated direct AGO mRNA interactions have found additional elaborations on the seed principle, including centered sites, single mutation seed sites, and extensive 3' compensatory sites (Chi et al., 2012; Loeb et al., 2012). Although these sites have been detected as physically bound by Ago/miRNA complex, the functional significance of these targets are unclear as these sites are either rare or do not promote transcript destabilization as strongly as traditional canonically seed-matched miRNA targeting. Irrespective of the target site, recruitment of RISC to a target transcript 3'UTR generally results in target gene suppression,

although some non-canonical examples of target gene stabilization and activation have been described (Mortensen et al., 2011). In mammals the typical result of targeting is transcript destabilization and translation inhibition (discussed in greater detail in Chapter 5). Although much of the miRNA biogenesis pathway and the components required for miRNA function have been well-described, many additional questions still remain about the mechanism of miRNA turnover after targeting a transcript and the possibility of additional RNA binding proteins or coregulators that may enhance and modify the activity of RISC and miRNA targeting.

USING THE SKIN TO DISSECT MIRNA BIOGENESIS AND FUNCTION

The skin is one of the first tissues in which functions of the miRNA pathway were delineated using genetically engineered mouse models. The first glimpse into the requirement for miRNA activity came from studies in which *Dicer* was ablated conditionally in the skin (Andl et al., 2006; Yi et al., 2006). Upon loss of the *Dicer* enzyme, small-RNAs, including miRNAs, cannot be processed from pre-miRNA to mature miRNA. These pioneering studies defined the requirement for the miRNA pathway in embryonic and neonatal skin development. Mice lacking canonical miRNAs in epidermal lineages have a severe phenotype resulting in neonatal lethality. The skin of these animals is severely perturbed, displaying a blistered, dry, and scaly skin. More strikingly however is that hair follicle migration is disrupted, resulting in hair follicle cell lineages failing to migrate into the dermis. Instead these cells form aberrant cyst-like structures residing in the interfollicular epidermis. More recent studies have extended these findings by ablating *dicer* in adult animals using inducible CRE deletion strategies (Teta et al., 2012). Loss of miRNAs results in perturbed hair follicle cycling, and

eventual failure to maintain the hair follicle. Apoptosis, which is normally a rare event in the epidermis and hair follicle stem cells, is more frequent, partially explaining the loss of hair follicle stem cells over time. Additionally, the balance of proliferation and differentiation of epidermal progenitors is improperly maintained, resulting in a hyperproliferative thickened epidermis (Teta et al., 2012; Yi et al., 2008).

In addition to these studies additional components of the miRNA pathway have been studied in the skin, such as *Dgcr8*, *Drosha* and the *Ago* proteins. *Dgcr8*, the cofactor of the microprocessor complex, specifically recognizes the stem loop of the primary miRNA transcript, providing specificity for the RNase-III cleavage event catalyzed by *Drosha*. Ablation of *Dgcr8* in the skin results in a nearly identical phenotype to loss of *Dicer*, in addition to a similar depletion of miRNAs from the small RNA pool (Yi et al., 2009). Importantly, these studies demonstrated that other small-RNA produced by *Dicer* but not processed by the microprocessor, have only minor functions during skin development. Similar to loss of *Dgcr8, Drosha*, was also ablated in the skin (Teta et al., 2012). Loss of *Dicer* and *Drosha* nearly phenocopied each other in postnatal skin and hair follicle phenotypes, further suggesting that the loss of canonical miRNAs is the likely cause of the phenotypes observed, and not likely due to non-canonical *Dicer*, or *Drosha* substrates.

The functions of the *Ago* proteins have also been studied in the skin. In mice and humans there are four *Ago* proteins, *Ago 1-4*. Constitutive loss of *Ago*1, 3, or 4 does not result in a developmental phenotype in mice (Cheloufi et al., unpublished data), whereas loss of *Ago2*, uniquely results in embryonic lethality (Liu et al., 2004). Within the skin *Ago2* is the most abundant Ago, followed by *Ago1* and *Ago3* (Wang et al.,

2012). *Ago4* is undetectable based on mass spectrometry. Combined deletion of *Ago1/Ago2* in the skin results in a very similar phenotype to loss of *Dicer*, albeit less severe, presumably due to residual amounts of *Ago3* protein. Combined loss of *Ago1/2* in the skin leads to ineffective RISC function, but also results in a ~90% reduction in the levels of mature miRNAs. Furthermore, loss of *Ago2* alone did not have a phenotype, demonstrating that the slicer activity of *Ago2* is not required during development. Additionally small-RNA sequencing of *Ago1*, *Ago2*, and *Ago3* immunoprecipitates demonstrated that miRNAs association with each Ago occurs in a stochastic manner, in which there is no strong miRNA bias for interacting with one Ago or another. Future studies into the miRNA biogenesis machinery will undoubtedly be focused on the mechanisms of pre-miRNA nuclear export mediated by Exportin 5, as it is unclear if Exportin 5 alone is the only nuclear to cytoplasmic transporter required for miRNA cytoplasmic transport (Xie et al., 2013). Additionally, the functions of the GW repeat containing proteins, *Tnrc6a*, *Tnrc6b*, and *Tnrc6c*, remain poorly described with currently only a *Tnrc6a* knockout described, with was embryonic lethal at day E10 (Jiang et al., 2012).

MIRNA EXPRESSION PATTERNS AND FUNCTIONS IN THE SKIN

Within the numerous cell types of the epidermis and hair follicle, many miRNA families are present, including stratified epithelia-enriched miRNAs such as *miR-203* and *miR-205*, as well as more ubiquitously expressed miRNAs, such as the *let-7*, *miR-125*, and *miR-17 ~ 92* families (Yi et al., 2006). Experimental manipulation of a small subset of individual miRNAs has demonstrated that no single miRNA examined to date is responsible for all the phenotypes that result from compromised miRNA biogenesis in

the skin. Instead, loss of individual miRNAs only contribute to a subset of the phenotypes, indicating that many miRNAs are likely working in concert with additional miRNA families and other regulatory pathways to control skin development (Figure 2).

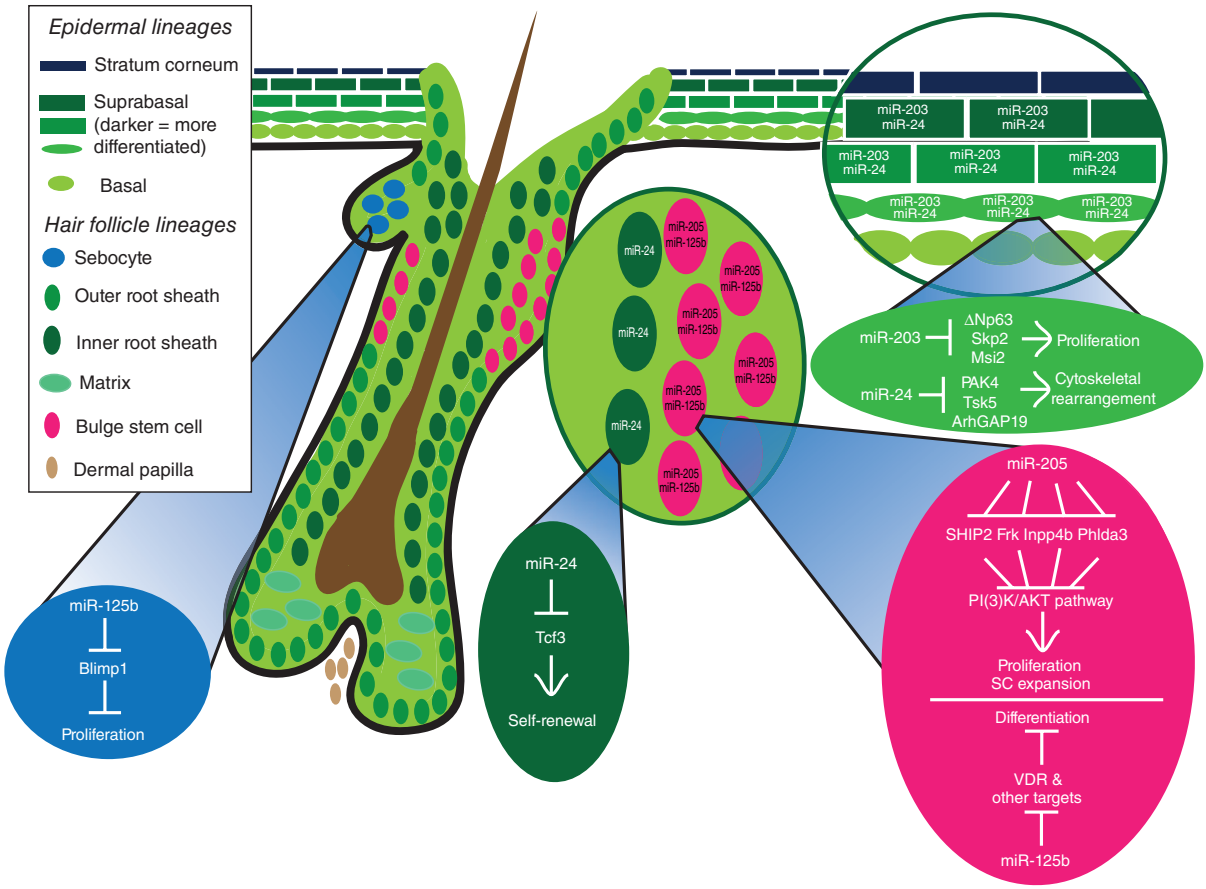

Figure 2. Expression patterns, functions, and targets of select miRNAs within the epidermis, hair follicle, and sebaceous gland. Reproduced/Adapted with permission (Riemondy et al., 2014).

miR-205, a microRNA broadly conserved throughout vertebrate lineages, is the most abundant microRNA expressed in purified hair follicle stem cells (Wang et al., 2013a). Ablation of *miR-205*, in contrast to most microRNA knockouts results in a severe phenotype with perinatal lethality. Within the skin and other stratified epithelia,

miR-205 loss results in impaired progenitor proliferation, and in disrupted epidermal and hair follicle morphogenesis. Mechanistically, *miR-205* regulates *AKT* signaling in part through suppression of negative regulators of the Pi3K pathway. Interestingly, the loss of hair follicle stem cells observed in the *miR-205*$^{-/-}$ mice is reminiscent of the loss of hair follicle stem cells observed in mice with postnatal deletion of *Drosha* or *Dicer*, suggesting that this miRNA is critical for stem cell maintenance. Besides *miR*-205, no other microRNA knockouts have been carefully examined to define roles in epidermal biology, in contrast transgenic overexpression or acute loss-of-function antagomiR approaches which have been employed to identify putative functions of candidate miRNAs.

miR-203 was the first miRNA to be studied in the skin with a genetic mouse model. *miR*-203 is the most abundant miRNA in epidermal samples, and is primarily expressed in the differentiated suprabasal cell populations (Sonkoly et al., 2007; Yi et al., 2008). Overexpression of *miR-203* within mouse stratified epithelia dramatically suppresses the proliferation of epidermal progenitors, a finding also further supported by studies in human keratinocytes, which are strongly growth-inhibited by *miR-203* (Lena et al., 2008; Nissan et al., 2011). These studies have prompted a model by which induction of *miR-203* during differentiation reinforces cell-cycle exit during differentiation, allowing for a robust transition from the proliferative basal layer to the fate-restricted differentiated suprabasal layers (Jackson et al., 2013) . This model is further substantiated by the finding that *miR-203* targets deltaN-p63 (*ΔNp63*), a master regulator of keratinocyte progenitor identity (Koster, 2010). However, although *miR-203*

has been studied extensively, the functions of this miRNA in early embryonic development, and in skin stress responses remains unknown.

A handful of other miRNAs have been studied in the skin, including *miR-24, miR-125b, miR-214* and *miR-31*. *miR-24,* a miRNA also broadly conserved in vertebrates, is very highly expressed in the epidermis, along with *miR-23* and *miR-27,* which are cotranscribed with *miR-24 (*Chhabra et al., 2010*). miR-24* is induced during keratinocyte differentiation, and is enriched in the suprabasal keratinocytes layers of the epidermis (Amelio et al., 2012). Transgenic overexpression in stratified epithelia (*K5-miR-24)* result in perinatal lethality, attributed to greatly reduced proliferation and thinning of internal epithelia. Intriguingly, sequestration of *miR-24* through use of an antagomiR, a cell permeable antisense oligonucleotide inhibitor, enhanced the proliferative capacity of basal progenitors *in vivo,* suggesting that endogenous *miR-24* may play a critical in regulation of keratinocyte differentiation. In support of this idea, *miR-24* overexpression in primary keratinocytes is sufficient to induce differentiation markers, and conversely, *miR-24* inhibition restrains differentiation induction. Additionally, *miR-24* overexpression also represses hair follicle morphogenesis, suggesting that *miR-24* broadly regulates targets critical to the proper development of both the epidermal and hair follicle lineages (Amelio et al., 2013). The identified targets for *miR-24* include *Pak4*, *Tks5*, and *Tcf3*, which regulate cytoskeletal dynamics, actin polymerization, and hair follicle stem cell dynamics respectively.

miR-125b, the mammalian *lin-4* homologue, is also highly expressed in the epidermal lineages. miRNA microarrays were used to define the relative abundances of miRNAs within the lineages of the hair follicle. It was discovered that *miR-125b* is

strongly enriched within the epidermal progenitors as well as the hair follicle stem cell (Zhang et al., 2011a). By combining a tetracycline-inducible *miR-125b* transgene with a *K14-rTTA* allele, Fuchs and colleagues were able to control the spatiotemporal expression of *miR-125* within stratified epithelial lineages. Sustained expression of *miR-125b* resulted in a unique phenotype with expansion of the hair follicle stem cell pool, at the expense of hair follicle, sebaceous, and epidermal differentiation. *miR-125b* directly targets vitamin D receptor (*Vdr)* and *Blimp1* which are required for proper hair follicle cycling and sebaceous gland differentiation respectively (Kretzschmar et al., 2014; Pálmer et al., 2008). Loss of function studies for *miR-125b* using a genetic approach have not been applied to study *miR-125b* in the skin, but such studies are of great interest given the unique and striking overexpression phenotype.

Early small RNA cloning datasets demonstrated that *miR-214* was one of the most abundant miRNAs present in developing hair follicles. Recently, a study of *miR-214,* was published that further characterized the expression pattern and established the functional consequences of *miR-214* overexpression in the skin (Ahmed et al., 2014). *miR-214,* is strongly expressed in hair follicles during anagen, the growth phase of the hair cycle, and becomes reduced during telogen, the resting phase of the hair cycle. Specifically *miR-214* shows a high level of expression in the hair follicle matrix population, the most proliferative cell-type in the skin. Additionally, *miR-214*, is expressed in the terminally differentiated suprabasal layers of the epidermis, suggesting that this miRNA may have cell-type specific functions. Inducible transgenic overexpression of *miR-214* in the skin resulted in attenuated epidermal and hair follicle proliferation, with reduced hair follicle density and cellularity in the hair follicle matrix.

Surprisingly, *β-catenin* was identified as a direct target of *miR-214,* which resulted in perturbed *Wnt* signaling in the hair follicle. *β-catenin* levels are most commonly regulated through the activity of the destruction complex of *Axin, APC,* and *GSK-B,* therefore the findings that *miR-214* regulates *β-catenin* demonstrates that post-transcriptional control of *β-catenin* synthesis can also regulate the Wnt pathway in the skin.

Lastly, *miR-31* was also identified as a miRNA that is dynamically expressed during hair follicle cycling. *miR-31* is strongly expressed in anagen hair follicles, within the matrix, as well as the outer and inner root sheath populations (Mardaryev et al., 2010). However during catagen and telogen the levels of *miR-31* decreased, with *miR-31* eventually disappearing in the telogen stage. Inhibition of *miR-31* through the use of a *miR-31* antagomiR, resulted in accelerated hair follicle entry into the anagen stage and hair shaft abnormalities, suggesting that *miR-31* promoted precocious stem cell activation and is required for hair shaft differentiation. Consistent with this hypothesis, miR-*31,* targets *Fgf-10*, which is required for hair follicle morphogenesis, and additionally *miR-31* targets keratins genes (*K16*,*K17*), which are expressed in the hair shaft and likely important for hair shaft structure.

Together the identified functions for miRNAs in the skin demonstrate that miRNA networks are intimately entwined in fundamental skin processes such epidermal proliferation, hair follicle stem cell maintenance and activation, as well as critical for regulating differentiation processes. Far less is known about the function of the miRNA pathway in regulation of skin stress responses. In animals with compromised miRNA biogenesis via inducible *Dicer* or *Drosha* epidermal specific the transit-amplifying matrix

cells fail to properly proliferate due increased apoptosis and DNA-damage induction, suggesting defective DNA-damage signaling (Teta et al., 2012). In another study, a subpopulation of *K5-Cre/Dicer*^{cko} animals that survived to adulthood were analyzed and found to have much higher rates of cellular senescence in the skin (Mudhasani et al., 2008).These studies point to miRNA as essential regulators of apoptosis, proliferation, and senescence processes in the skin lineages.

A handful of studies have additionally examined miRNAs functions in response to tissue damage and in tumorigenesis. miRNA expression profiles are dynamically regulated during wound healing (Li et al., 2015; Pastar et al., 2012). *miR-21* overexpression inhibits wound closure in ex vivo human wound healing assays and in a rat native wound healing assay. However, the role of the entire miRNA pathway has yet to be delineated using a *Dicer* or *Dgcr8* null mouse model, presenting an opportunity for additional functions to be uncovered. In addition to wound healing, miRNAs have also been implicated in regulating skin tumorigenesis. Combined loss of the miRNA pathway via *K5-Cre/Dicer*^{cko}, with epidermal loss of function mutations in *p53* result in greatly accelerated tumor induction and increased malignancy (Lyle et al., 2014), suggesting the existence of tumor suppressive miRNA networks in the skin .

MIRNA REGULATION OF TUMORIGENESIS

In the decade since microRNAs have been discovered, much work has been focused on delineating their functions in many biological processes, including roles for miRNAs in cancer. Identifying the functions of miRNAs in human cancer has been of particular interest due to the potential therapeutic avenues of miRNA based oligonucleotide therapies (Bader and Lammers, 2011). Early work identified that

miRNAs are commonly changed in expression in tumors and are being developed as diagnostic tools for identifying tumor types and stages of malignancy (Lu et al., 2005). Additionally genetic studies demonstrated that global reduction in miRNA expression due to mutation of miRNA biogenesis machinery promotes tumorigenesis in mouse models, a finding further supported by the identification of loss of function mutations in *Dicer* in some human cancers (Kumar et al., 2009; Stransky et al., 2011).

Small-RNA profiling techniques have identified many candidate oncogenic or tumor suppressor miRNAs, with many miRNAs being recognized as important regulators of tumorigenesis. For example the *miR-17~92* cluster and *miR-21* have been established as oncogenic miRNAs promoting lymphoid and solid malignancies respectively (He et al., 2005; Medina et al., 2010). In addition miRNAs can have tumor-suppressor activities. The *miR-34* family of miRNAs was originally found to be strongly upregulated by activation of the *p53* transcription factor (París et al., 2008). *miR-34* directly antagonizes cell proliferation and suppresses tumor growth in part through regulation of the *Cdk4*, *Ccne2* and *Met*, in addition to other targets (He et al., 2007). Furthermore, the founding member of the mammalian miRNAs *let-7*, is strongly associated with the onset of cellular differentiation *in vivo* and can suppress mouse models of lung cancer (Trang et al., 2011). Additionally, *let-7*, targets the proto-oncogenic *Ras* small GTPases thereby negatively regulating growth factor signaling. For both *miR-34* and *let-7,* these miRNAs are being pursued as possible cancer therapeutics due to their strong tumor suppressor activities.

miRNAs can be activated or suppressed in cancers through many different mechanisms, similar to protein coding genes. Direct mutation of the seed sequence,

while a plausible mechanism to disrupt a miRNA's function, is actually rarely observed based on human sequencing studies of small-RNAs in different cancers. However, miRNA genomic loci are located in regions of the genome that undergo frequent amplification and/or deletion in human cancers (Calin et al., 2004). For example the *miR-15/16* locus is commonly deleted in Chronic Myeloid Leukemia, contributes to upregulation of the anti-apoptotic protein *Bcl2* (Calin et al., 2002; Cimmino et al., 2005). Similarly the *miR-26a* locus is commonly amplified in glioma tumors, and functions to restrict *PTEN,* thereby providing a mechanism for downregulation of *PTEN* in tumors without loss of *PTEN* through other mechanisms (Huse et al., 2009). miRNA promoter methylation has also been described, but technical challenges in identifying promoter regions of primary-miR-transcripts have slowed genome-wide exploration of this mechanism.

Often the underlying changes in miRNA expression are due to changes in upstream transcriptional networks that then drive deregulation of miRNA expression. For example, oncogenic *KRas* suppresses the tumor suppressive *miR-143/145* family in pancreatic cancer cell lines while stimulating the oncogenic *miR-21* in many cancer types(Frezzetti et al., 2010; Kent et al., 2010). In another example *c-Myc* activates the pro-survival pro-growth *miR-17~92* cluster in lymphoid malignancies (Li et al., 2014). In addition to changes in miRNA expression profiles, target mRNAs can also be modified to escape or modify miRNA binding activity through modification of the 3'UTR sequences. Shortening of 3'UTRs due to alternative polyA site usage has been commonly observed in cancer cell lines in comparison to normal counterparts, in part as a mechanism to reduce negative regulation of critical oncogenic driver transcripts (Mayr

and Bartel, 2009). Lastly, mutations in 3'UTR miRNA binding sites have been observed in critical oncogenes such as a 3'UTR mutation observed in breast cancers in the *KRas* oncogene that relieves repression by the *Let-7* family of miRNAs (Paranjape et al., 2011). The myriad mechanisms by which miRNAs are deregulated in human cancers illustrates the importance of precisely defining miRNA and mRNA transcriptomes in tumorigenic cell populations, to accurately identify miRNA regulators of tumorigenic processes.

Within the skin, many miRNA are expressed that regulate tumorigenesis in other cancer models, including the *let-7* family*, miR-21, miR-125b, and the miR-17~92* family. However only a handful of studies have investigated miRNAs functions in skin cancer using mouse models. *miR-21*, one of the first described oncogenic miRNAs, is upregulated in nearly every cancer type investigated (Medina et al., 2010; Volinia et al., 2006). miR-21$^{-/-}$ are strongly resistant to chemical carcinogenesis in the skin, in part due to increased carcinogen induced apoptosis and reduced cellular proliferation under steady state conditions (Darido et al., 2011). In miR-21$^{-/-}$ skin, *miR-21* target genes were upregulated including *Pcdc4*, an apoptosis effector, *Spry1*, a negative regulator of *ERK* signaling, and the tumor suppressor *Pten*, which restrict *Pi3K* signaling. Additionally, *miR*-21 is strongly upregulated in SCCs derived from p53^{cko} animals and late stage SCCs that have progressed through epithelial to mesenchymal transition, known as Spindle Cell SCCs (SpSCCs)(Bornachea et al., 2012). Additionally, overexpression of *miR-21* also enhances epithelial-to-mesenchymal transition (EMT) in a xenografted cell line derived from skin SCCs. Interestingly in the skin, *miR-21* is not highly expressed, however in thyroid carcinoma cells, *miR-21* is strongly induced by oncogenic RAS,

suggesting that activation of *miR-21* by oncogenic Ras contributes to initiation of keratinocytes upon Ras activation *in vivo* (Frezzetti et al., 2010).

miR-125b, the mammalian lin-4 homologue, is highly expressed in HFSCs and functions to suppress HFSC terminal differentiation into epidermal, sebaceous and hair follicle lineages (Zhang et al., 2011a). miR-125b has also been implicated as an oncogene in human cancers (Guo et al., 2012), and negatively regulates *p53* (Le et al., 2009). Constitutive overexpression using a doxycycline inducible *miR-125b* transgene led to SCC tumor development in mice, a phenotype that reverted upon removal of sustained miR-125b expression (Zhang et al., 2014b). *miR-125b* overexpression activates MAPK activity in part through repressing an endosome recycling factor (*VPS4b*) that targets *EGFR.* These studies provide two examples of miRNAs with oncogenic activity in the skin, however no miRNAs have yet been demonstrated to suppress skin tumorigenesis with either a genetic model or chemically induced model of skin cancer.

THE DMBA/TPA MOUSE MODEL OF SKIN CANCER

Skin cancer is the most common cancer worldwide, resulting in an estimated 4 million yearly cases alone in the US (Guy et al., 2015). The two most common cancer types in the skin are Basal Cell Carcinoma (BCC) and Squamous Cell Carcinoma (SCC). BCCs account for about 80% of non-melanoma skin cancers, with SCCs accounting for approximately 20% of cases. Unlike BCC, SCC tumors can be locally invasive and have a significant risk of metastasis if left untreated (Alam and Ratner, 2001). However, skin SCCs are rarely fatal due to the ease of diagnosis and surgical excision. In contrast, SCCs derived from other stratified epithelia, such head and neck

SCC or SCC in non-small cell lung cancer, are rarely detected before the tumor burden is considerable and difficult to treat. Although the underlying genetics and etiologies differ between SCCs from different tissues, the study of SCC in the skin has provided a model to understand the general nature of tumorigenic processes.

The mouse skin chemical carcinogenesis protocol was roughly developed into its modern form in the 1940's. The historical roots of the protocol reach back to the earliest animal models of tumorigenesis in which application of coal tar to the skin of rabbits resulted in the formation of skin tumors (Yamagiwa and Ichikawa, 1918). Further refinement of the protocol in the 1940s, led to the functional separation of the exposure of a carcinogen, which results in irreversible "initiation" of the target tissue, from the tumor promoting agent, which reversibly "promotes" the expansion and proliferation of the initiated target cells (historically reviewed in (Balmain, 2014)).

In the modern protocol for skin carcinogenesis a single sub-carcinogenic dose of the polycyclic aromatic hydrocarbon, 7,12-Dimethylbenz(a)anthracene (DMBA) is painted onto the shaved backskin of mice (Figure 3). The mice are then treated with biweekly doses of a chemical tumor promoting agent, 12-O-Tetradecanoylphorbol-13-acetate (TPA), which results in a hyperproliferative, proinflammatory microenvironment within the epidermis (Abel et al., 2009). DMBA generates mutations through the formation of bulky DNA adducts that are repaired by the nucleotide excision repair pathway (Melendez-Colon et al., 1999). In this mouse model, DMBA induces mutations in a large field of skin cells, including epidermal progenitors, hair follicle stem cells, and differentiated progeny. The cell type of origin is generally thought to be a long-lived stem cell, although many cell types are competent for initiation (Lapouge et al., 2011;

White et al., 2011).

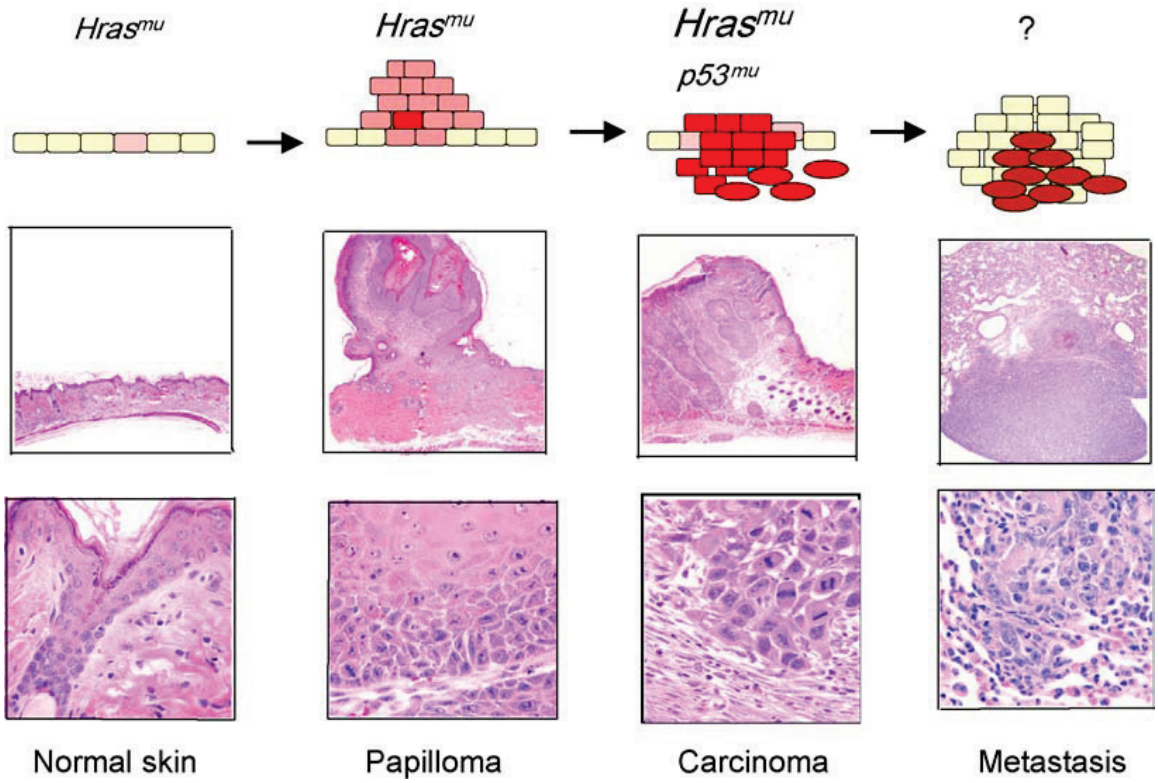

Figure 3. Schematic of tumor phenotypes produced in DMBA/TPA carcinogenesis. Initial *HRas* mutation produces the initiated state whereby in the absence of TPA the dormant initiated keratinocyte maintains proper homeostasis. Upon treatment with TPA, a subset of *HRas* mutant keratinocytes clonally expand to give rise to the benign papilloma state. After continual treatment for up to 50 weeks, a fraction of papillomas convert to malignant SCCs, a process potentiated by loss of p53 and further amplification of the *HRas* oncogenic allele. SCCs can also become metastatic with additional mutations, many of which remain to be defined. Reprinted from (Kemp, 2005) with permission from Elsevier.

Following DMBA, TPA is administered bi-weekly, which stimulates both proliferation and differentiation within the epidermis. A subset of initiated keratinocytes with an imbalance of regulatory control of proliferation and differentiation then go on to form a benign papilloma. Papillomas are exophytic lesions that display similar morphology as normal epidermis, with regions of hyperproliferative keratinocytes and large regions of suprabasal differentiated layers. The DMBA treatment step is

irreversible, as treatment with TPA will produce papillomas, even with up to one year of latency time after the initial single dose of DMBA (Van Duuren et al., 1975). The cell state change produced by DMBA treatment is defined as the “initiated” state. In contrast to the effects of DMBA, most papillomas are fully dependent on continual TPA for maintenance. Over the course of 25-50 weeks of treatment a subset of high-risk papillomas convert to malignant SCCs, a further subset of which can undergo EMT and metastasize to local lymph nodes or lungs, although this degree of malignancy usually requires additional genetic perturbations such as p53 ablation (Lapouge et al., 2011).

Seminal work in the 1980s demonstrated the central importance of *Ras* signaling pathway for mouse skin tumorigenesis. Over 90% of the tumors formed by DMBA/TPA method have a single nucleotide mutation in the *HRas* gene that results in a glutamine to leucine mutation in codon 61 (Quintanilla et al., 1986). In addition, skin tumors produced using alternative carcinogens, such as MNNG, MNU, or MCA, that induce divergent types of mutations also select for mutations in the *HRas* gene at a high frequency, although in different nucleotides of the *HRas* gene (Brown et al., 1990). The end result of these mutations is disrupted GTPase activity of the *HRas* protein leading to hyperactive and constitutive signaling to downstream *Ras* effector pathways (Pylayeva-Gupta et al., 2011). In addition to *Ras* activation due to specific mutation, the mutated *HRas* allele also is commonly amplified in SCCs that develop in the DMBA/TPA model, demonstrating further selection for high activity of the RAS pathway.

THE RAS SIGNALING PATHWAY IN SKIN TUMORIGENESIS

The *Ras* small GTPases regulates diverse cellular process and acts of central signaling node that controls the activity of many downstream effectors (Figure 4). The

Ras family includes *HRas, NRas, and KRas (KRas4a and KRas4b* in humans). Upstream signaling from many different membrane bound receptors (such as *Egfr* for example*)* leads to *Ras* activation, defined by *Ras* binding to GTP. Activation of RAS then serves to regulate numerous effector pathways to transduce the received extracellular signals into intracellular changes in downstream pathways (Figure 4).

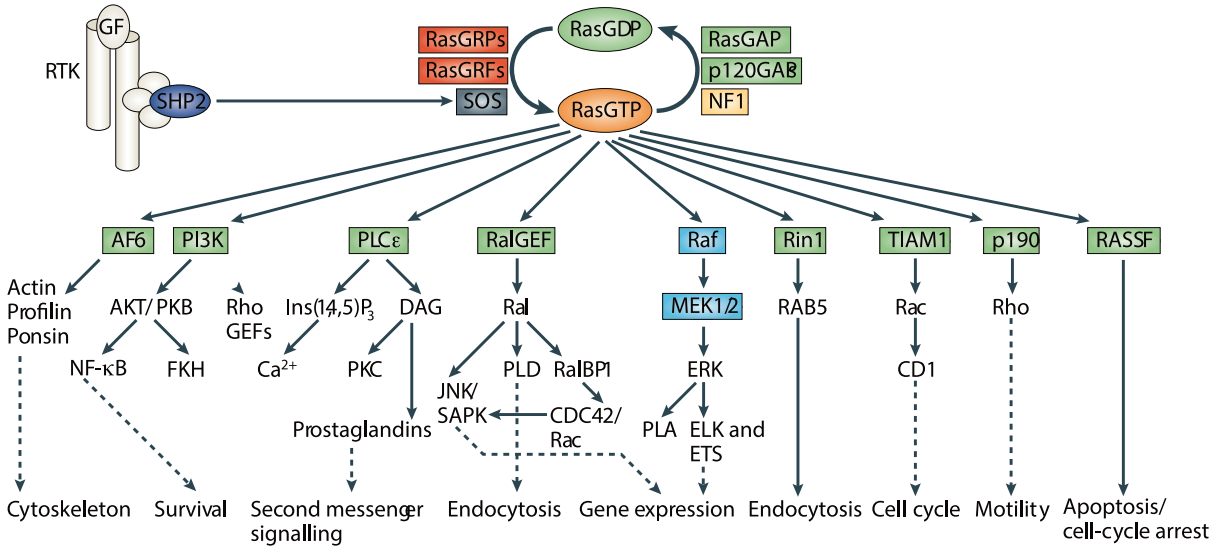

Figure 4. Schematic of the RAS signaling pathway, downstream effectors, and biological processes under regulation. Reprinted with permission from Macmillan Publishers Ltd: Nature Reviews: Molecular Cell Biology (Karnoub and Weinberg, 2008).

The outcomes of *Ras* activation are cell type and signal type specific, including cell-cycle progression, inhibition of apoptosis, modulation of cell migration, and activation of cellular differentiation pathways (Halfar et al., 2001). Normally, the activity of *Ras* is restricted by the activity of GTPase Activating Proteins (GAPs) that stimulate GTP hydrolysis, which switches *Ras* into an inactive state. However oncogenic *Ras* mutations prevent proper *Ras* binding to the GAP (G12 or G13 mutation) or prevent the necessary coordination of a water molecule to allow nucleophilic attack of the gamma-

phosphate of GTP (Q61 mutation) (Pylayeva-Gupta et al., 2011). Consequently the disrupted GTP catalysis stabilizes *Ras* in a primarily active form, leading to excessive downstream signaling.

Insights into the functions of many of the downstream effectors and upstream regulators of *Ras* in tumorigenesis have been gained using skin cancer as a model system. GTP bound *Ras* stimulates the activity of many downstream effector pathways including the *RAF/MEK/ERK* MAP kinase pathway, the *AKT* pathway through stimulation of *PI3* kinase, and the *Rac* and *Rho* small GTPases through *Tiam1* and *p190* (Figure 4) (Karnoub and Weinberg, 2008). The requirement for each of these effector pathways for DMBA/TPA driven skin tumorigenesis has been examined using loss of function mouse models. *c-Raf*, the first kinase target of *Ras* identified, is required for DMBA/TPA driven skin tumorigenesis. Keratinocyte specific *Raf-1* null mice are fully resistant to tumorigenesis, demonstrating a unique absolute requirement for this kinase in skin tumorigenesis (Ehrenreiter et al., 2009). *Raf-1* activation initiates the MEK/ERK MAP kinase cascade and in the DMBA/TPA model, loss of *Mek1* or *Erk1* signaling also reduces tumor development, but not as strongly as loss of *Raf-1*, suggesting that *Raf-1* may signal to additional pathways to promote tumorigenesis (Bourcier, 2006; Scholl et al., 2009) . Interestingly, ablation of *Cyclin-D1*, a well-established transcriptional target of RAF/MEK/ERK signaling, also does not result in as severe of a phenotype as *Raf-1* loss, further suggesting the existence of multiple targets of RAS/RAF that are required to initiate tumorigenesis (Robles et al., 1998).

The functions of the *Rac* and *Rho*-GTPase Ras effectors in skin tumorigenesis have also been examined. *Rac*-GTPase contribute to cell migration and cytoskeletal

dynamics, and are additionally transforming *in* vitro (Karlsson et al., 2009). *Tiam1* is activated by *Ras* to enhance the activity of the *Rac-1* GTPase by promoting GDP-GTP exchange. Ablation of *Tiam1* greatly reduces papilloma formation in part through reduced TPA dependent hyperplasia and enhanced DMBA driven apoptosis (Malliri et al., 2002). Similarly, *Rac-1* null mice display reduced tumor development (Wang et al., 2010), demonstrating the importance of RAS signaling through this pathway. Interestingly, loss of RhoB-GTPase, *increased* skin carcinogenesis, demonstrating that some of the downstream effectors act to restrain activated RAS signaling (Liu et al., 2001). Despite this observation, ablation of two Rho-GTPase GEFs, *Vav2* and *Vav3* severely restricts skin tumorigenesis, supporting an oncogenic role for Rho-GTPase activity, although the specific oncogenic *Rho*-GTPase(s) have yet to be identified (Menacho-Márquez et al., 2013). The copious number of effector pathways downstream of activated Ras required for tumorigenesis highlights the complexity in understanding the oncogenic mechanisms by which *Ras* drives skin tumorigenesis.

The cellular consequences of *Ras* effector pathways include hyperproliferation, a block in keratinocyte differentiation, modified cell migration, and a deregulated the transcriptional profile of the keratinocyte (Figure 5)(reviewed in (Cataisson and Yuspa, 2011)). Many molecular mechanisms have been described that contribute to these cellular phenotypes. *Ras* activation stimulates the production of *EGF* ligands, including *TGF-a* and *HB-EGF*. These ligands can act in a cell autonomous and non-autonomous manner to stimulate cell proliferation in keratinocytes through activation of the EGFR receptor tyrosine kinase (Dlugosz et al., 1997). Additionally, activation of the *Src/Fyn* family of kinases by oncogenic Ras antagonizes PKC dependent differentiation in

keratinocytes, through inhibitory tyrosine phosphorylation (Denning et al., 1996). These mechanisms provide some links between the activity of the *Ras* effectors and the cellular perturbations driven by oncogenic *Ras,* although many of mechanisms remain unexplored.

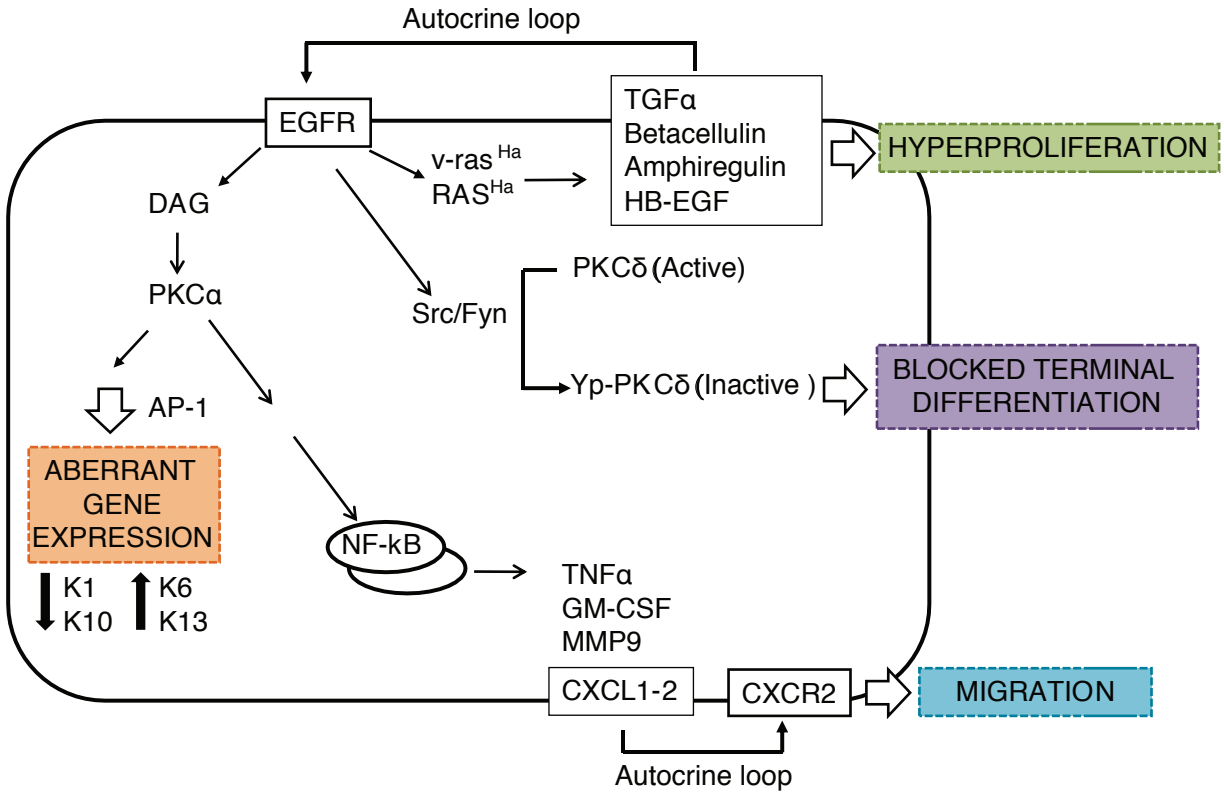

Figure 5. Schematic of cellular processes regulated by oncogenic RAS in keratinocytes. Figure reproduced from (Cataisson and Yuspa, 2011) with kind permission from Springer Science and Business Media.

Although the RAS/MAPK pathway has been intensely investigated for many decades, key questions still remain about the targets, mechanisms, and possible suppressors of this pathway. Of particular interest is defining the downstream network changes elicited by oncogenic *RAS* in the initiated keratinocyte. In the DMBA/TPA model, application of DMBA induces mutations throughout the backskin, however only a

few initiated keratinocytes are competent to form papillomas. Critical future questions to address are the cell autonomous and non-autonomous differences between the Ras initiated cells competent for tumorigenesis and those that remain dormant and do not become tumorigenic.

SCIENTIFIC PROBLEMS ADDRESSED IN THIS THESIS

It is now recognized that the miRNA pathway is a critical regulatory mechanism utilized in most biological systems examined. The challenge that now remains is to uncover the contributions of individual miRNA families to specific biological processes. Within the skin, much is known about how loss of all miRNAs perturbs developmental processes, however very little is known about which individual miRNAs controls developmental processes. *miR-203,* one of the most abundant miRNAs in the epidermis, was previously demonstrated to regulate epidermal progenitor proliferation, and thought to primarily function to drive cell-cycle exit during differentiation. However, prior to the work presented here, the functions of miR-203 in embryonic development, as well as the requirement for miR-203 for postnatal epidermal homeostasis were not addressed.

Additionally, while a handful of miRNAs are important for development, many miRNAs function to regulate stress responses in biological systems, suggesting many skin miRNAs are likely critical regulators of stress responses such as wound healing, infection and regulation of tumorigenesis. Oncogenic insult due to the inappropriate activation of proto-oncogenes occurs throughout the lifetime of an organism, however rarely results in tumorigenesis. In murine skin it is known that oncogenic *Ras* initiates keratinocytes to prime them for tumorigenesis in the skin, however the molecular

mechanisms responsible for driving or suppressing this initiated state remain inadequately defined. In particular, prior to the work herein presented, the identity of miRNAs regulated by aberrant *Ras* activity in keratinocytes, and their functions in controlling downstream oncogenic *Ras* driven processes were largely unexplored.

In this thesis I present the genome-wide identification of miRNAs regulated by oncogenic *Ras in* keratinocytes (Chapter 2). From these studies a candidate tumor suppressor miRNA, *miR-203* was identified. A mouse knockout model for *miR-203* was developed, and the phenotype was characterized initially for a function in regulation of epidermal homeostasis during development (Chapter 3). The mouse knockout model was next used to clarify the function of *miR-203* in skin tumorigenesis using a chemical carcinogenesis paradigm, which identified *miR-203* as a miRNA with tumor suppressor activities in the skin (Chapter 4). Moreover, to gain mechanistic insights into how *miR-203* controls epidermal homeostasis and restricts tumorigenesis, in Chapter 5 I present results obtained that utilized genome-wide expression profiling and *Ago2*-HITS-CLIP, to identify high confidence *miR-203* targets. This approach revealed a number of novel *miR-203* targets, a subset of which are involved in the regulation of the Ras/MAPK pathway and cell division. Lastly, in Chapter 6, I place my results in the context of existing knowledge about *miR-203* and suggest additional lines of experimentation that will further extend our understanding of miRNA's functions in skin cancer and improve existing methods to elucidate miRNA targets from genome-wide datasets.

CHAPTER 2

GENOME-WIDE PROFILING OF ONCOGENIC RAS INITATED KERATINOCYTES

INTRODUCTION

Oncogenic *HRas* was first the human oncogene discovered in year 1982 independently by many groups (Der et al., 1982; Parada et al., 1982; Santos et al., 1982). In the subsequent years, genome-wide mutation surveys have demonstrated that oncogenic mutations in the *Ras* family of small GTPases (*HRas, NRas, KRas*) are among the most common somatic mutations found in human cancers (Prior et al., 2012). The *Ras* signaling pathway is a critical molecular pathway for transducing extracellular signaling to modulate intracellular cellular processes, through a complex network of protein-protein interactions. The net sum effects of *Ras* activation results in cellular changes accompanied by activation of numerous effector gene-expression networks that promote cellular proliferation, migration, changes in cellular metabolism, and many cell type specific functions (Pylayeva-Gupta et al., 2011).

In mouse models of skin cancer activation of *HRas* is the initiating event for the development of benign papillomas. Treatment with the carcinogen DMBA results in keratinocytes with a specific Q61L amino-acid change in the *HRas* gene that abrogates GTPase activity, resulting in constitutive signaling (Quintanilla et al., 1986). The importance of oncogenic *Ras* for tumor initiation has been clearly demonstrated through multiple independent lines of evidence. First, direct infection of mouse skin *in vivo* with *v-HRas* expressing viral vectors bypasses the requirement for the mutagen DMBA for

formation of papillomas (Brown et al., 1986). Secondly, *in vitro* infection of primary keratinocytes with v-*HRas* viral vectors followed by grafting onto immunocompromised mice results in papilloma development, also without the need for DMBA treatment (Roop et al., 1986). Lastly, loss of the *HRas* gene strongly attenuates papilloma development, with the small number of tumors that do form acquiring *KRas* mutations to compensate for loss of *HRas* (Ise et al., 2000; Wong et al., 2013). Due to the central importance of oncogenic *HRas* for squamous tumor development in mice, intense efforts have been placed on dissecting the molecular mechanisms by which oncogenic *Ras* initiates tumor development.

In order to gain insights into the molecular changes driven by activation of *HRas*, I profiled the mRNA and miRNA changes driven by $HRas^{G12V}$. To define the consequences of activation of oncogenic *Ras*, I transduced primary keratinocytes with a control retroviral vector or one that overexpresses $HRas^{G12V}$, a similarly oncogenic mutation to $HRas^{Q61L}$ found in tumors produced with DMBA/TPA skin chemical carcinogenesis. From these samples, 3Seq and small-RNA-Sequencing datasets were generated. 3seq was used to map both the steady-state poly-A mRNA abundances and identify changes in 3'UTR usage patterns. Small-RNA-Seq was used to gauge changes in miRNA expression and identify individual miRNAs with potential tumor-suppressor or oncogenic activities. From these datasets I identified large-scale changes in mRNA abundances driven by $HRas^{G12V}$, suggesting rewiring of the keratinocyte cell-state. In addition I identified a subset of miRNAs that were strongly deregulated by $HRas^{G12V}$, including the most abundant miRNAs in the skin, *miR-203* and *miR-205*. Lastly, I examined the expression of *miR-203* in mouse models of skin cancer and human

SCCs, and provided evidence that *miR-203* is strongly silenced early in the development of SCC.

MATERIALS AND METHODS

3seq library construction:

3seq libraries were constructed using methods described previously (Wang et al., 2013b). Briefly, 500ng of total RNA isolated from primary keratinocytes was poly-A purified (Dynabeads™ Invitrogen) and chemically fragmented by treatment 95°C for 8 minutes in Fragmentation Buffer (Ambion). Fragmented RNAs were then oligoDT primed with a P7T20V oligo and reverse transcribed using SuperScript III™ (Invitrogen)(Appendix Table 1). Following ethanol precipitation, ligation competent cDNAs were generated via second-strand synthesis using RNase H and DNA Pol I enzymes, end-repaired using a mix of T4 DNA polymerase, Klenow DNA polymerase and T4 Polynucleotide Kinase in the presence of dNTPs, and A-Tailed using Klenow 3' to 5' exo- in the presence of dATP (NEB). Ligation was then performed using the P5 Adaptor with T4 DNA Ligase for 1 hour (NEB). Following reverse transcription with Superscript III™ (Invitrogen) and the RT-Primer, cDNA inserts 80-100nt in length were isolated from 8% PAGE gels and subject to PCR amplification using RP1 and RT-Primer oligos for 12-16 cycles (Phusion™ NEB) (Appendix Table 1). PCR products were isolated from PAGE gels and subject to 6 cycles of secondary PCR to introduce unique indices for multiplexed DNA sequencing on a HiSeq 2000™ (illumina).

Bioinformatics processing of 3seq data was performed as described previously, including adaptor trimming, read alignments, peak calling, peak filtering to remove internal polyA priming events, and transcript quantification with minor modifications

(Wang et al., 2013b). Following alignment to the mm10 genome, uniquely mapped alignments from every library were grouped together for peak calling and 3'end filtering to create a master set of high confidence 3' end peaks. From this 3'end dataset, reads counts mapping to each 3'end peak for each library were obtained (See Mapping Statistics, Appendix Table 2). To obtain transcript read counts, reads from all peaks that passed the internal priming filter and were 3'UTR localized were summed to obtain an overall transcript count for each transcript. Normalized transcript counts were calculated as Reads per Million reads Mapped (RPM). To determine differential transcript expression, low-abundance transcripts with less than 10 reads in two libraries were first excluded, then the remaining transcripts were analyzed with EdgeR with classical analysis parameters (Robinson et al., 2010).

To identify changes in 3'UTR distribution the UTR Index (UI) was calculated for every 3'UTR peak identified (Lianoglou et al., 2013). The UI is defined as the ratio of the number of reads mapping to a 3'UTR isoform compared to all reads mapping to all 3'UTR peaks for a particular gene. In order to determine if a particular isoform's UI relative usage is changed between conditions, the difference between the mean UI in one state (i.e. with $HRas^{G12V}$) was subtracted from the mean UI in the other state (i.e. vector only samples). A large positive change or negative change in the UI therefore indicates increased or decreased usage of that particular isoform. For identifying large changes in a 3'UTR usage a UI change of 0.5 was considered to be significant. Additionally to filter out infrequent 3'UTR usage events, a 3'UTR isoform required at least a UI of 0.1 in at least one of the conditions examined and additionally required a minimum of 10 reads mapping to the 3'UTR. Additionally in order to calculate the $\log_2$

fold change in a 3'UTR isoforms expression while incorporating information from biological replicates, the DEXSeq software package was utilized using a custom GTF file built that modeled each 3'UTR isoform as independent exons for a particular gene (Anders et al., 2012). For visualizing the 3'UTR distributions, only genes with multiple 3'UTRs were visualized, and only the isoform with the largest 3'UTR isoform expression change was chosen to represent each gene to avoid duplicate symmetric positive and negative change in UI values for a transcript.

Small RNA-Seq:

Small RNA-Sequencing libraries were prepared using minor modifications of a previously published protocol that reduces RNA-ligation biases and enables accurate miRNA quantification (Zhang et al., 2013). Briefly, two micrograms of total RNA, was first ligated to a pre-adenylated 3' adaptor (10uM) using truncated T4 RNA Ligase 2 (20 Units NEB) in the presence of PEG-8000 (10% w/v) RNase-Out™ (20 Units Invitrogen) for 4 hours at room temperature. Ligation reactions were then resolved on 7M Urea-15% PAGE gel to isolate the miRNA-3' adaptor hybrids. Following overnight elution from the acrylamide gel in HSCB buffer (400 mM NaCl, 25 mM Tris-HCl pH 7.5, 0.1% SDS), ligation products were ethanol precipitated, resuspended in 5' ligation reaction mixture containing a 5' Adaptor (10 uM), 1mM ATP, Peg-8000 (20% w/v), 1x T4 RNA Ligase buffer (NEB), denatured for 5 minutes at 70°C, after which RNase-Out™ (20 units) and T4 RNA Ligase 1 (10 units) were added. Following ligation at 37°C for 2 hours, cDNA was generated via reverse transcription using Superscript III™ (Invitrogen) in the presence of a 3'adaptor specific primer (See Table 1 for oligo sequences). cDNA products were then subjected to 10-14 PCR cycles and resolved on 8% native PAGE

gels. Libraries were then eluted as described above, precipitated, and submitted for sequencing on a HiSeq 2000™ (Illumina).

Small-RNA sequencing reads were analyzed following previous described methods with the following modifications (Zhang et al., 2013). Adaptor Sequences were trimmed from reads using CutAdapt using default parameters (Martin, 2011). Reads were then further trimmed 2 nucleotides on both the 3' and 5' end to remove randomized dinucleotides introduced by the adaptors. Reads were next aligned to a database of mouse miRNA sequences (miRbase) using blastn with the following settings (blastn -word_size 11 -outfmt 6 -strand plus) (Altschul et al., 1997). Blast alignments were then parsed with custom python scripts to extract and count the best miRNA alignment for each read with a minimum read alignment of 18 nucleotides. miRNA counts for each library were then filtered to keep only miRNAs with a minimum count of 50 reads in two libraries, and analyzed for differential expression using EdgeR, with classical analysis parameters.

Analysis of The Cancer Genome Atlas (TCGA) Data:

Head and Neck SCC miRNA-Seq data was obtained from the TCGA https://tcga-data.nci.nih.gov/tcga/ (Download date 10/23/2014). Patient matched normal and tumor miRNA quantification records were identified using custom R scripts (Regular Expression query for tumor and solid tissue normal samples respectively "TCGA-[0-9A-Z]{2}-[0-9A-Z]{4}-0", "TCGA-[0-9A-Z]{2}-[0-9A-Z]{4}-11"). The normalized reads_per_million quantification for miR-203 was then plotted to determine miR-203's relative expression in normal and tumor tissue samples. For analysis of RNA-Seq data from HNSCC samples, the RNA-Seq data was obtained from TCGA as listed above

(Download data 1/7/15). The TCGA barcode for patient matched tumor and normal tissue was parsed as listed above to obtain normal and tumor samples. The rsem.genes.normalized.txt files were then filtered to remove duplicate geneIDs, and then were used to calculate to normalized abundance of each transcript, represented as the mean normalized abundance for all tumor and normal samples respectively. Log_2 Fold changes were then computed. To compare the mouse 3seq data to the human HNSCC data, only mouse orthologues that had matching geneIds in the human TCGA data were plotted.

Primary Keratinocyte Culture, Retroviral Infections, RNA isolation, qPCR, and Western Blotting:

Primary keratinocytes were isolated from neonatal mice using previously described methods with the following modifications (Lichti et al., 2008). Isolated skin was incubated on a solution of Dispase enzyme overnight at 4°C to dissociate the epidermis from the dermis. The following day epidermal sheets were incubated in Trypsin at 37°C for 10 minutes to isolate keratinocytes. Primary keratinocytes were then plated in 6 cm or 10 cm dishes with E-Low Calcium media supplemented with .02 mM calcium chloride for the first 24 hours then switched to E-Low Calcium media with .05 mM Ca^{++} and passaged only once. Retroviral particles were produced by transient transfection of a pBabe vector alone or pBabe with $HRas^{G12V}$ cDNA (cDNA obtained from Dr. Geraldine Guasch), with PCL-Eco and pAdvantage packaging plasmids into 293FT cells using Mirus Bio LT1. After 16 hours, the media was changed to E-Low, and viral supernatant was harvested every 12 hours for up to 96 hours, pooled, filtered with 0.45μM filter, and frozen at -80°C. Retroviral infections were performed 3-4 days after plating primary

keratinocytes, using 4 ml to 6 ml of viral supernatant supplemented with 8ug/ml polyamine sulfate for 6-8 hours at 37°C. 48 hours after infection, keratinocytes were then selected with 2 ug/ml puromycin for 48 hrs, at which time non-infected control cell cultures were non-viable. Total RNAs were isolated from keratinocyte cultures using Trizol™, following manufacturer's instructions (Invitrogen). qPCR was performed using the Qiagen miR-script™ RT system with 500ng of Total RNA input and a BioRad CFX-384 qPCR machine. Fold-changes were computed using the ΔΔCt formula normalized to *sno25* and *Hprt* values. For detecting miRNAs, miRNA specific primers were obtained from Qiagen. For all qPCR figures error bars denote standard errors of the normalized mean. For calculating statistical significance the two-way Student T-test was utilized on the normalized relative quantity for each biological replicate. For qPCR experiments with both technical and biological replicates, the average normalized relative quantities for the technical replicates was calculated and used to represent each single biological replicate for statistical tests. qPCR primer sequences for those generated in house are shown in Appendix Table 1. Western blotting was performed using 20-40ug of clarified cell lysate in RIPA buffer run on 8-12% SDS-PAGE gels. Proteins were transferred to PVDF for detection of *HRas* and *Beta-Tubulin.* After blocking with 5% non-fat milk in TBST, primary antibodies were incubated in 5% BSA in TBST overnight and detected using HRP-conjugated secondary antibodies (1:10,000 dilution) and Amersam ECL-Plus™ reagents. See Appendix Table 4 for antibody descriptions and dilutions. X-ray films were scanned and processed with Fiji software.

miRNA in situ hybridization:

miRNA in-situ hybridization for *miR-203* was performed on frozen sections as described previously, using a LNA probe synthesized by Exigon (Yi et al., 2008). *miR-203* in situ hybridization on FFPE mouse and human tumor samples was performed with the following modifications, after deparaffinization in xylenes, the tissue was treated with proteinase K (20 ug/ml) for an extended period of 20min at an elevated temperature (37°C). Human SCC samples were obtained from Drs. Enrique Torchia and Dennis Roop (University of Colorado at Denver) with the pathological grade scored by an independent pathologist. The mouse SCC samples derived from $KRas^{G12V}$/$Smad4^{cko}$ mice were obtained from Dr. Xiao-Jing Wang (University of Colorado at Denver). Microscopy images were obtained using a Leica DM5500B microscope with a Leica camera and processed with the Leica image analysis suite, MetaMorph® (MDS Analytical Technologies) and Fiji software.

GO Term Enrichment, GSEA analysis, Hierarchical Clustering: Normalized transcript abundances (expressed as Reads Per Million) were used for mean-centered unsupervised hierarchical clustering using Cluster 3.0 software (Eisen et al., 1998). For 3seq data, only transcripts with at least 2-fold change were selected and for miRNA data, only miRNAs with at least an expression level of 1000 RPM and at least a 2-fold change were selected for visualization in JavaTree View (Saldanha, 2004). GO-term enrichment analysis was performed by *David* software using Gene-IDs as input, with the analysis being performed using GO Biological processes datasets (Huang et al., 2008). P-values displayed reflect Benjamini-Hochberg adjusted p-values. Gene Set Enrichment Analysis was performed on the 3Seq dataset using ranked expression values derived from log2 fold-changes using the default Signal2noise metric as the ranking criteria.

Genesets were permuted 5000 times to estimate FDR with the genesets selected from the referenced publications (Subramanian et al., 2005).

Statistical Analysis and Data Plotting:

Statistical analysis was performed using either R or Microsoft Excel. Unpaired two-sided student t-tests were used to assess statistical significance unless indicated otherwise in the figure legends. The hypergeometric test was used to assess the enrichment of gene lists in genome-wide studies. The Kolmogorov–Smirnov test was used to assess differences in cumulative distributions functions. Data plots were constructed using either Microsoft Excel, base graphics in R, or the ggplot2 package in R (Wickham, 2009).

RESULTS

Profiling the oncogenic HRas^{G12V} transformed transcriptome in primary keratinocytes

3Seq and small-RNA-Seq libraries were generated from total-RNAs isolated from independently derived primary keratinocyte cell cultures (Figure 6A-B). 3Seq is an RNA-Seq method that allows the simultaneous mapping of the 3'ends of poly-A containing RNAs, and the quantification of poly-adenylated RNA transcript abundance (Wang et al., 2013b). When applied to this system it permits the identification of differential poly-A site usage in addition to modification of transcript levels driven by oncogenic *Ras*. The 3Seq libraries generated were highly consistent based on comparisons of biological replicates (r = .989, pearson correlation) (Figure 6C). Additionally, examination of the proximal nucleotides nearest to the identified 3'ends of transcripts revealed the expected enrichment of a cleavage site adjacent to an adenine nucleotide (Figure 6D). After subjecting the identified 3' ends to a series of bioinformatics filters to exclude

internal priming events due to homopolymeric A nucleotides, I obtained a dataset of 15,772 unique 3'ends mapping to 10,010 unique genes.

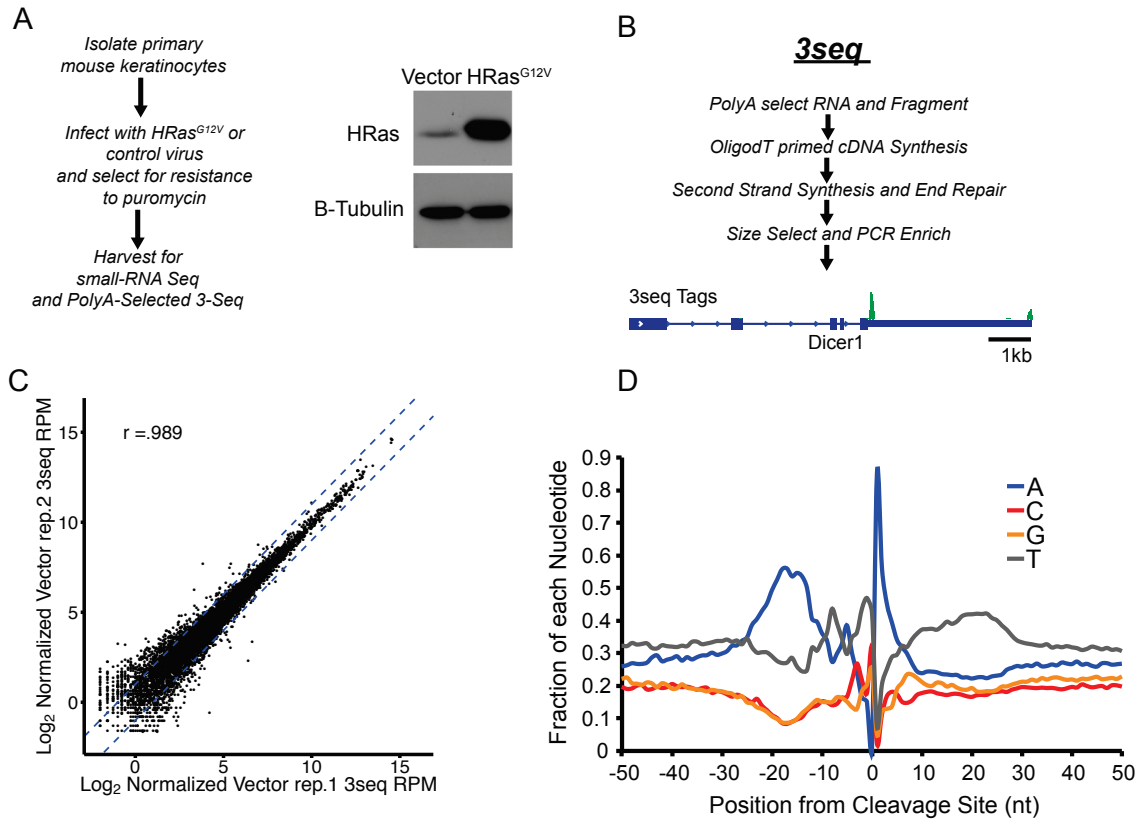

Figure 6. Identifying HRas^{G12V} regulated transcripts and 3'UTR usage dynamics with 3Seq. A) Schematic of primary keratinocyte sample preparation for 3seq and small-RNA-seq and western blot analysis of protein lysates to confirm *HRas* overexpression. (B) Schematic of 3Seq library preparation methods. (C) Correlation between gene expression between replicate wild-type samples (Pearson-correlation coefficient displayed) (D) Representative nucleotide distribution surrounding the 3'end cleavage sites identified via 3Seq.

The 3'UTR of a mRNA transcript contains important regulatory RNA sequences controlling diverse post-transcriptional processes including RNA stability, localization, and translational control. 3'UTR sequences for a given mRNA can be dynamic and altered between different cell types, developmental stages, or disease states (Mayr and

Bartel, 2009; Sandberg et al., 2008; Ulitsky et al., 2012). These observations suggest that an understanding of the 3'UTR sequences present in a given cell-type is critical to dissecting mechanisms of post-transcriptional control of an mRNA.

In order to determine if oncogenic *Ras* modified 3'UTR dynamics, I performed a computational analysis of differential 3'end usage. For mRNAs with multiple identified 3'ends, I determined the relative usage of each 3'end by calculating the UTR index (Lianoglou et al., 2013). The UTR index (UI) is a ratio of the normalized read density for a single 3'end compared to the total read density for all 3'ends in a transcript. Importantly, the difference in the UI in $HRas^{G12V}$ samples compared with controls provides a measure of the change in 3'end usage. For example, a positive change in UI for a given 3'end indicates that a 3'end is utilized more frequently in $HRas^{G12V}$ transformed cell populations. By applying this analysis, I determined that there were ~2300 multi-3'UTR transcripts in the 3Seq datasets. By applying a stringency filter that requires an absolute UI change of at least .5 to detect large changes in 3'UTR usage, I identified less than 5 transcripts that had large changes in 3'UTR usage (Appendix, Figure 32). The small number of 3'UTR switching events is consistent with analysis of 3'end distributions comparing different skin lineages, in which there are only minor changes between different skin cell populations (Wang et al., 2013b). However these results are in direct contrast to other reports that describe large-scale changes driven by cellular transformation, suggesting that 3'UTR switching may play cell-type specific roles in cellular transformation (Mayr and Bartel, 2009). Taken together these results demonstrate that the relative distribution of 3'ends in $HRas^{G12V}$ samples compared to controls underwent only minor changes in 3'end distributions genome-wide, indicating

that 3'UTR switching and shortening events are rarely driven by immediate expression of *HRas*^{G12V} and may reflect that changes at later stages in tumorigenesis drive 3'UTR shortening.

In contrast to the small changes observed in 3'end distributions, mRNA abundances were strongly deregulated by *HRas*^{G12V}. Over 1,100 transcripts were deregulated upon *HRas*^{G12V} expression (two-fold change, FDR < 0.05). In order to extract putative functional categories of the deregulated genes gene ontology enrichment analysis was performed. Genesets comprising the up (687) and downregulated (494) transcripts were compared to those defined by gene ontology (biological processes) .The upregulated transcripts grouped in major three major categories, including regulation of cellular migration, activation of pro-angiogenic processes, and regulation of wound responses (Figure 7A). Oncogenic Ras has previously been demonstrated to regulate expression of *Vegf*, a potent activator of angiogenesis, and modulate cell migratory processes through activation of the *Rho/Rak* kinase pathways (Parsons et al., 2010; Sodhi et al., 2001). Examination of the transcripts suppressed upon *HRas*^{G12V} revealed widespread suppression of genes critical for keratinocyte differentiation including the intermediate filaments *K1* and the major structural protein of the cornified envelope *Loricrin* (Mehrel et al., 1990; Porter et al., 1996). It is known that oncogenic *Ras* suppresses the differentiation of keratinocytes however the suppressive mechanisms remain poorly understood, yet critical to understand, as papilloma development is thought to be driven by an imbalance in basal

cell proliferation and suprabasal differentiation mechanisms (Driessens et al., 2012)

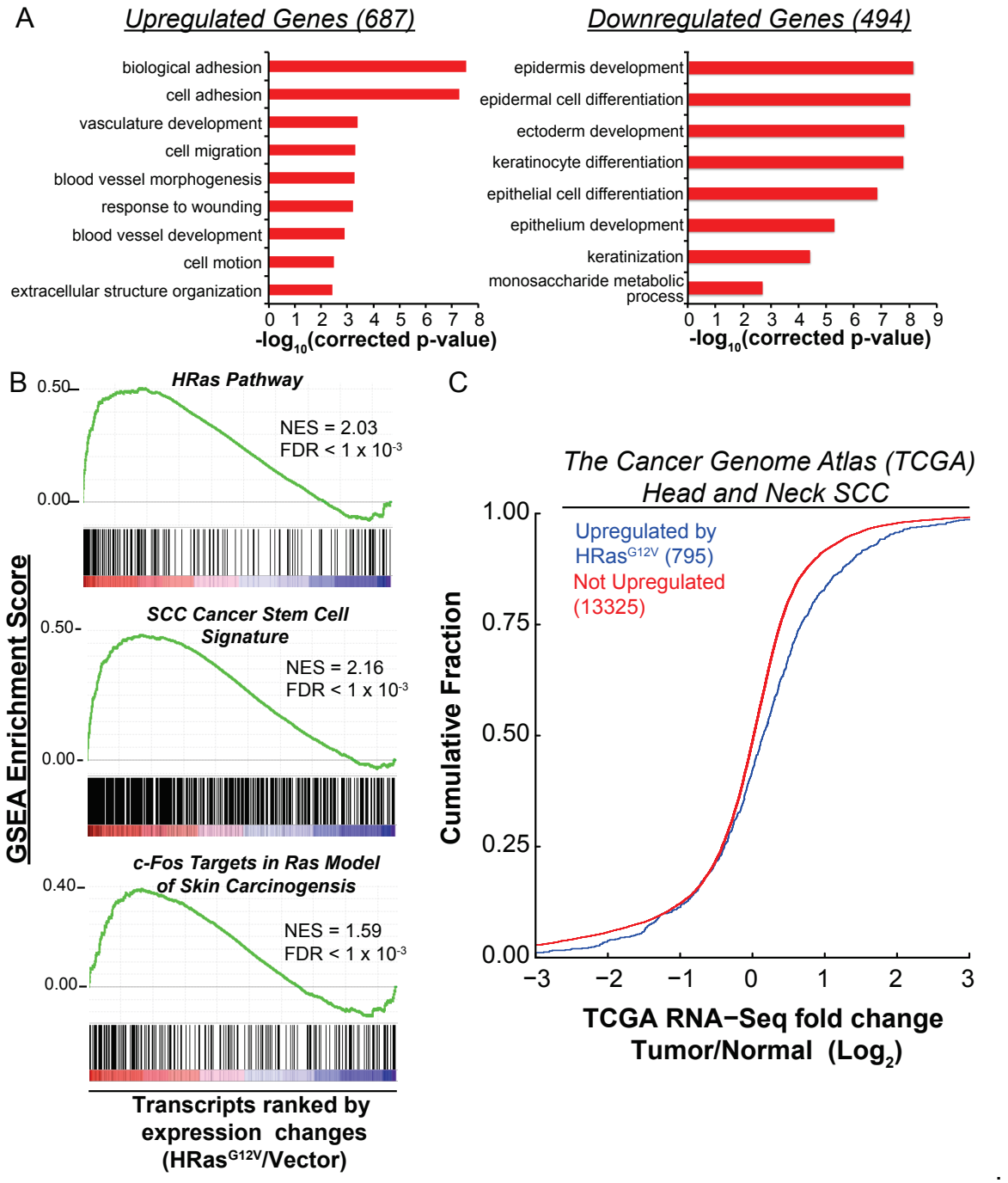

Figure 7. HRas^{G12V} regulated transcripts are enriched in tumorigenic processes (A) Gene Ontology (GO) enrichment of up and down-regulated transcripts in *HRas^{G12V}* samples (Two-Fold Change, FDR < 0.05) (B) GSEA analysis of selected gene-sets relevant to mouse skin carcinogenesis (C) Cumulative distribution of genes expression for targets of *HRas^{G12V}* in mouse keratinocytes (up-regulated and FDR<0.05) compared

to gene expression changes in tumor versus normal tissues from TCGA data ($p = 3.04 \times 10^{-13}$, KS Test).

In order to determine their relevance to tumorigenic process occurring *in vivo* I compared the 3Seq datasets to public available genesets using Gene Set Enrichment Analysis (GSEA) software. Genes classified as unique to the *HRas* pathway were strongly enriched in the upregulated genes in our dataset (Bild et al., 2006) (Figure 7B). Similarly, genes upregulated by oncogenic *Ras* were strongly enriched in a geneset of transcript defining a tumor propagating cell population from a murine SCC model (Schober and Fuchs, 2011). Additionally, genes upregulated by oncogenic *Ras* were also highly enriched for targets of the *c-Fos* oncogene in another *Ras* driven mouse model of skin cancer (Durchdewald et al., 2008). Furthermore, transcripts upregulated by oncogenic *Ras* were strongly upregulated in RNA-Seq data compiled from head and neck SCC tumors compared to patient matched controls (Figure 7c). Taken together these analyses demonstrate that the activation of *Ras* in primary keratinocytes captured a large number of gene expression changes, many of which are likely to have functional consequences for the establishment of the initiated keratinocyte state.

Profiling the oncogenic $HRas^{G12V}$ transformed miRNAome in primary keratinocytes

In addition to profiling mRNAs using 3Seq, small-RNA populations were sequenced using an updated high-efficiency library preparation protocol that reduces ligation dependent biases, and permits accurate quantification of small-RNAs (Zhang et al., 2013). Similar to the 3seq libraries, biological replicates from the small-RNA-Seq libraries were well-correlated (r >=.98). Overall, 15 miRNAs were differentially expressed upon $HRas^{G12V}$ *over*expression (FDR <0.05, two-fold change) (Figure 8A-B).

Two key patterns emerged in these profiles. First, the epithelial tissue-specific miRNAs, *miR-203* and *miR-205*, which represent the most abundant miRNAs expressed in murine skin and primary keratinocytes were strongly suppressed by *HRas*^{G12V}. Additionally, members of the abundantly expressed, *miR-23/24/27* miRNA cluster were also downregulated by *HRas*^{G12V}. Secondly, *miR-21* was strongly induced becoming the most highly expressed miRNA, consistent with its direct activation by oncogenic *Ras* reported in other systems (Talotta et al., 2009). The upregulation of *miR-21* is also consistent with its well-appreciated oncogenic function in skin cancer (Darido et al., 2011). Additionally, *miR-146* was also induced by *HRas*^{G12V}, however this miRNA is expressed 2-orders of magnitude lower than *miR-21*, suggesting that its upregulation may have limited contribution to *HRas* initiated tumorigenesis at this early stage.

A

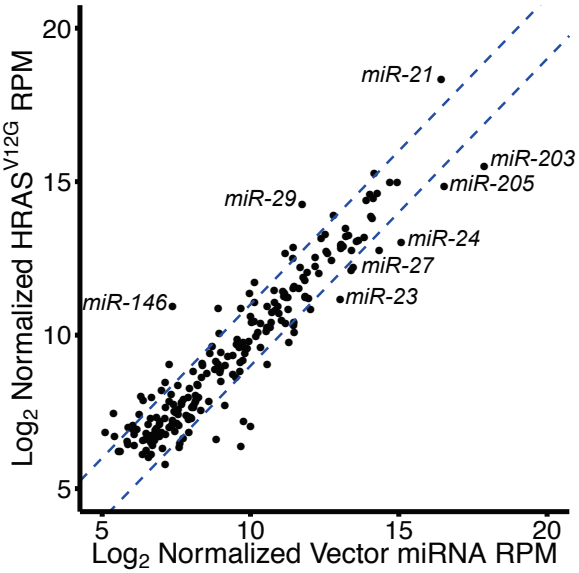

B

miRNA	Fold Change	FDR
mmu-miR-99a-5p	**-9.83**	3.60 x 10^{-06}
mmu-miR-335-3p	**-7.86**	3.00 x 10^{-06}
mmu-miR-203-5p	**-5.87**	**2.95 x 10^{-04}**
mmu-miR-203-3p	**-5.22**	**3.71 x 10^{-03}**
mmu-miR-335-5p	**-4.70**	1.16 x 10^{-03}
mmu-miR-24-3p	**-4.20**	1.70 x 10^{-02}
mmu-miR-23b-3p	**-3.62**	1.37 x 10^{-02}
mmu-miR-24-2-5p	**-2.89**	8.31 x 10^{-03}
mmu-miR-205-3p	**-2.83**	1.70 x 10^{-02}
mmu-miR-7a-5p	**2.68**	1.70 x 10^{-02}
mmu-miR-322-5p	**3.31**	1.55 x 10^{-02}
mmu-miR-21a-5p	**3.72**	**3.73 x 10^{-02}**
mmu-miR-29b-3p	**3.98**	8.40 x 10^{-04}
mmu-miR-29a-3p	**5.68**	6.12 x 10^{-04}
mmu-miR-146a-5p	**13.71**	3.00 x 10^{-06}

Figure 8. Identification of HRas^{G12V} regulated miRNAs (A) Scatterplot of mean normalized reads counts, Reads Per Million MicroRNA Mapped (RPM), for vector and *HRas*^{G12V} samples. Dashed Blue line represents a two-fold change (B) Expression values for 15 microRNA detected with FDR < 0.05.

Next the mature *miR-21*, *miR-203*, and *miR-205* miRNA were measured by qPCR. In support for the quantitative performance of the small-RNA-Seq, the differential expression of all three miRNAs measured by qPCR method was nearly identical to the quantification by miR-Seq (Figure 9A,B). To initially probe the mechanism through which $HRas^{G12V}$ suppresses *miR-203* expression, the level of *miR-203* primary transcript was examined. Previously the transcribed genomic region of *miR-203* including the promoter region and transcription start site was mapped (Jackson et al., 2013). Because the primary transcript *of miR-203* harbors a polyadenylation [AAUAAA] signal and generates a Poly(A) tail, the abundance of the primary transcripts was quantified by counting the 3'end reads of the primary miRNA obtained by 3seq (Figure 9C,D). This result was further confirmed by qPCR measurement specific to *pri-miR-203* (Figure 9 C,D). The degree of downregulation for both mature and primary *miR-203* transcripts was similar as judged by these two independent assays. Collectively, the results demonstrate that the repression of *miR-203* by $HRas^{G12V}$ is most likely mediated by suppressing the production of primary *miR-203* transcripts at an early stage of oncogenic cellular transformation, although an effect on RNA stability cannot be ruled out by the experiments performed.

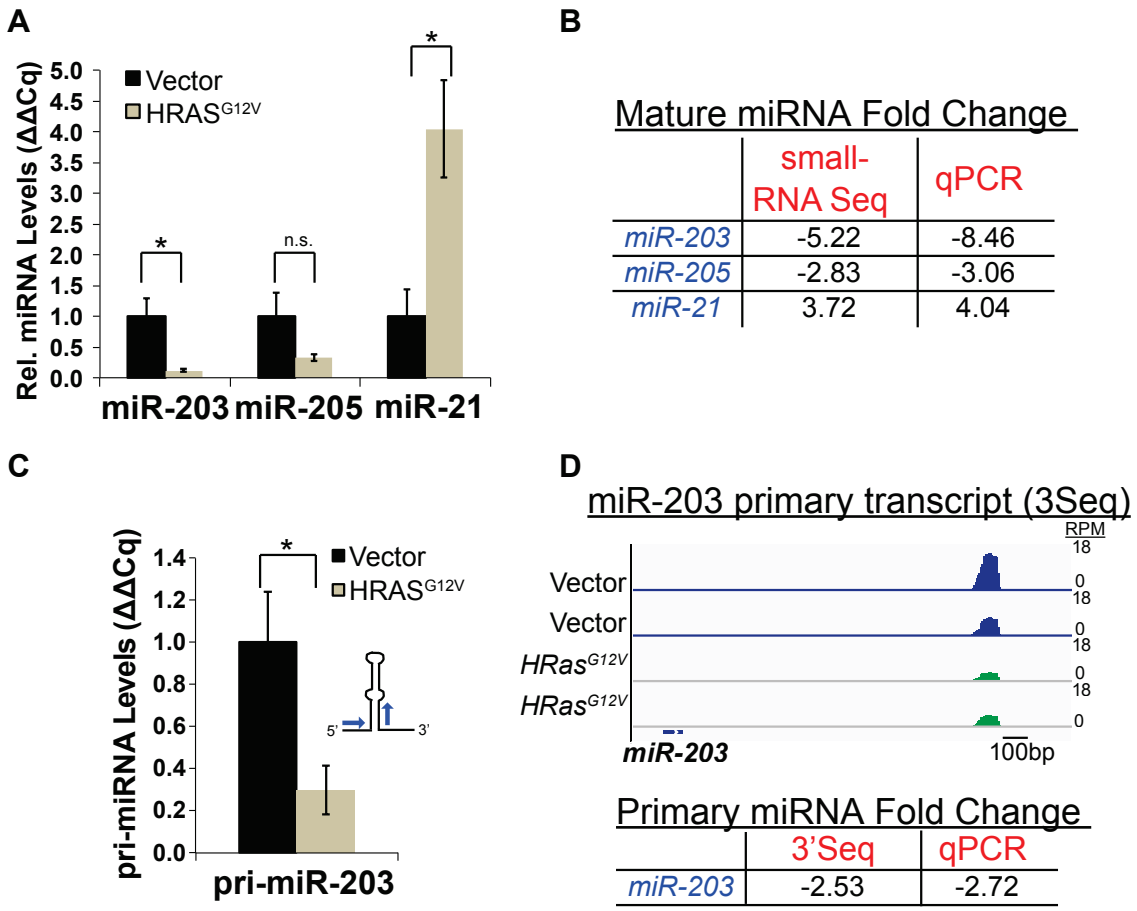

Figure 9. miR-203 is strongly downregulated by HRas^{G12V} (A) qPCR of mature miRNA expression in vector or HRas^{G12V} samples. Error bars represent S.E.M from qPCR reactions performed in technical duplicate on biological triplicate samples. * = p-value <0.05. n.s. = p >0.05. Student T-Test two-sided. (B) Comparison of mean fold-changes as measured by qPCR and small-RNA-Sequencing. (C) qPCR quantification of primary miR-203 transcripts in vector or HRas^{G12V} samples. Error bars represent S.E.M from qPCR reactions performed in technical duplicate on biological triplicate samples. * = p-value <0.05. Student T-Test two-sided. (D) Gene track view of miR-203 primary transcript displaying normalized read counts aligning to the 3' end of the miR-203 primary transcript and a tabular comparison between qPCR and 3Seq detection of primary miR-203.

miR-203 silencing is an early event in mouse and human SCC

The profiling data revealed robust silencing of *miR-203* by oncogenic *HRas* in an *in vitro* model. Therefore, *miR-203* expression was next accessed with in situ hybridization during skin tumorigenesis *in vivo*. In classic chemical carcinogenesis

models initiated by DMBA/TPA treatment of mouse skin, *HRas* is preferentially mutated, which compromises the GTPase activity and results in constitutive HRas activation. Mutating *HRas* at Q61 leads to papilloma development and infrequent malignant transformation to SCCs (Abel et al., 2009). *miR-203* expression in benign papillomas was first examined. Consistent with the *in vitro* results, *miR-203* expression was absent from epithelial compartments adjacent to tumor stroma (Figure 10A), the region where putative cancer stem cells reside. Although *miR-203* was detectable in tumor regions with evidence of cellular differentiation (keratin pearls and large differentiated morphology), the levels of *miR-203* were considerably lower in these regions compared to the suprabasal cells of adjacent normal skin, where *miR-203* is normally expressed (Figure 10A). Additionally, in an independent mouse model of SCC, *miR-203* expression was gradually lost in a $KRas^{G12D}$*/Smad4* KO model where skin tumors progressed to invasive SCC through serial tumor passaging (White et al., 2013) (Figure 10B). Taken together, these results demonstrate that *miR-203* is significantly downregulated in both papilloma and SCC stages of skin tumorigenesis in mouse models.

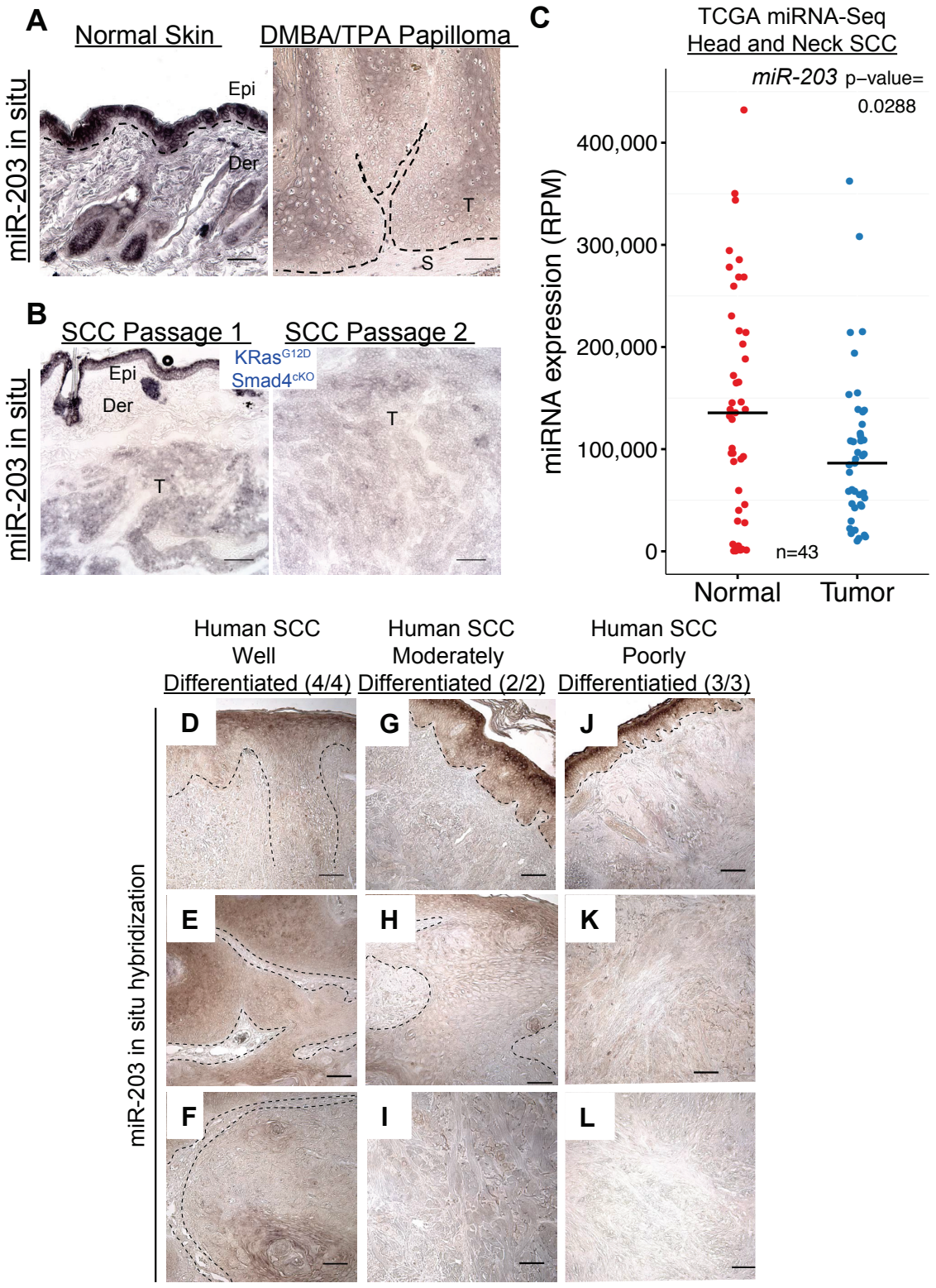

Figure 10 miR-203 is strongly downregulated in mouse and human SCC samples
(A) In situ detection of *miR-203* in normal adjacent skin or DMBA/TPA produced papilloma. Epi = Epidermis, Der = Dermis, T = Tumor, S = Stroma (B) In situ detection

of *miR-203* in SCCs sequentially passaged in immunocompromised mice. (C) TCGA data of normalized miRNA expression (Reads Per Million miRNA Mapped, RPM) in normal or tumor tissue from patient matched tissue samples. Bar indicates mean value. P <0.05 Student T-Test, two-sided. (D-L) In situ detection of *miR-203* in human skin SCC samples.of varying stages of differentiation (D,G,L) In situ detection in regions of hyperplastic tissue to confirm successful in situ hybridization. (E,H,K,F,I,L) In situ detection of *miR-203* in tumor regions. Scale bar = 50um.

Next, the levels of *miR-203* in human skin cancer were assessed by mining publically available TCGA small-RNA-Seq datasets. *miR-203* was significantly downregulated in head and neck SCC samples compared to patient matched normal tissue samples (Figure 10C), a finding that was recently collaborated by independent analysis by the TCGA consortium (Lawrence et al., 2015). To examine the dynamics of *miR-203* expression in different SCC stages 9 SCC samples were obtained from patients with the early, middle and late stages of skin cancer. In these human skin SCC samples, *miR-203* was downregulated well-differentiated tumors and progressively lost during the course of tumor progression, similar to the pattern observed in the mouse models. In the poorly differentiated SCC samples, the *miR-203* signal was completely absent, yet readily detectable in surrounding hyperplastic or normal epidermal regions (Figure 10D-L). Altogether, these results corroborate our observations in mouse models and further support the strong correlation between the loss of *miR-203* and the development of skin cancer at multiple stages of tumorigenesis. These expression analyses suggest that the loss of *miR-203* coincides with tumor-initiation and that *miR-203* might function as a tumor suppressing mechanism in skin cancer.

DISCUSSION

Somatic mutation of the *Ras* small-GTPases are some of the most common oncogenic mutations found in human cancers (Prior et al., 2012). In a mouse model for skin squamous cell carcinoma, oncogenic activation of the *HRas* gene is critical for tumorigenesis, and is the earliest event in the development of initiated tumorigenic state, making the study of mouse skin SCC a prime model to understand the mechanisms by which the *Ras* oncogene drives tumorigenesis (Kemp, 2005). Despite the discovery of the *Ras* oncogenes in human cancers in the year 1982 and the knowledge that the *HRas* gene is critical for mouse skin tumorigenesis, the downstream molecular mechanisms by which oncogenic *HRas* promotes the establishment of the initiated state, and drive mouse skin cancer, remain poorly understood.

To gain insights into the molecular networks disrupted by oncogenic *Ras* in murine skin cancer, the impact of oncogenic $HRas^{G12V}$ on the landscape of mRNA and miRNA expression was quantitatively measured. The 3Seq data confirmed the profound ability of $HRas^{G12V}$ to promote cellular transformation, through multiple mechanisms, including modifying transcript levels in processes that promote angiogenesis, suppress keratinocyte differentiation, and modulate cellular migratory processes, critical for proper epidermal homeostasis. Additionally the use of a 3Seq RNA-Seq approach allowed insights into potential 3'UTR switching events driven by $HRas^{G12V}$ during cellular transformation. However, in contrast to other cell-types, *Ras*-driven cellular transformation does not result in frequent shortening or changes to the distribution of 3'UTRs in keratinocytes.

Profiling miRNA populations revealed dynamic changes in highly expressed keratinocyte miRNAs driven by *HRas*^{G12V}. In particular, *miR-203*, one of the most highly expressed miRNAs in the skin was strongly downregulated by oncogenic *Ras*. Although the exact mechanism of by which miR-203 is downregulated has not yet been determined, the results presented suggest it likely occurs through a transcriptional mechanism, rather than modifying *miR-203* biogenesis. Oncogenic Ras is known to suppress markers of keratinocyte differentiation in cell culture through a mechanism that has not been fully defined (Cheng et al., 1990). It is tempting to speculate that a similar mechanism negatively regulates *miR-203* downstream of oncogenic *Ras*.

In order to determine if miR-203 suppression by oncogenic RAS was relevant to tumorigenesis *in vivo* tumor samples were obtained from both mouse and human SCC tumors. *miR-203* was strongly downregulated in two models of *Ras* driven skin tumorigenesis, in papillomas derived from DMBA/TPA chemical carcinogenesis, and in SCCs from a genetic model of skin cancer driven by *KRas*^{G12V} (White et al., 2013). These results demonstrate that *miR-203* downregulation occurs at an early stage of tumorigenesis in mouse skin cancer. Next, publically available small-RNA-Seq data from The Cancer Genome Atlas (TCGA) was analyzed, and it was found that in head and neck SCCs *miR-203* levels were reduced compared to patient matched normal tissues. Lastly, analysis of different stages of skin SCC tumors revealed that *miR-203* was lost in skin SCC tumors concomitant with reduced histological signs of keratinocyte differentiation.

Since the initial discovery of the miRNA pathway intense investigation has sought to identify the interactions between *Ras* signaling and miRNA regulation. Many

microRNAs have been identified that control upstream regulators of *Ras*, or processes that modulate the activation or abundance of *Ras*. For example, *Let-7*, the defining member of the mammalian miRNAs, directly targets the 3'UTRs of the human *Ras* genes, an interaction conserved in the small nematode *C. elegans,* that has important consequences for human lung cancer (Johnson et al., 2005). Additionally, *miR-143/145* directly target the *KRas* 3'UTR, resulting in reduced *KRas* activity, while simultaneously targeting the transcription factor *Rreb1*, a downstream transcription factor activated by *Ras* (Kent et al., 2010; Thiagalingam et al., 1996). *miR-21*, a microRNA induced by oncogenic *Ras* signaling, negatively regulates the ERK modulator *Spry1/2* and the p53-inducible gene *Btg2,* which suppress *Ras* transformation (Boiko et al., 2006; Frezzetti et al., 2010). In part through antagonizing both ERK activity downstream of oncogenic *Ras*, and suppressing a negative regulator of transformation, *miR-21* has potent oncogenic activities in many human cancers (Frezzetti et al., 2010). Lastly, the *miR-34* family of microRNAs strongly suppress cell proliferation in part through negative regulation of *Cyclin-D1, a* well-established downstream *Ras* target critical for the G1/S cell cycle transition (Sun et al., 2008).

The studies, presented in this chapter, sought to identify additional microRNAs regulated by *Ras* under the assumption that these miRNAs may have functional significance for *Ras*-driven cancer. Through the combinatorial use of mRNA and microRNA profiling, I identified wide-scale changes in the transcriptome driven by activation of *HRas* in primary keratinocytes. From these datasets I identified a microRNA, *miR-203,* that is strongly downregulated in mouse and human skin cancers, and actively antagonized by oncogenic *Ras*. These results place miR-203 within the list

of miRNAs that are regulated by oncogenic *Ras* and suggest that miR-203 may have tumor suppressor activity in skin cancer.

CHAPTER 3

GENERATION OF A MIR-203 CONDITIONAL MOUSE MODEL TO STUDY ITS FUNCTIONS IN SKIN DEVELOPMENT

INTRODUCTION

Since the initial findings that loss of all miRNAs with the skin results in a severe phenotype, intense effort has been placed on identifying individual miRNAs or miRNA families responsible for this phenotype. Loss of the whole microRNA pathway in stratified epithelia results in a unique phenotype not previously observed upon loss of any combination of protein coding genes (Yi et al., 2006). Of particular interest has been defining the miRNAs responsible for the early developmental phenotypes observed in the skin upon loss of the miRNA pathway.

Of all the microRNAs expressed in the skin, *miR-203* is the best studied. *miR-203* was originally identified via computational methods that compared sequence and structural conservation between vertebrate genome sequences (Lim et al., 2003). *miR-203* was found to be highly conserved in vertebrates, while being absent from *C.elegans*, and *D.Melanogaster* (Figure 11A). The expression pattern of *miR-203* in vertebrates was first determined by a genome-wide in situ analysis in zebrafish. In zebrafish, *miR-203* is found only expressed in the most distal epithelial tissues. Subsequently small-RNA cloning libraries generated from 250 unique samples derived from diverse organ systems, revealed *miR-203* expression predominately in epithelial tissues (Landgraf et al., 2007). In 2007, *miR-203* was found to be enriched in stratified epithelial tissues, including the skin, based on qPCR measurements, while being restricted from other cell types commonly found in the skin such as fibroblasts and

immunologic cells (Sonkoly et al., 2007) (Figure 11B). Importantly as well miR-203 was found primarily restricted to the suprabasal keratinocyte populations, a population of terminally differentiated cells undergoing cornification to produce the stratum corneum (Figure 11D). In addition to the strong enrichment of miR-203 within terminally differentiated keratinocytes, it is the most abundant miRNA found in the epidermis, based on small-RNA-Sequencing measurements (Figure 11C).

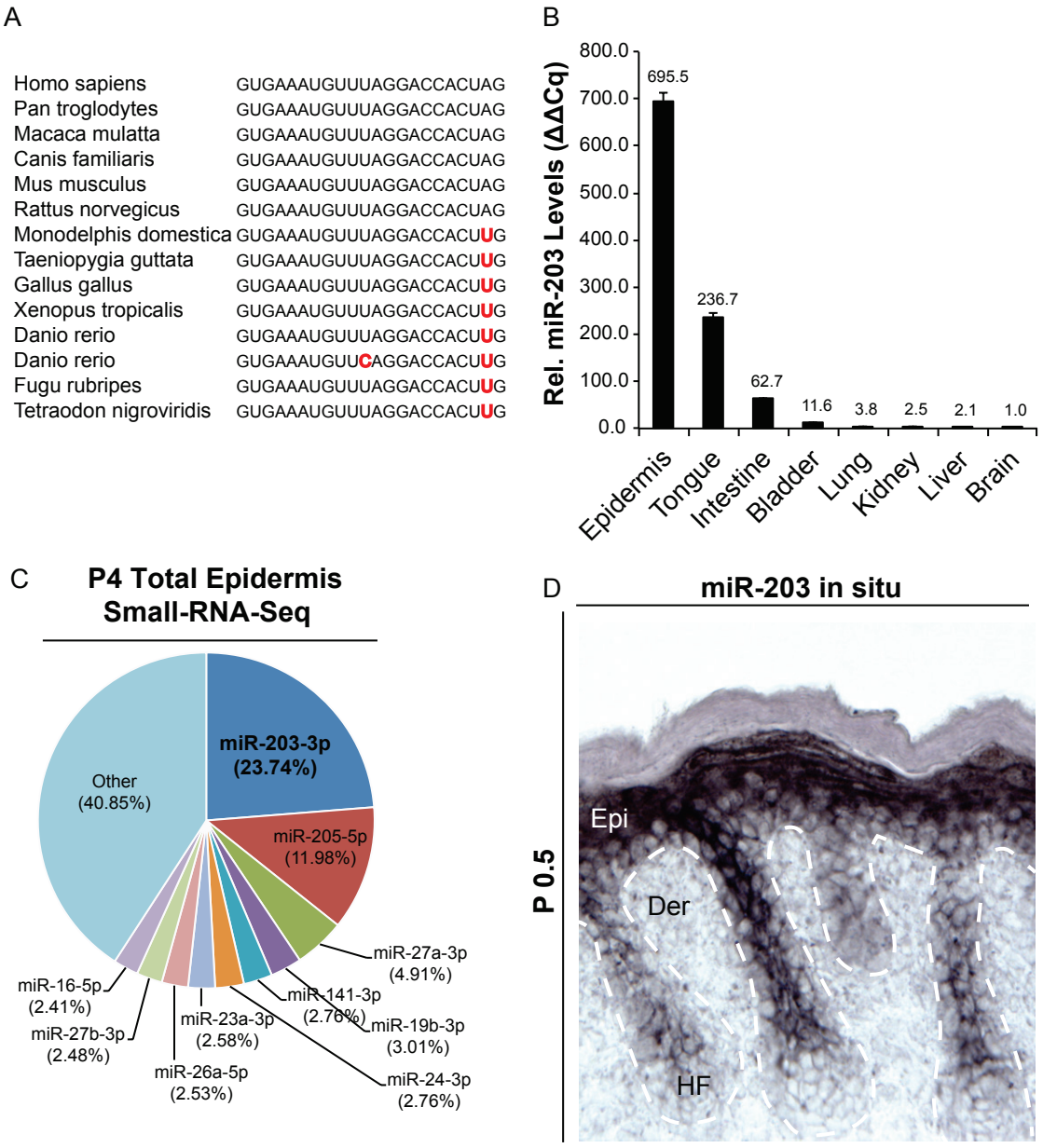

Figure 11. miR-203 is broadly conserved and highly expressed in suprabasal keratinocytes. (A) Multiple sequence alignment of all mature miR-203 sequences documented in miR-Base. Red indicates sequence variants compared to mouse *miR-203*. (B) qPCR detection of mature *miR-203* in various adult mouse organ tissues. Error bars represent S.E.M from reactions performed in technical duplicate. (C) Small-RNA-Seq from total epidermis isolated from a p4 mouse. Percentage of miRNA mapped of all miRNA mapped displayed. (D) In situ detection of *miR-203* in neonatal skin. Epi = Epidermis, Der = Dermis, HF= Hair Follicle.

The strong enrichment for *miR-203* in the differentiated keratinocyte populations suggests that *miR-203* may function to promote processes important for keratinocyte differentiation. The first experimental evidence for this function came from studies employing gain of function and loss of function approaches in mouse skin. Targeted overexpression of *miR-203* in the basal layer of stratified epithelia results in neonatal lethality, concomitant with strong and rapid suppression of basal progenitor cell proliferation (Yi et al., 2008). Interestingly, while *miR-203* overexpression suppressed the proliferation of basal progenitors, keratinocyte differentiation remained unperturbed based on analysis of markers of early (Keratin 10) and late differentiation (Loricrin), suggesting that *miR-203* primarily functions to regulate proliferation and not drive differentiation processes. Importantly, treatment of mouse skin with an anti-sense *miR-203* antagomiR results in ectopic proliferation in the normally mitotically inactive suprabasal layers. Additionally, this phenotype was also observed upon global loss of all epidermal miRNAs by ablation of *Dicer* in adult animals. These observations prompted the model that *miR-203* restricts the proliferation and expansion of epidermal progenitors, reinforcing cell-cycle exit required for keratinocyte differentiation.

Previous studies of miRNAs in the skin have generally relied on gain of function or short-term loss-of-function approaches to elucidate their functions. While these

approaches have provided great insights in the potential functions of miRNAs in diverse processes, it remains important to delineate miRNA function with traditional loss of function models. The phenotypes observed in miRNA transgenic models often exaggerate the importance of the miRNA during development, which rarely show strong phenotypes upon loss-of-function (Bejarano et al., 2012). Additionally, the functions of miRNAs during embryonic skin development have been poorly investigated, in part due to the fact that loss of *Dicer* or *Dgcr8* using the K14-Cre model only results in loss of miRNA late during embryogenesis, past a point in which epidermal fate specification and hair follicle morphogenesis has begun and thus obscuring potential functions for miRNAs in embryonic skin development.

Therefore to define the importance of miR-203 in the regulation of skin development a knockout mouse model was developed. *miR-203*$^{-/-}$ mice are viable and fertile, similar to many miRNA knockouts. Although the mice display no gross morphological phenotype, during embryonic epidermal development, epidermal progenitors are expanded in *miR-203*$^{-/-}$ epidermis. As development progresses*, miR-203*$^{-/-}$ epidermis returns to homeostasis, and is maintained throughout adulthood, suggesting that *miR-203* is dispensable for epidermal homeostasis in the adult.

MATERIALS AND METHODS

Generation of the conditional *miR-203* knockout mouse:

A gene targeting vector was constructed that contained 11kbp homologous region surrounding the *miR-203* locus Figure 11B). LoxP sited were inserted flanking the *pre-miR-203* sequence, with a neomycin selection cassette flanked by Frt sites. The

construct was electroporated into Cy2.4 ES cells (B6(Cg)-Tyr<c2J> genetic background). Positive clones were identified by southern blot analysis using a probe complementary to the 3' end of the targeted homologous region. ES cells were injected into blastocysts and chimeras were screened based on white/black coat color selection. Upon obtaining germline transmission, the neo cassette was excised by breeding the F1 progeny to an *Actb-Flpe* line maintained on a C57BL/6J background (obtained from Jackson Labs). *miR-203*^{floxed} animals were then bred to a *EIIA-Cre* line maintained on a C57Bl/6 background (obtained from Jackson Laboratory) or a *K14-Cre* line maintained on a mixed background (obtained from E. Fuchs Laboratory), to obtain germline or conditional ablation of miR-203. The *EIIA-Cre* transgene was removed from the germline *miR-203* deleted line by backcrossing to a C57Bl/6 line and subsequently maintained on a C57Bl/6 background. Mice were bred and housed according to the guidelines of IACUC at a pathogen-free facility at the University of Colorado (Boulder, CO, USA).

Immunofluorescence, EdU and BrdU detection, and miRNA in situ hybridization:

Frozen cryostat sections (8 uM) were fixed in 4% paraformaldehyde for 10 minutes at room temperature, washed thrice with PBS, and blocked for 10 minutes using Gelatin Block (0.1% Triton X-100, 2% gelatin, 2.5% normal goat serum, 2.5% normal donkey serum, and 1% BSA in PBS). Primary antibodies, diluted in gelatin block, were then incubated overnight (See Appendix table 4 for Antibody information). Following three washes with PBS, sections were incubated with appropriate Alexa-Fluor secondary antibodies (1:2,000) for 1-2 hours at room temperature. Following three washes with PBS, sections were stained with Hoescht Dye, and mounted in Anti-fade

solution. miRNA in-situ hybridization for *miR-203* was performed on frozen sections as described in Chapter Two. EdU detection was performed following manufacturer's instructions, with the following parameters. P4 animals were IP injected with 50 ug/g EdU 4 hours prior to tissue harvest. Following EdU detection, the sections were blocked and probed with antibodies as described above. BrdU detection was performed as previously described, with the following parameters. Pregnant female mice were IP injected with 50ug/g BrdU for 2 hours prior to embryo harvest in OCT compound. Microscopy images were obtained using a Leica DM5500B microscope with either a Leica camera (brightfield) or Hamamatsu C10600-10B camera (fluorescence) and processed with the Leica image analysis suite, MetaMorph (MDS Analytical Technologies) and Fiji software. BrdU or EdU image quantifications were performed by counting the number of K5+/EdU or BrdU positive cells in randomly chosen microscopy fields. The length of the basement membrane was used to represent the length of the epidermis analyzed and was determined by tracing the basement membrane and calculating line length using Fiji software. Epidermal thickness was assessed by tracing a line tangential to the basement membrane and extending to the beginning of the stratum corneum and measuring the line length.

Primary Keratinocyte Colony Formation Assays and Adenoviral Infections:

Primary keratinocytes were isolated from neonatal animals as described in the methods for Chapter 2. Following culture for 3-4 days, cell cultures were split and plated at a clonal density of 2,000 cells per well of a 6-well plate. Following 10-14 days of culture, the cells were fixed in 4% paraformaldehyde at room temperature, followed by staining with 0.2% crystal violet in 70% ethanol overnight. Plates were subsequently washed

with tap water to destain and visualize the colonies. Colony numbers were quantified by using the Fiji plugin ColonyArea, which autothresholds each well image, followed by the Fiji Analyze Particles function with a minimal size of 25 pixels (Guzmán et al., 2014). Adenoviral infections were performed on a *miR-203*$^{fl/fl}$ keratinocyte cell line, which was established through serial passaging on a NIH-3T3 subclone J2 feeder layer, until the cultures underwent spontaneous immortalization and proliferated in the absence of a feeder layer. Ad-eGFP or Ad-CREeGFP viruses were obtained from the Iowa Gene Transfer Core and used to infect the *miR-203*$^{fl/fl}$ cell line at a MOI of 50.

Other Methods:

Small-RNA-Seq analysis, miRNA qPCR, and statistical methods were performed as described in the methods for Chapter 2.

RESULTS

Genetic deletion of *miR-203* impacts early epidermal development in mouse

A conditional KO mouse model was generated to assess the function of *miR-203* in murine skin development. *miR-203* is located in an intergenic region, 3.3 kbp downstream from the *Asp* gene and 15.3 kbp upstream of the *Kif26a* gene. The primary transcript of *miR-203* begin approximately 100nt upstream of the mature sequence and extends ~1.3 kbp downstream (Figure 12A). To generate the conditional knockout allele two loxP sites were inserted to flank the *miR-203* hairpin (Figure 12B).

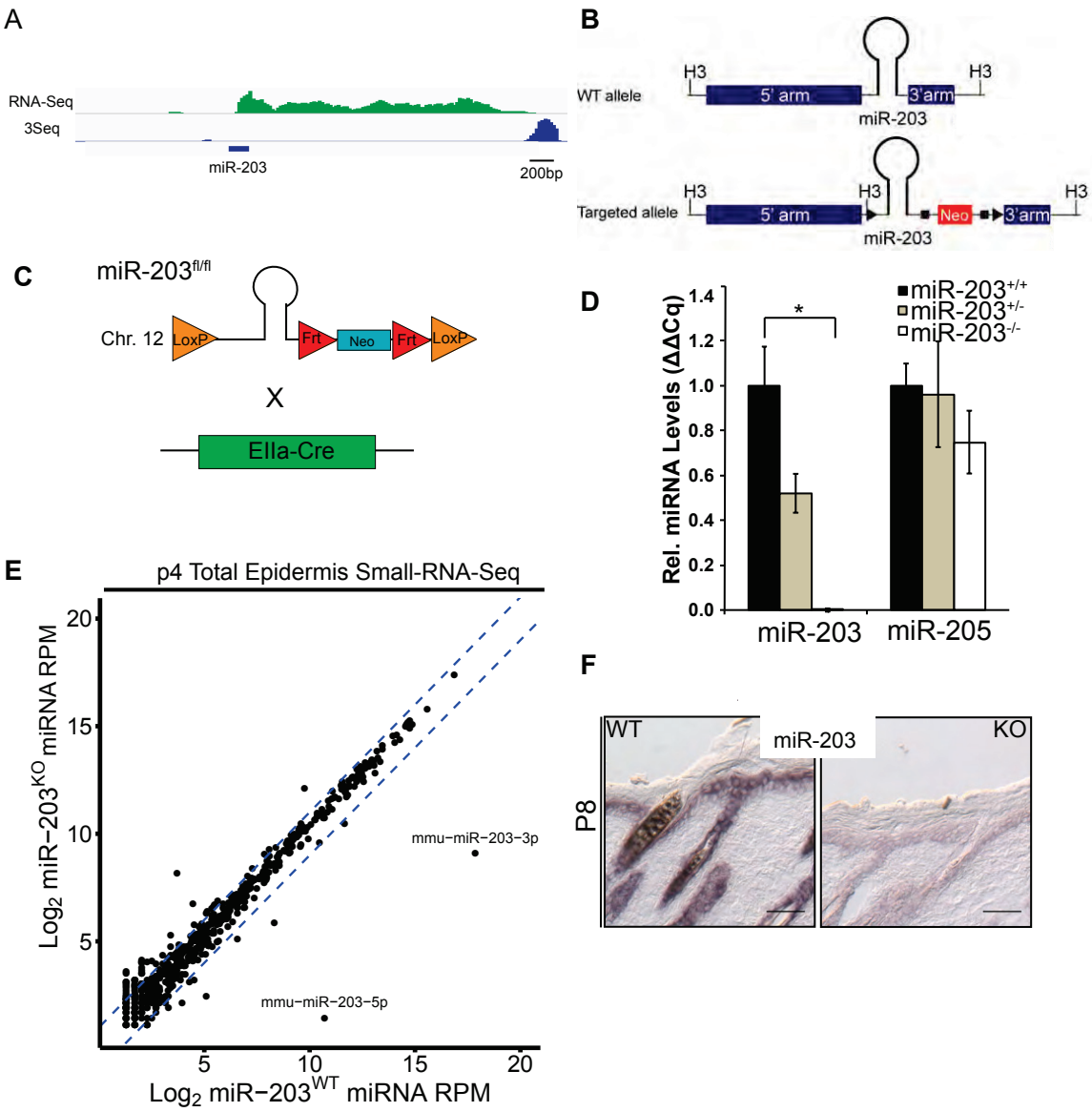

Figure 12. Generation of a miR-203 conditional knockout mouse (A) RNA-Seq and 3Seq detection of the miR-203 primary transcript (B) Schematic of the *miR-203* conditional allele. H3 = HindIII (C) Schematic of the *miR-203* KO strategy (D) qPCR validation of *miR-203* ablation from total epidermal samples. qPCR detection of mature *miR-203* in various adult mouse organ tissues. Error bars represent S.E.M from reactions performed in technical duplicate on triplicate biological samples. * = $p < 0.05$. (E) Small-RNA-seq confirmation of *miR-203* loss. Blue lines indicate two-fold change (F) miR-203 in situ confirms loss of *miR-203* in epidermal samples.

miR-203 was deleted by mating *miR-203*$^{fl/fl}$ mice with *EIIa-Cre* or *Krt14-Cre* mice, resulting in complete *miR-203* loss from all tissues or only from stratified epithelial

tissues, respectively. The expression of *miR-203* is primarily restricted to stratified epithelial tissues where the K14 promoter is active. Consistent with this observation, there are no discernible phenotypic differences between constitutive miR-203 null (*miR-203*$^{-/-}$) mice and skin-specific cKO (*K14-Cre/miR-203*$^{fl/fl}$) mice. Both strains were born at the expected mendelian ratio and showed no signs of gross developmental defects as adults (Figure 13A and data not shown). The constitutive *miR-203*$^{-/-}$ mice were maintained on the C57BL/6 background, whereas the K14-Cre/miR-203$^{fl/fl}$ mice were generated on a background that was heavily mixed. To reduce any confounding complications due to the use of a mixed genetic background the constitutive *miR-203*$^{-/-}$ maintained on the C57/Bl6 background was therefore chosen for further analysis. *miR-203* ablation was confirmed by qPCR and small-RNA-Seq on total epidermal samples (Figure 12D,E) and in situ for *miR-203* in postnatal skin (Figure 12F).

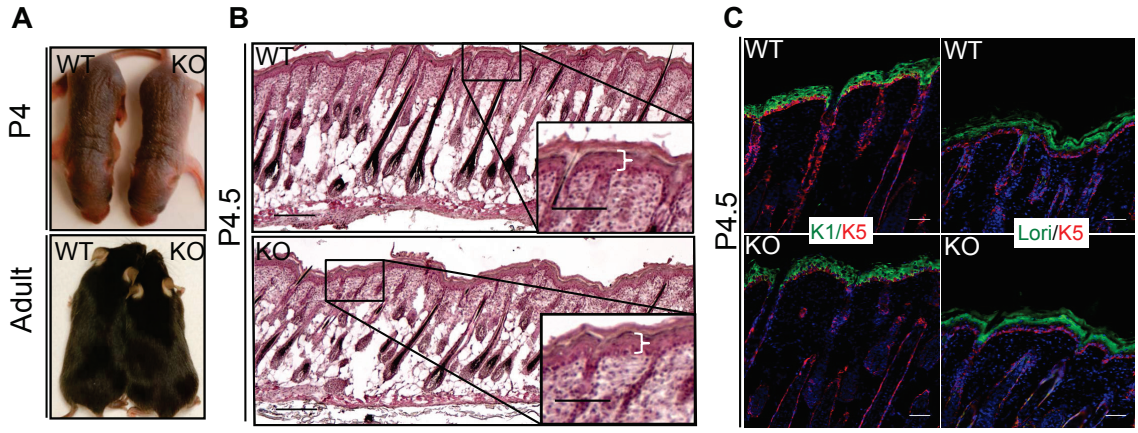

Figure 13. miR-203*$^{-/-}$ *animals develop normally and do not have epidermal differentiation defects. A) *miR-203*$^{-/-}$ animals do not display gross morphological phenotypes (B) *miR-203*$^{-/-}$ skin is histologically normal in postnatal animals. (C) Epidermal differentiation markers are normally expressed in *miR-203*$^{-/-}$ epidermis. K1 = Keratin 1, K5= Keratin 5, Lori= Loricrin. Scale bar = 100um in (B), 50 in inset (B) and (C).

At P4.5, at a timepoint when epidermal development has neared completion, *miR-203*$^{-/-}$ mice displayed a normal histological appearance of the epidermis. In addition, there was no evidence of perturbed differentiation in *miR-203*$^{-/-}$ mice based upon analysis of early and late epidermal differentiation markers, Keratin 1 and Loricrin, for the spinous and granular layers, respectively (Figure 13C). In addition the pre-cortex region of the hair follicle, where hair follicle differentiation commences, and *miR-203* is highly expressed was examined. *Lef1*, a transcriptional regulator activated by Wnt/B-catenin signaling, was normally expressed in the pre-cortex demonstrating proper induction of hair follicle differentiation (Figure 14A). Additionally, matrix cell proliferation was not expanded into the differentiated *Ae13* layers. Lastly, *Ae13* and *Ae15* immunostaining patterns were similar demonstrating proper organization of the hair cortex and cuticle; and the inner root sheath and medulla respectively (Figure 14B,C). Collectively these results demonstrate that loss of miR-203 did not impact epidermal homeostasis and hair follicle differentiation in postnatal animals.

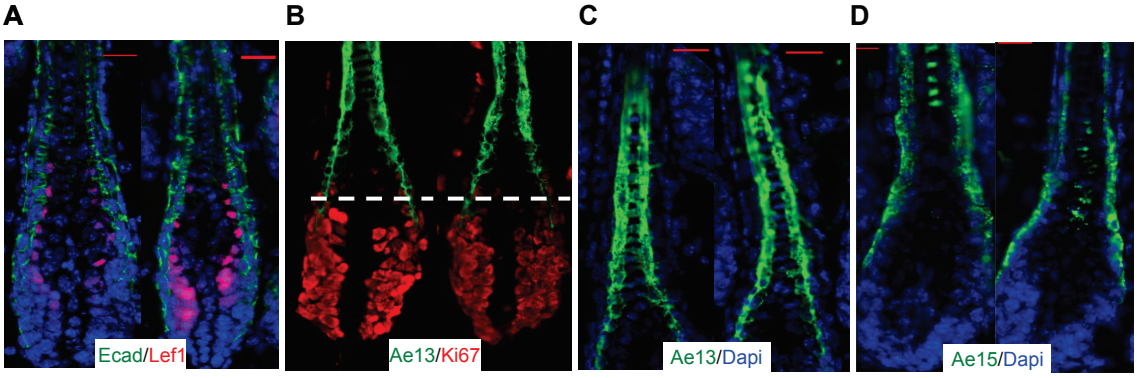

Figure 14. miR-203*$^{-/-}$ *hair follicle differentiation is normal. (A) Ecad and Lef1 immunostaining of the hair bulb in P4.5 hair follicles.Left panel is *miR-203*$^{+/+}$, right panel is *miR-203*$^{-/-}$ (B) Ae13 and Ki67 immunostaining. White-line denotes boundary between the proliferative matrix cell populations and the pre-cortex differentiating hair follicle cells. (C) *Ae13* and Dapi staining. (D) *Ae15* and Dapi staining. (Scale bar = 20um).

miR-203 begins to be expressed by E13 when the epidermis begins to stratify and reaches a maximum at p4.5 (Yi et al., 2008). I therefore reasoned that loss of *miR-203* could impact the each stratification and expansion of epidermal progenitors during embryogenesis, and be dispensable for adult epidermal homeostasis. To investigate epidermal development, samples were collected at multiple stages during embryogenesis and examined for proliferation and epidermal thickness defects. At E16, the thickness of the KO epidermis was strongly increased, compared to the WT littermates (Figure 15). Coincident with the increased thickness, we observed mildly elevated cell proliferation in the KO, as measured by BrdU incorporation, although this difference did not achieve statistical significance (p-value= 0.16) (Figure 15B). Additionally, as development progressed the *miR-203*$^{-/-}$ epidermis remained thickened (E17) but this difference waned as development progressed into postnatal stages (P4.5). Together, these results suggest that *miR-203* functions to limit cell division early during development, but is not required for homeostasis of the epidermis in postnatal stages.

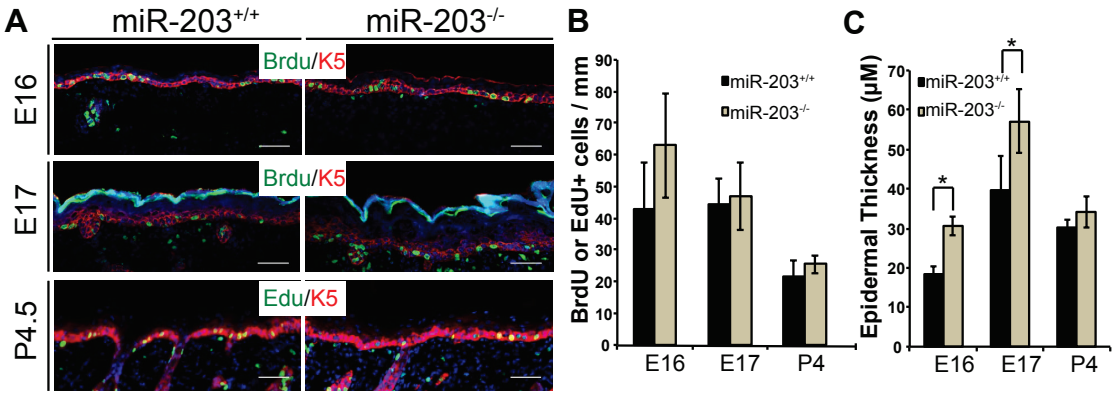

Figure 15. miR-203 ablation results in mild epidermal hyperplasia during embryonic development. A) BrdU and EdU detection in embryonic and postnatal epidermis. (B) Quantification of BrdU (E16 and E17) or EdU (P4.5) and K5 positive basal epidermal cells (C) Quantification of epidermis thickness throughout epidermal

development. * = $p < 0.05$, Student T-test two-sided. n=2 animals E16 and n=3 animals E17 and P4.5.

The impact of loss of *miR-203* upon embryonic epidermal development was later compensated for during development. However, the embryonic proliferation rate of epidermal progenitor is approximately 50% higher than that of postnatal keratinocytes, suggesting that *miR-203* may control the expansion of highly proliferative keratinocytes (Figure 15C). To test whether *miR-203* functions to restrict the expansion of highly proliferative keratinocytes, I next investigated the roles for *miR-203* in regulation of primary and established keratinocyte cell lines, respectively. *miR-203*$^{-/-}$ keratinocytes displayed ~2-fold higher colony forming capacity of, compared to the WT controls (Fig. 16A). To further confirm the ability of *miR-203* to suppress cell proliferation cell-autonomously, a *miR-203*$^{fl/fl}$ keratinocyte cell line was generated. By treating these cells with *Adeno-Cre*, *miR-203* was completely depleted within 48h of *Adeno-Cre* exposure (<1% remaining as measured by qPCR)(Figure 16B). Again there was a similar, ~2-fold higher colony forming capacity by the *Adeno-Cre* treated *miR-203*$^{fl/fl}$ cells, compared to the *Adeno-GFP* treated control cells (Figure 16B). In both cases, although there were some slightly larger clones with more cells formed by the *miR-203* null keratinocytes, the biggest differences were the significantly increased number of clones formed by the *miR-203* null cells. These results suggest that *miR-203* limits expansion of normal keratinocytes in culture, suggesting that *miR-203* regulation of cell-proliferation may be required under stress response conditions.

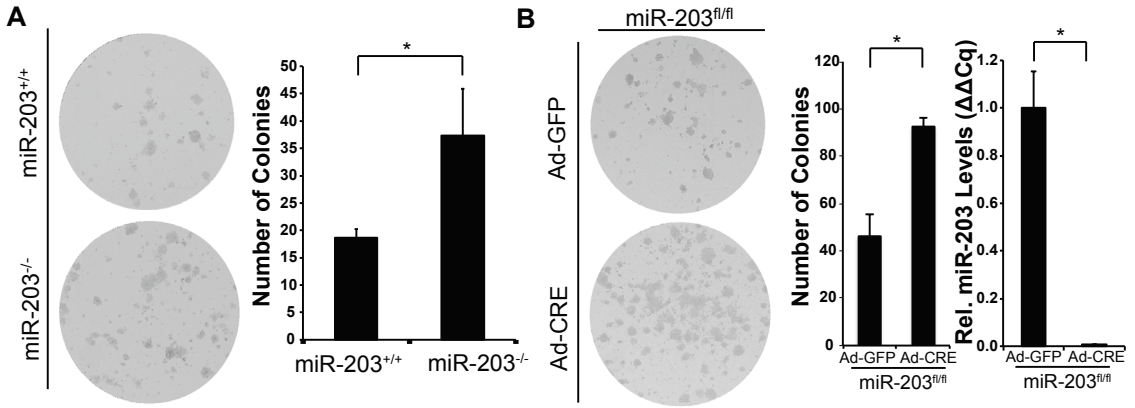

Figure 16. miR-203$^{-/-}$ keratinocytes have increased colony forming ability. (A) *miR-203$^{-/-}$* primary keratinocytes are more clonogenic than wild-type cultures. Representative of n=7 independent experiments. (B) Conditional Ablation of *miR-203* from a spontaneously immortalized *miR-203$^{fl/fl}$* culture results in increased colony-forming ability. Representative of n=3 independent experiments.

DISCUSSION

miR-203 has been long thought to play a gatekeeper role in enforcing epidermal differentiation. Through the use of a knockout mouse model we demonstrate that *miR-203* acts to suppress the expansion of early epidermal progenitor populations. However, this function is compensated for and the epidermis restores homeostasis as development progress. This finding is not entirely unexpected, in part because miRNA knockouts typically have subtle phenotypes during development often in stark contrast to the strong and dramatic developmental phenotypes often observed with miRNA transgenic models (Bejarano et al., 2012). In *C.elegans* deletion of most miRNA individually, or most miRNA families identified only as handful of miRNAs that were essential for development, with the vast majority phenotypically normal (Alvarez-Saavedra and Horvitz, 2010; Miska et al., 2007). Similarly in mammals, most miRNA knockouts do not show developmental phenotypes, although there are many miRNAs

that have not been studied (Mendell and Olson, 2012). While miRNA loss of function mouse models generally have subtle phenotypes, environmental or genetic conditions that introduce stress have uncovered a wide-range of sometimes-unexpected phenotypes. This observation has lead to speculation that miRNAs confer robustness to biological systems, by acting to buffer against noise processes driving cell state changes due to stochastic variations in mRNA metabolic processes (transcription, stability, etc) (Ebert and Sharp, 2012).

The mild developmental phenotypes observed in *miR-203*$^{-/-}$ mice, are reminiscent of the subtle epidermal phenotypes of knockouts of cell-cycle regulatory proteins. For example, individual inactivation of *p21, p27,* or *p53* in the skin does not result in epidermal proliferation phenotypes (Guinea-Viniegra et al., 2012; Missero et al., 1996). However when keratinocytes derived from these genetic backgrounds are placed into culture, these cells often demonstrate defects in growth control and modulation of keratinocyte differentiation. Importantly however overexpression of all of these factors leads to strong inhibition of the cell cycle, similar to *miR-203* overexpression in the skin. These observations suggest that the epidermis has robust redundant pathways to control proper proliferation or differentiation during development, and that the functions of many regulatory networks may be in reinforcing epidermal homeostasis during stress conditions.

Importantly, the results obtained from analyzing *miR-203* ablation in all tissues are in contrast to the previously published phenotypes observed using an antagomiR to disrupt *miR*-203 transiently in postnatal animals. I reason that this discrepancy could be due to compensation for loss of *miR-203* during development, or due to differences in

genetic background of the animals used in the experiments (C57BL/6 for *miR-203*$^{-/-}$ and CD-1 for the *miR-203* antagomiR experiment). However, these discrepancies can be addressed by utilizing an inducible CRE driver such as *K5-CreER* to determine if acute ablation of *miR-203* postnatally would recapitulate the observed defects obtained by using an antagomiR approach. It is also worth noting that the findings of many studies that originally reported miRNA loss-of-function phenotypes using antagomiRs have not been replicated with miRNA knockout mice (Sun and Lai, 2013), suggesting that the timing of a miRNA deletion may play a critical role in the phenotypes observed or additionally that antagomiR approaches may have unintended off-target effects.

The discovery that *miR-203*$^{-/-}$ mice are relatively normal, and maintain epidermal homeostasis postnatally, prompted me to investigate the role of *miR-203*$^{-/-}$ in stress responses in the skin. Given that I found *miR-203* was strongly downregulated by oncogenic *Ras* in Chapter 2, and predicted to be a tumor suppressor based on it's ability to restrict keratinocyte proliferation, I next investigated *miR-203* function in skin tumorigenesis using the mouse model developed and described in this chapter.

CHAPTER 4

ANALYSIS OF THE FUNCTION OF MIR-203 IN SKIN TUMORIGENESIS

INTRODUCTION

Defining miRNA functions in tumorigenesis has attracted considerable interest due to the possibility of identifying new pathways for therapeutic intervention. In addition to having functions in tumorigenesis, miRNA expression profiles have been proposed as novel biomarkers for tumor diagnosis (Lu et al., 2005). In mouse models of skin cancer, *miR-21* and *miR-125b* have been demonstrated to promote tumor development, but a miRNA with tumor suppressor capacities has not been identified to date. Based on the finding that miR-203 was strongly downregulated by oncogenic *Ras,* and that *miR-203* loss of function promotes keratinocyte expansion in culture, similar to many tumor suppressors, I was promoted to investigate a function for *miR-203* in skin tumorigenesis.

Many lines of evidence suggest that *miR-203* functions as a miRNA tumor suppressor gene. *miR-203* expression is reduced in many human cancers through diverse mechanisms. *miR-203* downregulation has been reported in prostate, liver, lung, oral, head and neck, cervical, leukemia and other cancers (Bueno et al., 2008; Furuta et al., 2010; Kozaki et al., 2008; Viticchiè et al., 2011). In a meta-analysis of miRNA expression profiles from 51 cancer types and 50 normal tissue controls, representing over 3000 human samples, *miR*-203 was the most downregulated microRNA found in solid cancers (Volinia et al., 2010). The most commonly described mechanism for *miR-203* downregulation in cancers is suppression by oncogenic or pro-metastatic pathways.

For example, the EMT activating factors, *Zeb1* and *Snai1/2*, can stimulate EMT, and in the process strongly downregulate *miR-203* (Taube et al., 2013; Wellner et al., 2009). In addition, activation of growth factor signaling, via treatment of keratinocytes with keratinocyte growth factor or epidermal growth factor, results in dose-dependent suppression of *miR-203* (Sonkoly et al., 2010). Additionally, the human papilloma viral oncoproteins *E6* and *E7*, both suppress *miR-203* in cervical cancer cell lines (McKenna et al., 2010; Melar-New and Laimins, 2010). Hypermethylation of the *miR-203* promoter has also been observed in oral and hepatocellular carcinoma cell lines (Furuta et al., 2010; Kozaki et al., 2008). Lastly, there are examples of loss of the *miR-203* locus in leukemias and endometrial cancers, although the functional significances of these observations to human cancers remain unclear (Bueno et al., 2008; The Australian National Endometrial Cancer Study Group et al., 2015). *miR-203* is expressed at it's highest levels in stratified epithelial tissue, however the pattern of *miR-203* downregulation in diverse cancer types, suggests that even low levels of *miR-203* are selected against in tumors (Landgraf et al., 2007; Sonkoly et al., 2007).

Since the initial finding that *miR-203* suppressed keratinocyte proliferation, many groups have speculated that *miR-203* functions as a tumor suppressor miRNA. Initial investigation into a tumor suppressor role demonstrated that *miR-203* was induced by UVC irradiation and suppressed the cell proliferation of head and neck squamous cell carcinoma cell lines and normal human keratinocytes (Lena et al., 2008). In the intervening seven years, numerous reports have demonstrated that ectopic expression of *miR-203* in diverse human neoplastic and normal cell lines results in suppression of the cell-cycle and in some cases increased apoptosis (Li et al., 2011; Viticchiè et al.,

2011; Zhang et al., 2011b). Of particular note, xenograft models have additionally shown that overexpression of *miR-203* results in reduced tumor burden and metastasis (Ding et al., 2013; Garofalo et al., 2012; Zhang et al., 2014a).. The relatively low-expression level of miR-203 in established cancer cell lines minimizes the utility of loss-of-function approaches to determine miR-203s function in human tumorigenesis. Nevertheless, a function for miR-203 in suppressing metastasis came from studies in which *miR-203* was suppressed in a head and neck cancer cell line with relatively higher levels of *miR-203*. Inhibition of *miR-203* enhanced lung metastasis number and size and enhanced sphere-forming capacity upon serial passage, nicely demonstrating complementary phenotypes to *miR-203* overexpression (Benaich et al., 2014). Taken together the current experimental evidence strongly demonstrates that high-levels of miR-203 antagonize tumor cell proliferation, burden and metastasis in xenograft models. These results provide insight into possible therapeutic potential of miR-203 based interventions in established human cancers.

miR-203 is suppressed by many human oncogenes which can function as driver mutations and therefore is silenced at very early stages in tumorigenesis. These observations suggest that *miR-203* may act to suppress tumor initiation, in addition to suppressing later development and metastasis. However, the importance of *miR-203* for the initiation of tumorigenesis and early development are difficult to resolve by the study of established human cancer cell lines, which often are used to model end-stage processes in tumorigenesis.

In order to define the importance of *miR-203* during multiple stages of tumorigenesis, I employed the two-stage mouse skin chemical carcinogenesis protocol.

Loss of *miR-203* results in a higher tumor burden compared to wild-type counterparts. While *miR-203* loss of function increased the number of tumors, the tumor sizes were similar between wild type and knockouts, suggesting that *miR-203* impacted tumor initiation. Additionally, *miR-203*$^{-/-}$ tumors contained *HRas*^{Q61L} mutations at the expected frequency suggesting that *miR-203* ablation did not substitute for oncogenic *Ras* activity. Moreover, miR-203$^{-/-}$ keratinocytes transduced with oncogenic *Ras* were more clonogenic in culture upon serial passage. Lastly, restoration of *miR-203* in *HRas*^{G12V} transduced keratinocytes potently suppressed their cell-cycle progression and clonogenicity. Taken together our results demonstrate that *miR-203* loss sensitizes mice to skin tumorigenesis and promotes the clonogenicity of transformed keratinocytes, providing further evidence that *miR-203* is a tumor suppressive miRNA in the skin.

MATERIALS AND METHODS

DMBA/TPA carcinogenesis:

DMBA/TPA carcinogenesis was performed as described previously (Abel et al., 2009). The backskin of 7-9 week old mice was shaved and 48 hours later the backskin was painted with a single dose of 25 ug of DMBA in 200ul of acetone. Two weeks following DMBA treatment the mice began receiving bi-weekly treatments of 4 ug of TPA in 200ul of acetone. The number of palpable tumors of at least 1 mm in diameter, persisting for at least two weeks, was recorded weekly. Tumor diameters were measured using a digital caliper. Following 21 weeks of TPA treatment, mice were euthanized and tumors were collected for *HRas*^{Q61l} genotyping, OCT embedding, and paraffin embedding.

HRas^{Q61L} *genotyping of DMBA/TPA tumors:*

Tumor DNA was isolated by incubating tumor tissue in a DNA Lysis Buffer (400mM NaCl, 0.1% SDS, 1mM EDTA, 1ug/ml Proteinase K) at 55° C for 4 hours. Lysates were then vortexed and lightly centrifuged to liberate DNA from the partially-digest tumor tissue. The supernatant was then removed and subject to phenol-chloroform extraction, followed by isopropanol precipitation. Isolated DNA pellets were then resuspended in TE buffer and quantified by UV spectrophotometry (10mM Tris pH 8.0, 1 mM EDTA). The *HRas* gene was PCR amplified using primers that flank exon 2. Following amplification, the PCR reactions were digested with 5 units of XbaI restriction enzyme at 37° C. The reaction products were then resolved and visualized on a 3% agarose gel. DNA isolated from the tails of animals in the DMBA/TPA experiment was treated in parallel as a negative control for detection of the $HRAS^{Q61L}$ mutation. Primer sequences are shown in Appendix Table 1.

Colony formation assays, Edu flow cytometry, qPCR, and Immunostaining:

Colony formation assays were performed as described in Chapter 3 with the following modifications. To perform the serial colony formation assays, after the first plating for the colony formation assay, one well for each sample (always the right most well of the cell culture plate to avoid selection-bias) was trypsinzed to harvest the keratinocytes. The cells were counted then replated at 2,000 cells per well. This procedure was then repeated for the third passage of the assay. EdU flow cytometry was performed using the Click-IT Plus ™ kit following the manufacturers instruction (Life Technologies). Keratinocytes were pulsed with 10uM EdU for 1 hour before harvesting for flow cytometry. qPCR for *miR-203* and immunostaining was performed as described in Chapter 2.

Statistical Analysis:

Statistical analysis was performed using either R or Microsoft Excel. Unpaired two-sided student t-tests were used to assess statistical significance unless indicated otherwise in the figure legends. Non-parametric Whitney-Mann U-Tests were used to assess significance for the tumor multiplicity measurements (Abel et al., 2009).

RESULTS

miR-203 ablation sensitizes skin to chemical carcinogenesis

Results presented in Chapter 2 demonstrated that loss of *miR-203* is an early event in the initiation and development of both mouse and human skin SCCs. Furthermore, genetic deletion of *miR-203* confers ~2-fold higher colony forming ability on primary keratinocytes. Because oncogenic *HRas* is a potent driver for tumorigenesis in the skin and the observations from the small-RNA-seq data that revealed strong repression of *miR-203* by $HRas^{G12V}$, I was prompted to investigate whether the loss of *miR-203* plays a role in skin carcinogenesis.

WT and *miR-203* null littermates were subject to a two-stage chemical (DMBA/TPA) carcinogenesis regimen (Figure 17A-C). The chemical carcinogenesis experiments were terminated at week 21 when tumor burden had plateaued and tumor sizes were beginning to regress. Because the mice were generated in the C57BL/6 background and these mice are known to be resistant to two-stage chemical carcinogenesis, all tumors generated were papillomas, with no evidence for malignant

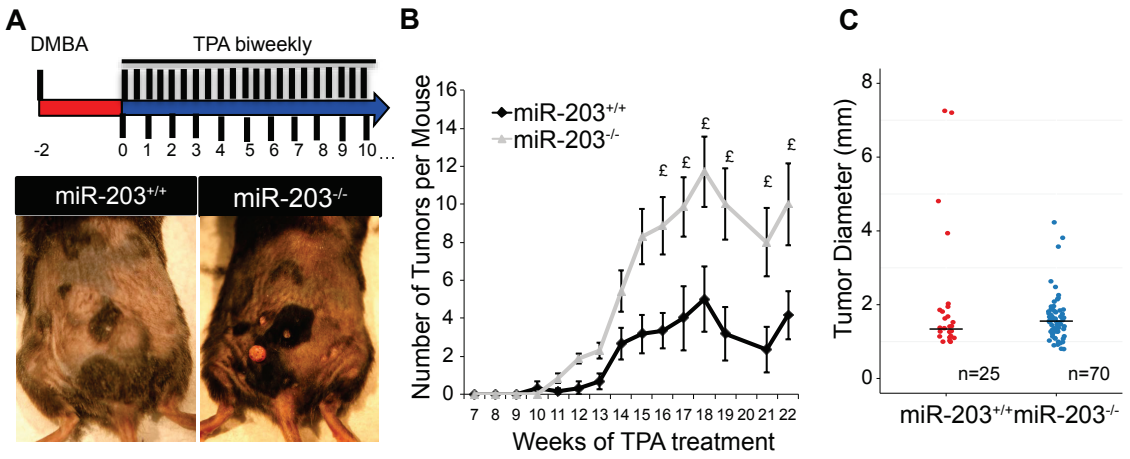

Figure 17. miR-203 ablation sensitizes mice to DMBA/TPA chemical skin carcinogenesis (A) Schematic of DMBA/TPA dosing schedule and representative pictures of tumor burdens in mice at week 17. (B) *miR-203* loss results in increased tumor multiplicity (£ = p< 0.05, Whitney-Mann Rank Test, one-sided). (C) Tumor diameters at week 18. Median bar displayed. p > 0.05 Student T-test, one-sided.

conversion to squamous cell carcinomas consistent with documented observations (Abel et al., 2009). To reveal a role for *miR-203* tumor formation I examined the temporal and numeric characteristics of the tumor development. At the point of a maximal tumor response, *miR-203* null animals developed ~2.5-fold more tumors, when compared to WT control animals (Figure 17B). However, measurement of tumor sizes at week 17 showed no statistically significant difference in tumor sizes between genotypes although *miR-203* null animals were more susceptible to tumor formation (Figure 17C). These results demonstrate that loss of *miR-203* does not alter the tumor type distribution or growth properties of the papillomas, but instead suggest that *miR-203* impacts the process of tumor initiation.

Traditionally about 90% of DMBA/TPA produced tumors contain activating $HRas^{Q61L}$ mutations (Quintanilla et al., 1986). In order to rule out the possibility that *miR-203* loss bypassed oncogenic *Ras* activation to promote tumorigenesis, I isolated DNA

and genotyped the *HRas* allele in a subset of papillomas. The Q61L mutation results from an A to T transversion, in *HRas* gene. This specific mutation can be identified by the generation of a novel *XbaI* restriction site by the mutation. PCR amplification of exon two of the *HRas* gene followed by restriction digest reveals the presence of the mutated allele. I profiled the mutation frequency in 5 and 14 papillomas from wild type and null papillomas respectively and found a similar mutation frequency of 80% and 85.7% for wild type and null papillomas respectively ($p > 0.05$, chi squared test)(Figure 18A,B). These results demonstrate that *miR-203* null papillomas did not form due to bypassing the canonical initiating mutation, $HRas^{Q61L}$.

A

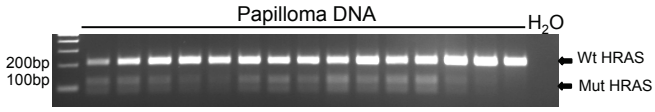

B

	Number of Tumors with $HRas^{Q61L}$ mutations	Percentage of tumors with $HRas^{Q61L}$ mutations
miR-203$^{+/+}$	4/5	80%
miR-203$^{-/-}$	12/14	85.7%

Figure 18. The $HRas^{Q61L}$ mutation is common in both miR-203$^{+/+}$ and miR-203$^{-/-}$ tumors (A) Representative end-point PCR followed by *XbaI* digestion. The $HRas^{Q61L}$ allele 120bp and 87bp, wild-type 207bp (B) Table with quantification of genotyping results. non-significant $p > 0.05$, Chi-Squared Test.

I next performed histologic examination of the papillomas. Hematoxylin and Eosin staining revealed that the papillomas produced had a similar morphology, displaying exophytic lesions with evidence for squamous differentiation (Figure 19A). Additionally, assessment of proliferation (*Ki67*) and differentiation markers (*K1*, *Lori*) revealed similar dynamics between *miR-203*$^{+/+}$ and *miR-203*$^{-/-}$ tumors (Figure 19A-C), suggesting that loss of *miR-203* did not impact tumor growth or differentiation, consistent with the similar tumor sizes observed for wild type and knockout tumors.

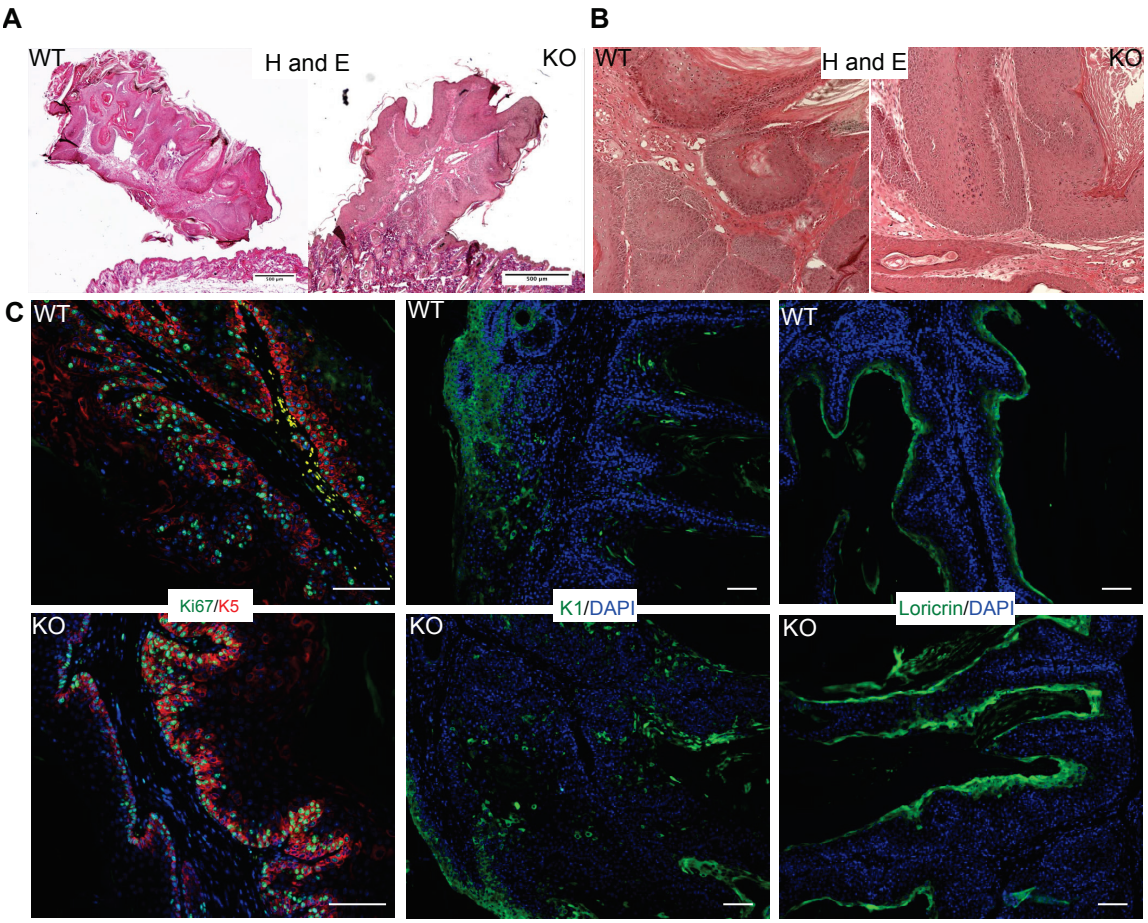

Figure 19. miR-203$^{-/-}$ tumors are histologically papillomas, and display similar proliferation and differentiation dynamics to wild-type papillomas (A) Hematoxylin and Eosin staining of *miR-203*$^{+/+}$ and *miR-203*$^{-/-}$ papilllomas. Scale bar = 500um (B) Hematoxylin and Eosin staining of *miR-203*$^{+/+}$ and *miR-203*$^{-/-}$ papilllomas, Scale Bar =50um. (C) *Ki67*, Keratin 1 (*K1*), and Loricrin (*Lori*) immunostaining.

<u>miR-203 represses the clonogenicity of oncogenic *HRas* transformed cells in vitro:</u>

To further probe *miR-203*'s role in tumorigenesis, I infected *miR-203* WT and null primary keratinocytes with *HRas*^{G12V} or a control virus. At the passage 1, the loss of *miR-203* led to ~40% increase in colony forming capacity (Figure 20A). However when I passaged the *HRas*^{G12V} transduced cells, I observed a gradual reduction in the number of colonies that were formed by both the WT and null cells (Figure 20A). This was likely due to senescence that primary keratinocytes undergo during extended culture without

feeder cells. However, in contrast to the WT cells that generally formed smaller colonies in subsequent passages and, by passage 3, failed to generate many productive colonies, the *miR-203* null cells generated more clones at each passage (Figure 20A). Collectively, the results from this serial passage assay support the notion that loss of miR-203 potentiated keratinocyte growth upon oncogenic *HRas* induction.

To further characterize the ability of *miR-203* to suppress the growth of oncogenic *HRas* transformed cells, I used the previously established *K14-rtTA/pTRE2-miR-203* inducible model (Jackson et al., 2013). After infecting the inducible keratinocytes with either the *pBabe* vector control or *pBabe-HRas*^{G12V}, I treated the cells with 5ug/ml doxycycline to induce ~4-7-fold increase in *miR-203* expression, a physiologically relevant level of *miR-203* typically observed during epidermal differentiation (Figure 20B). Introduction of *miR-203* resulted in suppression of keratinocyte proliferation and colony formation ability (Figure 20B,C,D), as noted previously (Benaich et al., 2014; Jackson et al., 2013; Yi et al., 2008). Furthermore, whereas oncogenic *HRas* enhanced S-phase entry, short-term (~24h) induction of *miR-203* abolished the gain of S-phase entry (Figure 20D). Over a longer term, induction of *miR-203* severely compromised the colony forming capacity of the transduced cells (Figure 20C). However, there was no evidence for enhanced apoptosis caused by *miR-203*, as measured by the absence of sub-G1 keratinocytes. Taken together, these results suggest that the loss of *miR-203* contributes to the expansion of primary keratinocytes harboring the oncogenic HRas mutation and that high levels of *miR-203* can effectively suppress the growth of these cells.

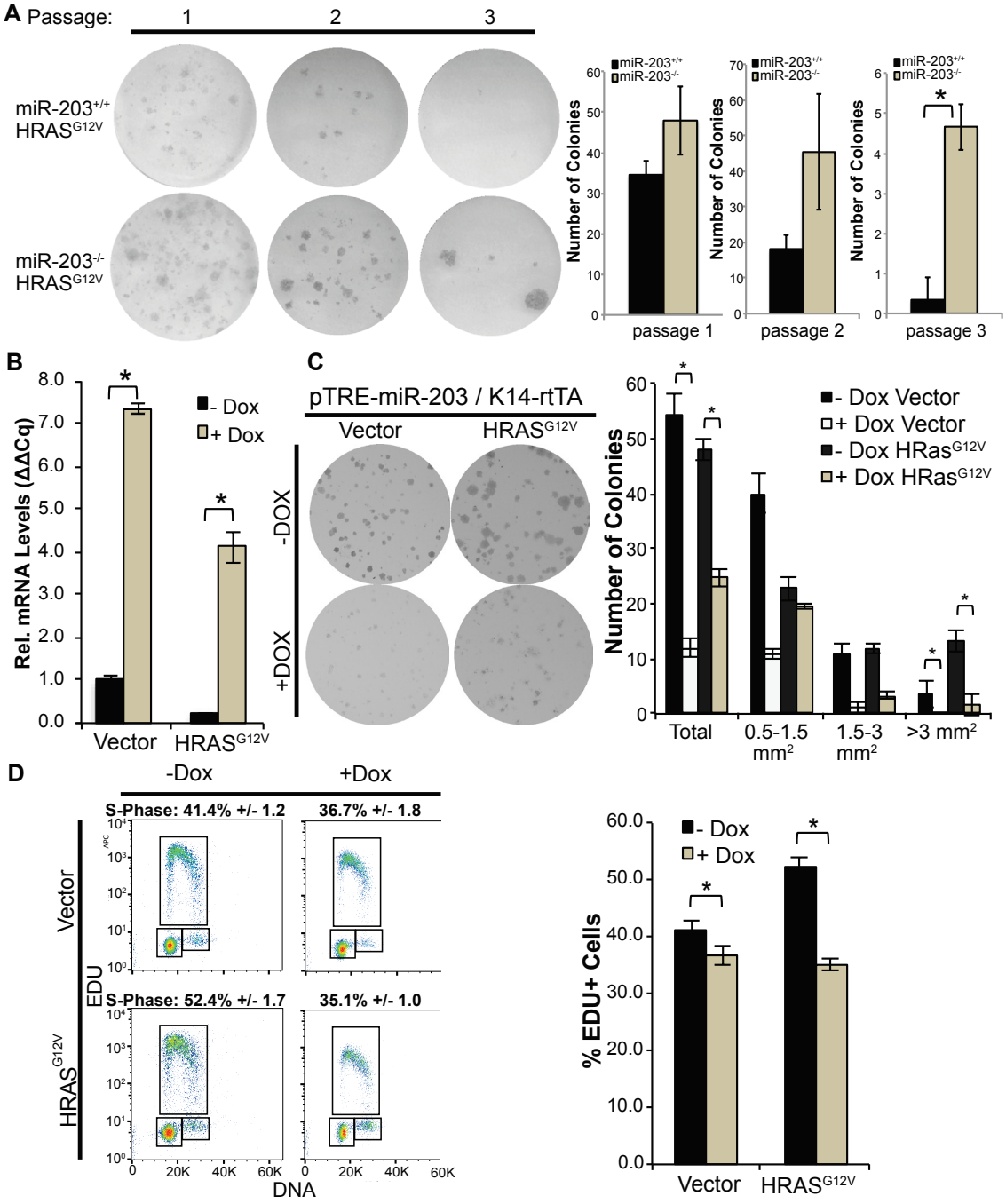

Figure 20. miR-203 antagonizes HRas^{G12V} driven keratinocyte proliferation. (A) *HRas^{G12V}* transduced *miR-203$^{-/-}$* primary cultures are more clonogenic upon serial passage than wild-type controls (representative of n=2 independent experiments, mean +/- standard deviation displayed. * = p-value <0.05, Student T-Test two-sided) (B) qPCR of *miR-203* induction upon addition of doxycycline. (mean +/- SEM displayed, n=3 biological replicates) (C) Restoration of *miR-203* using a doxycycline inducible

transgene, results in suppression of colony formation ability in *HRas*^{G12V} transduced and control keratinocytes. *miR-203* was induced with doxycycline (5ug/ml) 24 hours after plating (representative of n=3 independent experiments, mean +/- standard deviation displayed, * = p-value = <0.05). (D) *miR-203* restoration suppresses *HRas*^{G12V} driven s-phase entry. *miR-203* was induced for 24 hours prior to harvesting for flow cytometry. (n=3, mean +/- standard deviation displayed, * = p-value = <0.05).

DISCUSSION

The data presented in this chapter provides strong evidence that *miR-203* loss contributes to skin cancer in a mouse model. This data represents the first demonstration of a miRNA in the skin with tumor suppressor activity *in vivo.* Additionally the results presented suggest that a key function of this miRNA is restricting tumorigenesis at the very early stages of tumor initiation.

The finding that miR-203 loss sensitizes mice to chemical carcinogenesis was a somewhat surprising result for the following reason. miR-203 levels are strongly suppressed by oncogenic *Ras*, the initiating mutation for the tumor development. The prediction was that loss of *miR-203* via genetic ablation would have minimal impact, as the loss of *miR-203* is already accomplished by activation of oncogenic *Ras* (Figure 8A). The conceptual scenario is analogous to the function of *p53* in squamous cancers initiated by HPV infection. The HPV oncogene *E6* directly inactivates *p53*, and consequently in HPV+ tumors, p*53* mutations are unnecessary to inactive *p53* function and are rarely observed (Lawrence et al., 2015). However, the results presented here suggest that the relatively low remaining *miR-203* in a *Ras* transformed keratinocyte have regulatory functions that contribute to suppressing tumor development.

In the benign papilloma stage, keratinocyte differentiation is strongly maintained, and is only lost during later progression to malignant SCC. As such it is thought that

keratinocyte differentiation acts to restrict the tumor growth, a hypothesis supported by recent clonal analysis of papillomas and SCC formed by DMBA/TPA treatment (Driessens et al., 2012). Given that *miR-203* remains expressed in the differentiated regions of DMBA/TPA produced papillomas, it is possible that *miR-203* loss alters the differentiation potential of the *Ras* initiated keratinocytes, skewing the differentiation capacity more towards self-renewal. The results presented in this chapter support this suggestion as *Ras* initiated miR-203$^{-/-}$ keratinocytes have increased clonogenicity *in vitro.* However, demonstrating that *miR-203* loss increases the number of tumor-initating keratinocytes *in vivo* is beyond the scope of this study, but could be assessed by determining the frequency of tumor initiating keratinocytes using limited cell dilution and grafting in immunocompromised mice (Boumahdi et al., 2014).

Another key question that remains is how loss of *miR-203* would impact the proliferative keratinocyte populations to promote tumorigenesis, given that *miR-203* is most highly expressed in the suprabasal differentiated keratinocytes. One possibility is that loss of *miR-203* potentiates the ability of suprabasal keratinocytes to initiate tumor development. Hair follicle stem cells and epidermal progenitors are the primary cell types thought to be responsible for tumor development in multi-stage chemical skin carcinogenesis. However suprabasal keratinocyte populations are also competent to initiate tumorigenesis. Overexpression of oncogenic *HRas* in suprabasal keratinocytes using the keratin 10 promoter, a marker of differentiation committed keratinocytes, results in spontaneous papilloma development, with more pronounced papilloma development in sites of mechanical wounding (Bailleul et al., 1990). In another example, the alpha6/beta4 integrins were transgenically overexpressed in the suprabasal layers,

which resulted in dramatically enhanced papilloma development and malignant conversion to SCC after DMBA/TPA treatment (Owens, 2003). These results demonstrate that changes in suprabasal gene expression can modify the tumor phenotype. Lastly, recent experiments using endogenously expressed knock-in allele of oncogenic *KRas*^{G12D} demonstrated that targeting the suprabasal differentiated keratinocytes with a *Involucrin-CREER* resulted in papilloma development 2-4 months after single tamoxifen injections (Lapouge et al., 2011). These results are especially intriguing, as they suggest that a subpopulation of suprabasal keratinocyte are able to self-renew, resist differentiation, and ultimately initiate tumor development upon receiving an oncogenic *Ras* mutation, without requiring sustained transgenic *Ras* expression in all suprabasal cells. In order to determine if *miR-203* loss enhances suprabasal keratinocyte tumor formatting capacity, it would be necessary to develop sophisticated lineage-tracing mouse models to track the fate of suprabasal keratinocytes after tumor initiation. Following the fate of suprabasal *Ras* initiated keratinocytes during chemical carcinogenesis would also be of more general interest, as this cell population is much more prominent in human epidermis and may play a more important role in human skin cancers.

The results presented here demonstrate a role for *miR-203* in the early stages of skin tumorigenesis, but we were unable to assess the consequences of *miR-203* loss o n malignant progression. The *miR-203* conditional allele was generated on the C57BL/6 strain, which is highly resistant to tumor formation, compared to other strains such as FVB or CD-1 (Abel et al., 2009). Only about 5-10% of papillomas typical undergo malignant conversion to SCCs, therefore due to the small numbers of papillomas

formed we were unable to determine if the loss of *miR-203* also promoted malignant progression. Of note however, a few studies have implicated *miR-203* in regulating epithelial-to-mesenchymal (EMT) transitions in human cancer cell lines. EMT is observed in highly malignant SCCs, known as spindle cell carcinomas that form upon combined deletion of a strong tumor-suppressor such as $p19^{ARF}$ with DMBA/TPA. It is intriguing to speculate that loss of *miR-203* could also impact conversion to EMT, as miR-203 is known to be suppressed by EMT promoting factors *Zeb1, Snai1/2,* and *Tgf-Beta* and negatively regulates *Snai1/2* levels (Moes et al., 2012; Taube et al., 2013; Wellner et al., 2009; Zhang et al., 2011b). Studying the role of *miR-203* could be studied best with use of a genetic model of SCC, such as the combined knock-in $KRas^{G12D}/p53^{cko}$ mice which readily form malignant SCCs.

Collectively, the results presented in this chapter present experimental evidence for an important role of *miR-203* in repressing skin tumorigenesis. Additionally, these results further support the findings obtained from studies of established human SCC cell lines, which also demonstrate that *miR-203* has tumor suppressive properties in human cancers.

CHAPTER 5

IDENTIFICATION OF MIR-203 TARGETS VIA GENOME-WIDE EXPRESSION PROFILING AND AGO2-HITS-CLIP.

INTRODUCTION

A major challenge in studying miRNA is identifying *bona fide* target genes from large-scale genome-wide studies. miRNAs are predicted to target hundreds of transcripts in human cells, and select targets through the use of 6-8 nucleotide motifs, making high confidence identification of miRNA targets challenging (Witkos et al., 2011). Furthermore, miRNA targeting typically results in very minor suppression of targeted transcripts, on the order of 20-40% downregulation in many cases (Guo et al., 2010). miRNA regulation therefore likely functions primarily through regulation of a network of targets, whose net downregulation elicit a biological response. Therefore determining the relevant targets of a microRNA for a given cellular processes requires identifying not just individual targets, but entire networks of target genes.

In the previous chapters I have provided evidence that *miR-203* restricts skin tumorigenesis in part through suppression of cell proliferation. To provide insights to the mechanism by which *miR-203* restricts tumorigenesis, I sought to identify direct *miR-203* targets in keratinocytes. In this Chapter I will introduce the molecular mechanisms of miRNA target repression, the sequence motifs responsible for recruiting miRNAs targeting, and the approaches used to identify targets from genome-wide expression data.

miRNA identify target transcripts through basepairing to the target transcript. The miRNA provides targeting specificity to the RNA Induced Silencing Complex (RISC)

directing the complex to target messages. The outcome of miRNA targeting is principally determined by the amount of the basepairing between the miRNA and the targeted transcript. Extensive or complete basepairing can result in cleavage of the target mRNA between position 10 and 11 on the targeting miRNA (Hutvagner and Simard, 2008). Cleavage can only occur if the miRNA is loaded into an *Ago2* protein, which is competent for RNA cleavage activity, in contrast to the other mammalian *Ago* proteins, *Ago1*, *Ago3*, and *Ago4* (Meister et al., 2004). However such cleavage events rarely occur in canonical miRNA targeting events in mammals as most miRNA binding sites do not have extensive complementarity to the miRNA, in contrast to miRNA binding sites in plants, which have near perfect complementarity (Jones-Rhoades and Bartel, 2004). Instead of mRNA cleavage, the imperfect basepairing of the miRNA and the targeted mRNA results in mRNA destabilization and translational repression of the message.

The molecular mechanisms by which miRNAs repress their target has been extensive studied and remain controversial to this day (Eichhorn et al., 2014). Two general mechanisms have been proposed, mRNA destabilization through deadenylation, and repression of translation through blocking initiation. Genome-wide expression analyses have demonstrated that upon modulation of a miRNA, changes in target mRNA abundance are frequently observed prior to modulation of ribosome occupancy on the transcript, supporting a role for mRNA destabilization as the primary mechanism for miRNA targeting (Eichhorn et al., 2014; Guo et al., 2010). However, in some contexts, such as during zebrafish embryonic development, translational inhibition predominates as the initiating event, with decay secondary to translational repression

(Bazzini et al., 2012; Subtelny et al., 2014). Additionally, in many single gene studies, translational repression is observed with only minor or undetectable changes in mRNA abundance (Ding and Grobhans, 2009). The *Gw182* proteins, or *TNRC6a/b/c* in mammals, play critical roles in both mRNA destabilization and repression of translation. *GW182* is part of the RISC, associates with *Ago* proteins directly through a Glycine-Tryptophan (GW) repeat domain, and is required for miRNA targeting functions (Tritschler et al., 2010). *Gw182* directly binds to the cytoplasmic Poly-A Binding Protein (*Pabpc1*), titrating *Pabpc1* away from *Eif4g*, which is hypothesized to decrease target mRNA circularization resulting in reduced translation initiation (Zekri et al., 2009). Additionally, *Gw182* also directly binds components of the *Ccr4/Not1* deadenylase complex, which promotes targeted message deadenylation but also contributes to repression of translation in some contexts (Chekulaeva et al., 2011). It is therefore likely that modulation of *Gw182* activities is critical for determining the relative importance of initial mRNA deadenylation or inhibition of target mRNA circularization and translation initiation. In addition these findings further suggest that the miRNA targeting mechanism is also likely heavily influenced by the suite of other RNA-binding proteins bound to a targeted mRNA (Schwamborn et al., 2009).

The sequence motif responsible for miRNA targeting is the 5’ region of the miRNA known as the seed sequence. The pioneering study of miRNA noted that the *C.elegans lin-4* miRNA was complementary to 3’UTR sequences in the targeted *lin-14* transcript, a singular example that two decades later is still exemplary of how miRNAs targeting is thought to occur (Lee et al., 1993). Although miRNA targeting events have been described in non-3’UTR sequences, including coding sequences (CDS) and

5’UTRs, the functional impact of these interactions on miRNA targeting is minimal compared to miRNA targeting in the 3’UTR region (Bartel, 2009). However there are cases where a high number of CDS miRNA target sites, or miRNA binding sites in poorly translated regions with rare codons, in which CDS targeting can be effective (Gu et al., 2009; Schnall-Levin et al., 2011).

In the early 2000s, the seed region was identified as the critical determinant of microRNA targeting, based on computational predication, preferential evolutionary conservation, and experimental evidence (Lai, 2002; Lewis et al., 2003). The seed sequence has since become the primary predictor for identifying miRNA target sites in transcript 3’UTRs. The minimal miRNA seed region is composed of a hexamer sequence of nucleotides from position 2-7 from the 5’ end of the microRNA. The strength of the seed sequence for predicting targeting is further increased by additional base-pairing to include 7mer and 8mer sequences, with most functional miRNA binding sites having a minimal 7mer match or a 6mer match with a 3’ terminal A nucleotide (Bartel, 2009). There exist additional classes of miRNA targeting motifs, include central pairing, 3’ compensatory sites, and mismatched seed sites however these targeting interactions have limited impact on targeted message abundance or translation (Chi et al., 2012; Grimson et al., 2007; Shin et al., 2010). Broadly speaking the predictive power of a 3’UTR seed match can be ranked as 8mer > 7mer > 7mer> 6mer, with 8mer sites being the most predictive for regulation.

The identification of the seed sequence prompted the development of numerous computation approaches to predict miRNA binding sites genome-wide. These methods generally employ some combination of seed match identification, strength of miRNA

hybridization, local 3'UTR context, and sequence conservation (Witkos et al., 2011). Although the computational algorithms have aided miRNA target identification, the poor degree of overlap between the predictions made between different software programs demonstrate a high rate of false positives and false negatives predictions (Alexiou et al., 2009). The commonly employed approach of combining predictions from multiple algorithms can decrease the false positive rate, but will result in missing many targeting events and detecting only the most confidently predicted targets. Due to these complications, experimental methods for identifying miRNA targets are necessary to identify miRNA targeting events. By combining computational predictions with gene expression datasets in which a miRNA has been experimentally overexpressed or inhibited can further increase the ability to detect *bona fide* targets (Jackson et al., 2013). However these approaches lead to an overly reductive view of miRNA targeting in which only a handful of targets are identified and taken as representative of the true suite of miRNA targets relevant for a particular miRNAs function. The recent development and expansion of high-throughput methods for identifying RNA-binding protein targets, and the increased accessibility of transcriptome profiling methods now provide more unbiased approaches to identify miRNA targets with the goal of identifying entire networks of miRNA targets.

Techniques to identify the RNA targets of RNA-binding proteins (RBPs) genome-wide have been developed in recent years. By using microarray or RNA-Seq techniques, the RNA bound to RBPs can be recovered from immunoprecipitated complexes using RIP-Chip or RIP-Seq approaches. These approaches have provided insights into the mRNA targets under regulation of a particular RBP, but lack the

sequence resolution to define exact RBP binding site in the targeted transcripts. Additionally, for RBPs such as *Ago*, which is predicated to target a third of all mRNAs, this caveat severely limits the utility of RIP-Seq approaches to identify targets for an individual miRNA as multiple unique miRNAs can target a transcript. These limitations were overcome in 2008 with the development of the HIgh-Throughput Sequencing of RNA isolated by CrossLinking ImmunoPrecipitation (HITS-CLIP) method (Licatalosi et al., 2008; Wang et al., 2009). Briefly, intact cells or tissues are irradiated with high energy 254nm UVC light resulting in a zero-length irreversible cross link between amino acids and nucleic acids (Greenberg, 1979). The nucleotide and amino acid preferences for crosslinking are complex, varied, and depend on the structural interactions between the RNA and RBP (Hockensmith et al., 1986). After crosslinking and cell lysis, specific RBP-RNA complexes can be isolated by immunopreciptation with stringent purification via SDS-PAGE followed by nitrocellulose transfer. Crosslinked protein-RNA complexes can be readily identified after nitrocellulose transfer by radiolabeling the RNA with ^{32}P after immunoprecipitation. Following isolation of the protein-RNA complex from the nitrocellulouse membrane, the protein is digested with protease liberating the crosslinked RNA and allowing for the generation of a cDNA library competent for high-throughput sequencing. By adding varying amounts of RNase into the cellular lysate, the size of the recovered RNA fragments can be titrated to a size useful for mapping the RBP binding-site. Additionally, during reverse-transcription, mutations are often introduced into the RNA-amino acid crosslink site due to remaining amino acid-nucleic acid adducts after protease digestion. These cross-linked sites can be used to map the RBP binding sites genome-wide at single nucleotide resolution (Moore et al., 2014).The

HITS-CLIP technique has been used to construct genome-wide binding profiles for many RBPs involved in the miRNA pathway, including *Dgcr8, Dicer,* and *Ago* . By performing *Ago* HITS-CLIP, miRNA targets can be predicted genome-wide based on the mapped binding site and the presence of miRNA seed sequences, greatly improving miRNA target identification genome-wide (Loeb et al., 2012).

In this chapter I present a genome-wide approach to identify *miR-203* targets in keratinocytes that faithfully recovered *bona fide* targets. By integrating multiple genome-wide gene expression datasets a high-confidence list of *miR-203* targets was identified that responded to alterations in *miR-203* levels. Additionally, by performing *Ago2*-HITS-CLIP I identified transcriptome-wide *Ago2* binding-sites allowing identification of *miR-203* targets additionally based on *Ago2* association in keratinocytes. By integrating the HITS-CLIP datasets with the expression meta-analyses I identified a set of novel *miR-203* targets. These novel targets have functions in diverse biological processes, however I validated a subset of these targets with previously known functions in the *RAS/MAPK* pathway and DNA replication. Lastly, the *Ago2* binding profiles obtained predicted targets of multiple additional miRNA families in keratinocytes, providing mechanistic insights into the functions of additional miRNA families in keratinocytes.

MATERIALS AND METHODS

Affymetrix microarray analysis:

For the miR-203 epidermal loss-of-function microarray analysis, RNA was isolated from total epidermal samples from two-pairs of *miR-203*$^{+/+}$ and *miR-203*$^{-/-}$ animals at p4. For the doxycycline-inducible *miR-203* over-expression microarray analysis, total RNA was isolated from two pairs of doxycycline induced or uninduced

K14-rtTA/pTre-miR-203 animals using FACS sorting for *K14-H2B-GFP+* cells as described previously (Jackson et al., 2013). The microarray analysis of *miR-203* overexpression in basal epidermis was previously published (Jackson et al., 2013). Subsequently Total RNAs (500 ng) were processed and hybridized to the Mouse Genome 430 2.0 array (Affymetrix, USA) following the manufacturer's instruction at the MCDB microarray facility. Microarray image files were processed using the R Bioconductor suite and Mas5 normalization. Probesets were then filtered to include only those probes with Present or Absent calls in at least two arrays. Probesets were then collapsed using the probeset with the maximum averaged probeset intensity to represent each GeneID. Log2 fold changes were then computed using the *limma* Bioconductor package.

Ribosome Profiling:

Ribosome profiling was performed on primary keratinocyte lysates using the ARTSeq™ Ribosome profiling kit (Epicentre). Briefly, lysates from a 10cm dish of primary keratinocytes were isolated in the presence of cycloheximide (Sigma Aldrich, 50 µg/ml) and subject to limited RNase I digestion (10 units) for 45min at room temperature. RNase digestion was terminated by addition of 15ul of Super-RNase IN (Ambion) followed by ribosome isolation using illustra™ MicroSpin™ S-400 HR Columns (GE Healthcare). Following RNA extraction and precipitation, rRNA was depleted using the Ribo-Zero Gold™ kit (Epicentre), with the remaining RNA then fractionated through 18% PAGE gels. RNA species 28-32 nt were isolated for adaptor ligation, reverse transcription, circularization, and PCR amplification following the

manufacturer's protocol. PAGE gel isolated PCR products were then sequenced on a HiSeq 2000™ (Illumina).

Raw reads were first trimmed to removed 3' adaptors using cutAdapt with default parameters. Read were aligned to mm10 rRNA, tRNA, and ncRNA (Ensemble annotation) databases using Bowtie (default settings) to exclude reads aligning to rRNA, tRNA, and ncRNA sequences. Unaligned reads were then aligned to the mm10 genome via Tophat using default settings, with a supplied .gtf annotation file containing Refseq gene annotations (iGenomes Illumina downloaded 9/4/2013). Uniquely aligned read counts were quantified across each CDS using HTSeq Count (settings: -s yes -m union -t CDS) using the above-mentioned GTF annotation database. Mapping statistics are provided in appendix Table 5. Transcripts with low reads counts were excluded by only keeping transcripts with at least 50 reads in at least two libraries. Filtered transcript reads count data was then analyzed for differential expression using EdgeR with classical analysis parameters. To calculate translation efficiency for each transcript, Reads Per Million Mapped (RPM) values from 3Seq were divided by Reads per Million Mapped to coding-sequences for the Ribo-Seq. The change in translation efficiency was then computed as the ratio of translation efficiency in the *miR-203*$^{-/-}$ and *miR-203*$^{+/+}$ libraries (Guo et al., 2010).

Ago2 HITS-CLIP:

Ago2-HITS-CLIP was performed as previously described with minor modifications (Leung et al., 2011; Wang et al., 2009). 15 cm^2 dishes of primary keratinocytes were irradiated twice at 200mJ/cm with 254 nm UVC light. Following irradiation cell lysates were harvested by scraping and stored at -80°C. Following

thawing, lysates were further lysed by trituration 3 times through pre-chilled 25 and 30 gauge needles. Lysates were then treated with 10 ul Turbo DNase™ (Promega) and 5 ul RNase-Out™ (Invitrogen) per ml of lysate. Limited RNase digestion was performed using 10ul per ml of lysate of a 1:20 dilution of an RnaseA/T1 mix (Sigma/Ambion 1x mix = 3.33ul RnaseA (2 ug/ul) with 6.66 ul RnaseT1 (1 U/ul)). Crosslinked *Ago2* was recovered via immunoprecipitation for 2 hours at 4°C with 3 ug of a monoclonal anti-mouse Ago2 antibody (Wako Chemicals USA clone 2D4) complexed with Protein-G Dynabeads™ (Invitrogen). Immunoprecipitates were washed twice with High-Salt Buffer and PNK buffer, then end-labled with 25 μCi ^{32}P γ-ATP using PNK 3' phosphatase minus (NEB) for 5 minutes at 37°C. After washing the beads as listed above, 5' adaptor ligation was performed for two hours at room temperature using T4 RNA Ligase 1 with 10uM 5' RNA Linker, 20% PEG-8000 (w/v final), 1mM ATP, and RNaseOut™ (Invitrogen). Beads were again washed twice with PNK buffer then resuspended in a phosphatase reaction with 5uL FastAP™ (ThermoFisher) with RNaseOUT. Following washing twice with PNK buffer, Protein-RNA complexes were eluted from the beads using 1x Novex™ Loading buffer supplemented with 50mM DTT at 70°C for 10 minutes. Protein-RNA complexes were then resolved on an 8% Bis-Tris Gel and transferred to nitrocellulose. Membranes were exposed to a phosphor screen for 1-2 hours to obtain an autoradiograph. Subsequently, RNA-protein complexes migrating in the 110-130kD range were excised from the nitrocellulose. RNA was recovered from the nitrocellulose using Proteinase K treatment followed by phenol-chloroform extraction and ethanol precipitation. Isolated RNA was next ligated to a 3' adaptor using the same ligation reaction conditions as for the 5' ligation, and ligated

RNA species were fractionated away from adaptor-adaptor ligation products on 10% UREA Page gels. The RNA was eluted from the PAGE gel with HSCB buffer overnight at 4°C, then ethanol precipitated and resuspended for reverse transcription with SuperScript III™ (Invitrogen). cDNA products were then subjected to PCR amplification for 20-24 cycles and fractionated on an 8% native PAGE gel. PCR products representing cDNA inserts of 20-50nts were recovered and subject to sequencing on a HiSeq 2000™ (Illumina)

HITS-CLIP reads were analyzed as follows. First, reads were processed to identify miRNA alignments using the same pipeline that we use for Small-RNA-Seq listed in Chapter 2. Reads not mapping to miRNAs were next processed as follows. Reads were trimmed with Cutadapt to remove adaptor sequences using default settings. To avoid PCR duplicates from biasing the analysis, duplicate reads were then collapsed to a single read using Fastx_collapser (default settings). The 5' and 3' adaptor sequences contain randomized dinucleotides on their 3' and 5' ends respectively, which were next trimmed from the reads. The reads were then aligned to the mm10 genome assembly using NovoAlign requiring a minimum alignment length of 25 nucleotides (settings –s 1 –t 85 –l 25) (Novocraft). Mapping statistics are provided in appendix Table 6. All unique alignments from each library were then pooled to identify Ago2 HITS-CLIP clusters. Clusters were defined as two read alignments that overlap by a minimum of one nucleotide. Clusters were next annotated to gene features in a hierarchical manner in which clusters were annotated to protein coding RefSeq 3' UTRs (with 5kbp extension allowed), RefSeq CDS regions, RefSeq 5' UTRs, Ensemble ncRNA regions, and RefSeq intron regions. Clusters not found in these regions were annotated as

intergenic clusters. For predicting miRNA target sites, 3'UTR cluster sequences were searched for 6mer seed-sequence matches for miRNA species that accounted for 90% of miRNAs expressed in epidermis based on small-RNA sequencing (Appendix Table 8).

Meta-analysis of miR-203 targets:

Gene Symbols were used to compare across microarray, 3Seq and Ribo-Seq datasets. Log_2 fold changes were used to assess differential gene expression in each dataset. In total 6,365 genes were detectable in all the datasets, from which 294 satisfied the criteria of being upregulated in all the *miR-203* knockout datasets and downregulated in the *miR-203* overexpression datasets (Appendix Table 10). Negative control datasets were constructed to analyze the enrichment of genes containing *miR-203* seed matches with the following criteria, randomly selected genes from the list of detected transcripts in the meta-analysis, or genes that have a positive correlation to *miR-203* expression (downregulated in *miR-203* knockout datasets and upregulated in *miR-203* overexpression datasets).

In order to compare gain-of-function and loss-of-function datasets in aggregate, a ranked correlation to *miR-203* metric was calculated. Transcripts were assigned a rank in each knockout dataset with the most upregulated gene given a rank of 1. Transcripts were next assigned a rank in each overexpression dataset with the most downregulated gene given a rank of 1. The ranked values from each of the 5 datasets were then summed and ranked with the transcript most upregulated upon miR-203 ablation and downregulated upon overexpression being assigned a value of 1.

3'UTR motif-searching:

De novo motif searching was performed using the HOMER package to search for 7 or 8mer motifs in RefSeq 3'UTR sequences for selected gene-sets (Heinz et al., 2010). For genes with multiple 3'UTR isoforms, the longest 3'UTR was selected for motif searching. For the CDF plots, transcripts were classified into 8mer, 7mer, 6mer, or not seed containing by first searching with a Python script FASTA sequences with regular expressions ([^C]ATTTCA | ^ATTTCA for a 6mer *miR-203* match, [^A]CATTTCA | ^CATTTCA for a 7mer *miR-203* match and ACATTTCA for an 8mer *miR-203* match). Transcripts with multiple seed matches were hierarchically assigned to avoid duplicate assignments. If a 3'UTR contained a 8mer match, it was assigned to the 8mer category, regardless of the presence of 7mer or 6mer matches. Similarly a 3'UTR was only assigned to the 7mer category if it did not contain a 8mer match. 3'UTRs in the 6mer category only contained 6mer matches. Lastly 3'UTRSs with no 6mer, 7mer or 8mer matches were assigned to the no-match category. miRNA seed-sequence searches in Ago2-HITS-CLIP clusters were performed with a Python script on FASTA sequences using regular expressions for position 2-7 nucleotide 6mer seed matches for 26 miRNA families which accounted for 90% of the miRNAs expressed in mouse epidermal samples (Appendix Table 8).

qPCR and western blotting:

qPCR was performed as described in Chapter 2. Western blotting was performed as described for Chapter 2. Proteins were transferred to PVDF for detection of *Pola1*, *Beta-Tubulin*, or *Ccnd1.* See Appendix Table 4 for antibody descriptions and dilutions. X-ray films were scanned and processed with Fiji software to calculate relative protein abundance.

Primary Keratinocyte cell culture, viral infections, and shRNA knockdown:

Lentiviral particles were produced by transient transfection of pLKO-shRNA constructs, PsPax.2, and pVSVG into 293Ft cells using Mirus-Bio LT1. 24 hours post transfection the media was changed to E-Low calcium. Viral supernatant was harvested every 12 hours for up to 96 hours, pooled and filtered with .45μM filter. A spontaneously immortalized wild type mouse keratinocyte cell line was also generated in house via serial passage on mitomycin-C treated NIH-3T3 feeder cell culture layer and utilized for luciferase assays and shRNA knockdowns. For colony formation assays, 500 cells were split into individual wells of 6-well plates, cultured for 10-14 days, fixed with 4% PFA, and stained with 0.2% Crystal Violet in 70% Ethanol. Sigma-Aldrich TRC lentiviral shRNAs against *Hbegf* and *Pola1* were obtained from the Functional Genomic Facility (University of Colorado at Boulder, sequences listed Appendix Table 7).

3'UTR Luciferase Assays:

3'UTR reporter constructs were generated by PCR amplification of 3'UTRs from cDNA or gDNA and subcloning of the fragments into pGL3-Control (Promega) (Appendix Table 1). 50,000 keratinocytes from a spontaneous immortalized cell line were plated into each well of a 24 well plate. The following day 2ng renilla luciferase control, 20ng pGL3-3'UTR reporter, and 380ng of K14 empty vector, or K14-*miR-203* were transiently cotransfected into keratinocytes in each well of a the 24 well plate using 1.2 ul of Mirus Bio LT1 reagent (MirusBio). 24 hours later cell lysates were collected and renilla and firefly luciferase activity were measured using Dual-Glo Luciferase Assay system (Promega) as described previously (Yi et al., 2008). Data are represented as

the ratio of firefly to renilla RFU values, normalized to Pgl3-Control values. Error bars represent propagated standard deviations.

GO enrichment analysis:

GO enrichment analysis was performed using the TopGO R package (Alexa and Rahnenfuhrer, 2010). This package allows the user to upload the most recently updated GO annotations, and perform multiple different statistical enrichment tests. For the analyses presented in this chapter the Weighted statistical test was performed which assigns go terms based not only on enrichment, but also based on the GO-hierarchical assignment and the enrichment of go terms in interrelated GO terms(Alexa et al., 2006). GO annotations for biological processes were downloaded from http://geneontology.org/ on 1/8/2015. For all tables presented the p-values are not subject to adjustment, as per the recommendation of the topGO documentation.

Statistics and Data Plotting:

Statistical analysis was performed using either R or Microsoft Excel. Unpaired two-sided student t-tests were used to assess statistical significance unless indicated otherwise in the figure legends. For comparisons with multiple categories, ANOVA was used with Tukey's HSD post-hoc test. The hypergeometric test was used to assess the enrichment of gene lists in genome-wide studies. The Kolmogorov–Smirnov test was used to assess differences in cumulative distributions functions.

Data Access:

All sequencing data, microarray data, and relevant analyzed datafiles have been deposited at the Gene Expression Omnibus and is accessible through the GEO superseries # GSE66056.

RESULTS

Identification of miR-203 targets with meta-analysis of genome-wide expression datasets:

The data presented so far have provided evidence a role for *miR-203* in suppressing tumorigenesis driven by oncogenic *HRas*. To decode the underlying mechanism, I carried out complementary lines of experimentation to identify *miR-203* targets in the skin. As mentioned in the introduction, recent studies have demonstrated that measuring mRNA expression changes can largely capture the impact of miRNA targeting. I therefore generated multiple gene expression datasets upon modulation of *miR-203* levels to identify *miR-203* targets. In parallel, I performed High-Throughput Sequencing of RNA isolated by CrossLinking ImmunoPrecipitation (HITS-CLIP) on *Ago2* to identify the physical interaction between RISC and predicted miRNA targets.

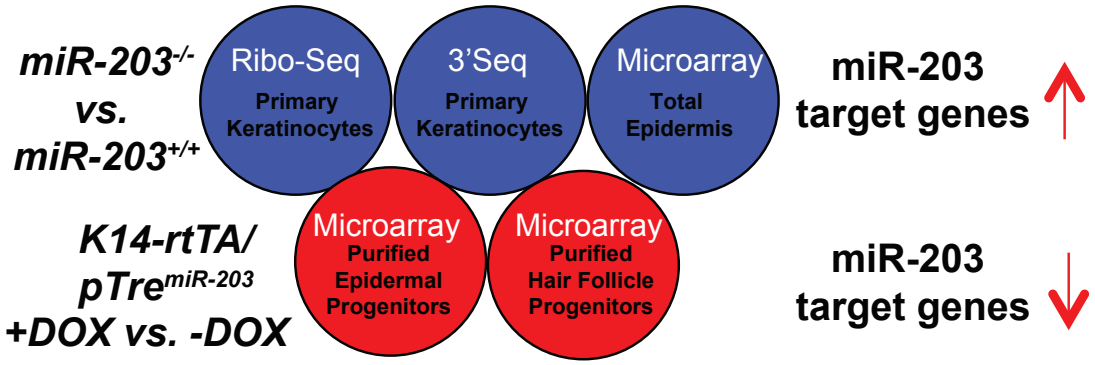

Figure 21. Meta-analysis approach to identify bona fide miR-203 targets in mouse keratinocytes. Microarray, RNA-Seq (3Seq), and Ribosome Profiling datasets were individually generated to identify miR-203 targets.

I applied several different profiling techniques that included: ribosome profiling, RNA-Seq (3Seq), and microarray to determine up-regulated genes in *miR-203* KO

samples and down-regulated genes in *miR-203* induced samples (Figure 21). This approach allows identification of targets negatively regulated by *miR-203.* Although reports exist that suggest that miRNAs can positively regulate their targets, such examples are rare, and in our datasets not observed as a common outcome of targeting (Figure 23A) (Mortensen et al., 2011).

I first examined the transcriptome-wide impacts of *miR-203* gain-of-function using an inducible mouse model that allows spatiotemporal control of *miR-203* expression. The *K14-rTTA/pTre2-miR-203* mouse model was previously generated in the lab and used to determine the impact of short-term *miR*-203 expression on basal epidermal progenitors *in vivo* and identify novel *miR-203* target genes (Jackson et al., 2013). Additional datasets were also generated during these studies by Zhaojie Zhang and Dejiang Feng, which used microarray profiling to identify transcripts downregulated upon *miR-203* induction in hair follicle progenitor populations although this data was not published.

I first reanalyzed the epidermal and hair follicle microarray datasets to identify the impact of *miR-203* on biological pathways to gain further molecular insight into *miR-203's* function (Figure 22A). To maximize the likelihood of detecting *miR-203* targets, both datasets were combined, and genes that exhibited downregulation in both datasets were selected. This approach was taken as many miRNA targets are regulated with very minor mRNA expression changes, sometimes less than 20% changes for a particular target. Therefore filtering the dataset based on fold-change metrics, or p-value estimates can lead to excluding potential targets. This approach leads to a high false-positive rate, which can be overcome by including additional datasets, however this

approach provides the benefit of a low false-negatives rate, allowing detection of additional targets. The combined analyses indicated that 1704 transcripts were jointly downregulated in the hair follicle and epidermal datasets. *miR-203* induction perturbed many biological processes, including regulation of cell proliferation, cell division, process involving nucleotide metabolism, and DNA damage responses (Figure 22C).

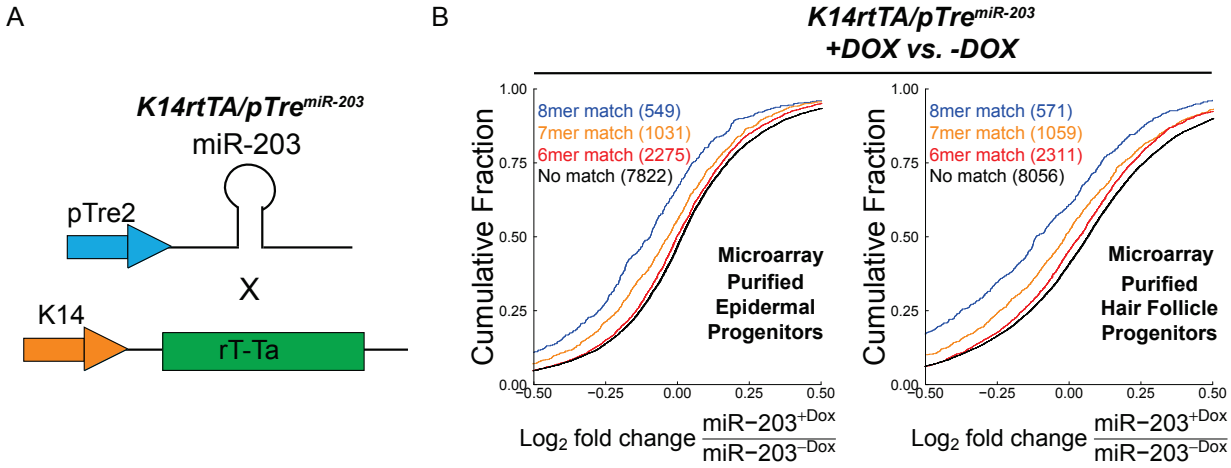

C

GO.ID	Term	Gene Count	P-Value
GO:0006260	DNA replication	9.20E+01	< 1e-30
GO:1903047	mitotic cell cycle process	1.49E+02	< 1e-30
GO:0006306	DNA methylation	1.50E+01	0.00011
GO:1902186	regulation of viral release from host cell	8.00E+00	0.00011
GO:0006287	base-excision repair, gap-filling	4.00E+00	0.00012
GO:0006297	nucleotide-excision repair, DNA gap filling	4.00E+00	0.00012
GO:0008635	activation of cysteine-type endopeptidase activity...	4.00E+00	0.00012
GO:0016072	rRNA metabolic process	2.30E+01	0.00012
GO:0031145	anaphase-promoting complex-dependent proteasomal...	6.00E+00	0.00014
GO:0006413	translational initiation	1.70E+01	0.00014
GO:0034976	response to endoplasmic reticulum stress	2.10E+01	0.00014
GO:0009200	deoxyribonucleoside triphosphate metabolic process	7.00E+00	0.00014
GO:0046148	pigment biosynthetic process	1.10E+01	0.00015
GO:0001841	neural tube formation	2.00E+01	0.00018
GO:0045333	cellular respiration	2.10E+01	0.00019
GO:0055114	oxidation-reduction process	1.05E+02	0.00022
GO:0050678	regulation of epithelial cell proliferation	3.70E+01	0.00022
GO:0097193	intrinsic apoptotic signaling pathway	3.90E+01	0.00024
GO:0045814	negative regulation of gene expression, epigenetic	1.00E+01	0.00028
GO:0018105	peptidyl-serine phosphorylation	3.00E+01	0.00029

Figure 22. miR-203 overexpression dramatically downregulates seed matched transcripts, and deregulates cell-cycle related processes. (A) Schematic of the *K14-rTTa/pTre-miR-203* allele. (B) Cumulative distribution plots of *miR-203* seed containing transcripts in epidermal and hair follicle datasets. ($p < 0.05$ for 8mer to No match comparison). (C) GO biological process enrichment analysis. All downregulated transcripts in both datasets were queried for GO term enrichment (1704 transcripts). P-Value calculated using weighted GO term analysis (See Methods).

These observations are not altogether unexpected as *miR-203* expression strongly suppresses cellular proliferation, which is indicated by the large number of genes involved in cell-cycle processes that are downregulated.

Next, I used these datasets to determine the regulatory impact of *miR-203* on putative targets. As shown in Figure 22B, transcripts containing *miR-203* 8mer seed matches in their 3'UTRs are strongly downregulated upon *miR-203* induction (p-value = $3.3x10^{-23}$ for epidermis and $5.4x10^{-28}$ for hair follicle, respectively). Importantly, as suggested by previous studies of miRNA targeting efficacy, transcripts with 8mer matches are more strongly regulated than those with 7 or 6mer matches. These results demonstrate that *miR-203* behaves similar to other miRNAs by utilizing seed based targeting to repress transcripts, and additionally defines a subset of genes that are downregulated by *miR-203* induction.

miRNA overexpression commonly results in strong perturbation of cellular processes and leads to wide-scale downregulation of many transcripts. In contrast, miRNA knockout or inhibitor studies generally results in far more subtle and minor regulatory effects upon the transcriptome (Bartel, 2009). I generated three independent datasets to examine the impact of *miR-203* ablation on gene expression profiles. For all datasets generated, miR-$203^{+/+}$ and miR-$203^{-/-}$ samples were harvested in biological duplicate. Microarray profiling was performed on total epidermal samples isolated from p4.5 mice, 3seq was performed on primary keratinocytes, and ribosome profiling was performed on primary keratinocyte samples. Ribosome profiling was conducted to test the hypothesis that *miR-203* primarily regulates it's targets through translational mechanisms.

In striking contrast to the overexpression analyses, loss of *miR-203* resulted in far more mild deregulation of gene expression (Figure 23A,B). In the combined datasets, 786 transcripts were jointly upregulated in all the knockout datasets. GO analysis of this geneset demonstrates poor enrichment for any particular biological process, with most categories having less than 5 genes overlapping (Figure 23C). Some insights can be gained as components of the spindle assemble checkpoint and genes responding to radiation stress are among this list. However, the mild overall enrichment, and unclear biological implications of these enriched pathways argued against further lines of experiments to address these observations.

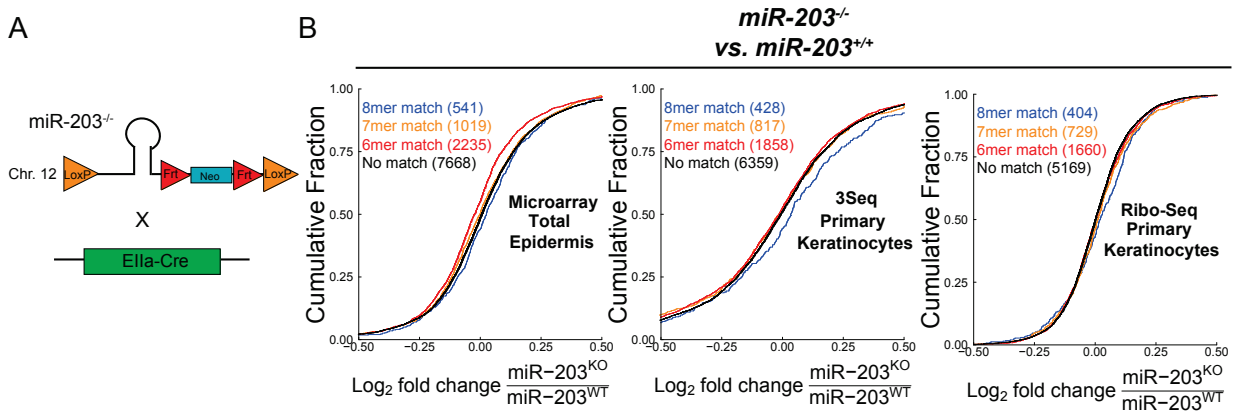

C

GO.ID	Term	Gene Counts	P-Value
GO:0006888	ER to Golgi vesicle-mediated transport	9.00E+00	0.00012
GO:0032204	regulation of telomere maintenance	5.00E+00	0.00012
GO:0071173	spindle assembly checkpoint	6.00E+00	0.00016
GO:0010212	response to ionizing radiation	1.20E+01	0.00018
GO:0009891	positive regulation of biosynthetic process	8.10E+01	0.00021
GO:0014812	muscle cell migration	9.00E+00	0.00022
GO:0034227	tRNA thio-modification	3.00E+00	0.00033
GO:0010629	negative regulation of gene expression	6.10E+01	0.00039
GO:0042274	ribosomal small subunit biogenesis	8.00E+00	0.00039
GO:0055114	oxidation-reduction process	5.20E+01	0.00044
GO:0034613	cellular protein localization	7.20E+01	0.00044
GO:0043518	negative regulation of DNA damage response	4.00E+00	0.00045
GO:0060070	canonical Wnt signaling pathway	1.70E+01	0.00045
GO:0051262	protein tetramerization	1.10E+01	0.00055
GO:0048660	regulation of smooth muscle cell proliferation	1.10E+01	0.00055
GO:0031572	G2 DNA damage checkpoint	6.00E+00	0.00062
GO:0050687	negative regulation of defense response to virus	4.00E+00	0.00064
GO:0043648	dicarboxylic acid metabolic process	9.00E+00	0.00067
GO:0045732	positive regulation of protein catabolic process	1.50E+01	0.00071
GO:0031334	positive regulation of protein complex assembly	1.50E+01	0.00092

Figure 23. miR-203 loss of function mildly upregulates seed matched transcripts. (A) Schematic of the *miR-203* ablation strategy. (B) Cumulative distribution plots of *miR-203* seed containing transcripts in epidermal and primary keratinocyte datasets (p <0.05

for 8mer to No match comparison for all datasets). (C) GO biological process enrichment analysis. All upregulated transcripts in both datasets were queried for GO term enrichment (786 transcripts). P-Value calculated using weighted GO term analysis (See Methods).

Examination of seed dependent *miR-203* targeting demonstrated that ablation of miR-203 lead to mild increases in targeted transcripts (p value =0.041, 0.0043, 4.58 x 10^{-05} for comparing 8mer to non-targeted for epidermal microarray, 3seq, and Ribo-seq respectively). Given that these datasets displayed *miR-203* seed dependent upregulation of transcripts, similar to the overexpression datasets, I next combined both the overexpression and knockout datasets based on gene symbols to further identify *miR-203* regulated transcripts.

The combined dataset of transcripts represents 6,365 transcripts detectable in all 5 datasets. I next sought to confirm that the aggregate dataset showed similar miR-203 seed dependent regulation as the independent analyses of the overexpression and knockout datasets. To compare transcripts across all datasets I computed a summed rank correlation metric. Transcripts in the knockout datasets were ranked based on fold changes with the transcript most upregulated given a rank value of 1. Transcripts in the overexpression datasets were similarly ranked based on fold changes with the transcript most downregulated given a rank value of 1. The rank values from the 5 datasets were then summed for each transcript, and the transcript with the smallest summed rank value assigned a rank of 1, which indicates the transcript with the strongest gene expression changes correlated to miR-203 gain or loss of function. This “Ranked expression correlation” then allowed direct comparison between groups of genes with 8mer, 7mer, 6mer, no seed matches. As shown in Figure 24A, genes with 8mer or 7mer seed matches had a higher ranked expression correlation metric, consistent with

A

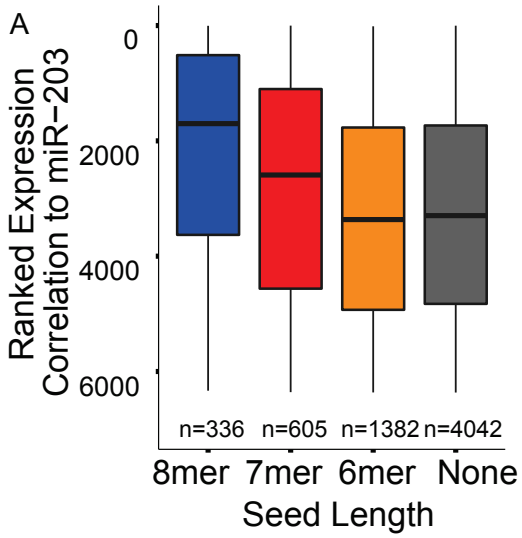

B

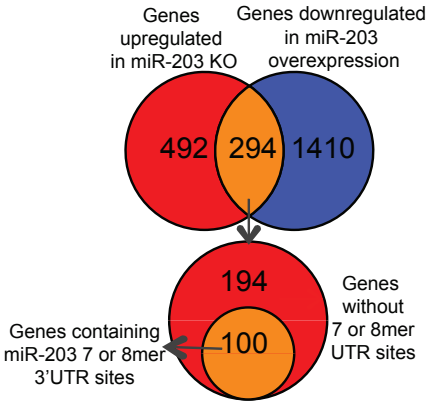

C

Seed Type	miR-203 Targets (294)	P-Value	Non-Targets (353)	P-Value	Random Targets (294)	P-Value
6mer	49	9.9E-01	79	4.2E-01	66	4.2E-01
7mer	**52**	**7.4E-06**	27	9.2E-01	28	5.5E-01
8mer	**48**	**7.0E-13**	8	1.0E+00	16	4.8E-01

D

Gene Symbol	Microarray Epidermal Progenitors (+DOX)	Microarray Hair Follicle Progenitors (+DOX)	Microarray Isolated Epidermis (KO)	3'seq Primary Keratinocytes (KO)	Ribo-Seq Primary Keratinocytes (KO)	Log_2FC
Sh3bgrl	-0.83	-1.67	0.42	0.91	0.57	
Vopp1	-0.74	-1.34	0.51	0.38	0.37	
Pola1	-1.42	-1.83	0.36	0.58	0.18	
Rapgef1	-0.29	-1.29	0.49	0.87	0.60	
Lasp1	-1.13	-1.31	0.28	0.33	0.22	
Rap1b	-0.43	-0.55	0.43	0.44	0.31	
Tax1bp3	-0.57	-0.79	0.27	0.38	0.23	
Cav1	-0.95	-1.07	0.10	0.97	0.28	
Gbe1	-0.65	-1.26	0.46	0.69	0.08	
Ndufb2	-0.67	-0.91	0.29	0.24	0.20	
Lnx2	-0.42	-0.29	0.45	0.75	0.25	
Pgam5	-0.39	-0.79	0.47	0.22	0.31	2.00
Slc12a4	-0.64	-0.66	0.38	0.33	0.13	1.50
Sh3pxd2b	-0.99	-0.43	0.31	0.59	0.12	1.00
Yars2	-0.61	-0.60	0.48	0.32	0.11	0.50
Ctps2	-0.84	-0.69	0.09	0.44	0.26	0.00
Ppap2c	-0.42	-0.38	0.33	0.25	0.37	-0.50
Prmt6	-0.54	-0.19	0.58	0.60	0.15	-1.00
Dhx36	-0.24	-0.58	0.22	0.51	0.22	-1.50
Tprkb	-0.24	-0.42	0.42	0.74	0.15	-2.00

E

GO.ID	Term	Gene Count	P-Value
GO:0006270	DNA replication initiation	4.00E+00	0.00011
GO:0051259	protein oligomerization	1.50E+01	0.00019
GO:0071173	spindle assembly checkpoint	4.00E+00	0.00026
GO:0050680	negative regulation of epithelial cell proliferation	7.00E+00	0.00057
GO:0031116	positive regulation of microtubule polymerization	3.00E+00	0.00058
GO:0045740	positive regulation of DNA replication	5.00E+00	0.00058
GO:0030178	negative regulation of Wnt signaling pathway	7.00E+00	0.00070
GO:0046716	muscle cell cellular homeostasis	3.00E+00	0.00072
GO:0044774	mitotic DNA integrity checkpoint	5.00E+00	0.00082
GO:0032204	regulation of telomere maintenance	3.00E+00	0.00088
GO:0044319	wound healing, spreading of cells	3.00E+00	0.00106
GO:0006355	regulation of transcription, DNA-templated	5.70E+01	0.00143
GO:0030866	cortical actin cytoskeleton organization	3.00E+00	0.00148
GO:0001885	endothelial cell development	4.00E+00	0.00165
GO:0045070	positive regulation of viral genome replication	3.00E+00	0.00173
GO:0016573	histone acetylation	7.00E+00	0.00203
GO:0043648	dicarboxylic acid metabolic process	5.00E+00	0.00207
GO:0018107	peptidyl-threonine phosphorylation	6.00E+00	0.00209
GO:0006975	DNA damage induced protein phosphorylation	2.00E+00	0.00213
GO:0042542	response to hydrogen peroxide	6.00E+00	0.00243

Figure 24. Expression meta-analysis enriches for miR-203 seed matched targets and known targets for miR-203 . (A) Comparison of genes with or without miR-203 seed matches with ranked expression correlation to miR-203. A summed rank metric was calculated to rank transcripts accordingly to their negative correlation to miR-203. A rank of 1 indicates the gene most upregulated gene in miR-203 KO and downregulated in miR-203 overexpression datasets (See Methods) ($p < 0.05$ for 8 and 7mer compared to no match) (B) Schematic of bioinformatics to identify candidate miR-203 targets in the meta-analysis (C) De novo motif searching of 3'UTRs for the 294 transcripts identified, top motif found displayed. Table of miR-203 seed match enrichment in meta-analysis identified transcripts compared to background frequencies, or negative control datasets (See methods). (D) Top 20 transcripts detected and Log_2 Fold Changes in each dataset. Red transcripts contain miR-203 7 or 8mer seed matches. (E) GO analysis for biological process enrichment.

observations from each individual dataset ($p < 10^{-7}$ for 7 and 8mer comparison to no match, ANOVA with TukeyHSD post-hoc test).

By demanding all potential targets be upregulated in all the miR-203 KO samples and downregulated in all the miR-203 induced samples, I identified 294 transcripts as candidates for miR-203 targeting (Figure 24B). In order to validate this method for identifying miR-203 targets I performed de novo motif searching on the 3'UTR sequences of the 294 transcripts identified. Under the assumption that these identified transcripts are likely miR-203 targets, I expected to find a sequence motif corresponding to miR-203. Satisfying this analysis revealed that the most enriched motif (ACAUUUCA, $p=1x10^{-13}$) perfectly matched to nucleotide position 2-9 of miR-203, the 8-mer seed sequences of miR-203 (Figure 24C). To further validate that our meta-analysis has enriched for miR-203 targets I tabulated the number of genes with 6,7 or 8mer matches in our meta-analysis, and assessed the enrichment over the background frequency of these motifs in all detectable genes in the datasets. Of the 294 transcripts identified in the meta-analysis, 49 contained a 6mer, 52 a 7mer, and 48 an 8mer seed match in their 3'UTRs, representing a strong enrichment over the frequency of miR-203 seed matches

in background keratinocyte transcripts for 7 and 8mers ($p = 7.4 \times 10^{-6}$ and 7.0×10^{-13} for 7mer and 8mer targets.)(Figure 24C). To further substantiate this enrichment I randomly selected 294 transcripts detectable in the combined dataset, and performed an analogous statistical test, demonstrating non-significant enrichment for miR-203 seeds in the randomized dataset ($p > 0.05$). Lastly, I queried the set of transcripts that behaved in an opposite fashion to miR-203 targets (upregulated upon miR-203 overexpression and down-regulated upon miR-203 knockout). These 353 transcripts also showed no statistical enrichment in miR-203 seed matches (Figure 24C). Taken together these analyses demonstrate that by combining multiple gene expression datasets we compiled a dataset strongly enriched for putative miR-203 targets.

Among the top 20 most differentially expressed transcripts when *miR-203* was deleted or induced, 15 of them contain at least one 7-mer or 8-mer match in their 3'UTRs (highlighted in red, Figure 24D). The meta-analysis identified many known miR-203 targets including *Lasp1* (Mori, 2012; Viticchiè et al., 2011)*, Cav1* (Cheng, 2014), *Bmi1* (Wellner et al., 2009), *Snai2* (Ding et al., 2013; Zhang et al., 2011b*), Zfp281* (Yi et al., 2008)(Appendix Table 10). Interestingly the analysis failed to detect known targets of miR-203 in keratinocytes including *Trp63*, *Skp2*, and *Msi2* (Jackson et al., 2013; Yi et al., 2008), suggesting that our analysis may have been conservative in the identification of targeted transcripts. To determine if the subset of predicted direct target genes comprised a network of targets with a coherent biological function I assessed the GO term enrichment for the transcripts identified in the meta-analysis. As shown in Figure 24E, *miR-203* predicted targets are mildly enriched in a some pathways that are consistent with it's function in suppressing the cellular proliferation, including DNA

replication initiation, Positive Regulation of DNA replication, and Regulation of telomere maintenance. However other pathways were also identified whose significance to *miR-203's* function is unclear (i.e. Negative regulation of epithelial cell proliferation), suggesting that the network of *miR-203* target may regulate cellular processes in an incoherent manner, with targeting of both activators and repressors of a given pathway.

Identification of *miR-203* targets via Ago2 HITS-CLIP:

I next applied HITS-CLIP to identify direct interactions between *miR-203* and it's mRNA targets. Four *Ago2* HITS-CLIP libraries were constructed from primary WT keratinocytes, which abundantly express *miR-203* (Figure 25C). *Ago2*-RNA complexes were isolated from a region extending from approximately 110kd – 130kd as expected (Figure 25B). Sequencing libraries from *Ago2* HITS-CLIP samples were generated and analyzed using previously described method (See Appendix Table 8 for mapping statistics). The HITS-CLIP captured miRNA species expressed in keratinocytes, including *miR-203* (Figure 25C), although the rank distribution of miRNAs was notably different from those obtained with small-RNA-Seq from the same cell type (Figure 25D). This discrepancy likely is due to the poor overall recovery of Ago2 crosslinked RNA fragments resulting in poor ligation efficiencies, which can severely bias the faithful quantification of miRNAs (Zhang et al., 2013).

Overall the HITS-CLIP reads and clusters were similar to previously published results with a significant portion aligning to 3'UTRs (Figure 26A) (Leung et al., 2011). Interestingly, there are many intronic, repeat, and intergenic alignments, however the overall significance of these findings is unknown although these binding events have been observed in other *Ago2* HITS-CLIP experiments (Leung et al., 2011). Due to the

focus on identifying microRNA binding with canonical regulatory activity, I focused further analysis on the ~6700 HITS-CLIP clusters aligning to 3'UTR regions.

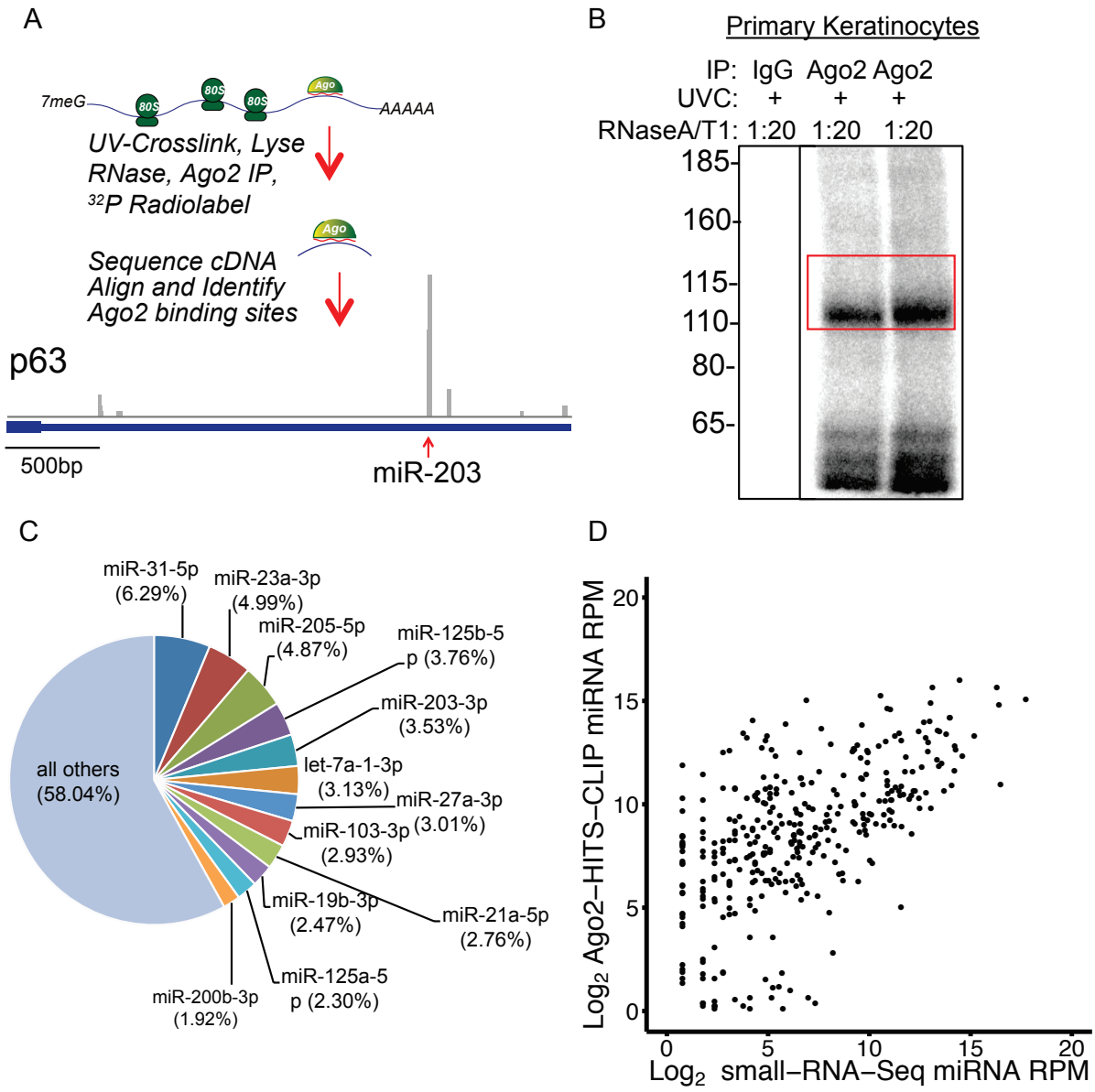

Figure 25. Ago2 HITS-CLIP analysis identifies Ago2 binding-sites genome-wide. (A) Schematic of HITS-CLIP library preparation method and IGV gene track for a *miR-203* target gene *p63*. (B) Autoradiogram of isolated *Ago2*-RNA complexes and control IgG immunoprecipitation. (C) Distribution of miRNA species detected in combined *Ago2*-HITS-CLIP libraries. Percentage represents percentage miRNA mapped out of all miRNA mapped. (D) Comparison between miRNA species detected by *Ago2* HITS-CLIP and small-RNA-Seq from primary keratinocytes. (Pearson correlation coefficient of .59)

To validate that the HITS-CLIP faithfully captured miRNA binding events, I analyzed the sequence motifs present within the 3'UTR CLIP clusters to determine if miRNA binding events were enriched. For each cluster, the region with the highest density of read alignments was determined and defined as the peak summit. I next searched for 6mer seed matches for miRNAs highly expressed in epidermis in a +/- 40 nucleotide region surrounding the peak summit (see methods). As expected miRNA seeds were strongly enriched in a +/- 15 nucleotide region surrounding the peak summit, relative to two control distributions, either randomized cluster positions in keratinocyte 3'UTRs, or clusters with dinucleotide shuffled sequences (Figure 26B). Interestingly, when the same analysis was performed for each miRNA individually, some miRNAs, such as the *miR-23-34-27* cluster and the *let-7* family showed a strong positional bias, whereas *miR-203* showed only minor positional bias (Appendix Figure 33). This biased approach demonstrates that miRNA seeds are present in captured 3'UTR clusters, but does not demonstrate that they are the predominate sequences present. To address this concern, I next performed a *de novo* motif search on the 3'UTR HITS-CLIP clusters to identify sequences enriched over a 3'UTR background (Figure 26C). I found numerous motifs corresponding to miRNA families highly expressed in keratinocytes, such as the aforementioned miRNAs, *miR-23/24/27* and *let-7*, as well as the abundant *miR-203* and *miR-205.* Satisfyingly, the sequence motif for *miR-203*, ACAUUUCA ($p=1x10^{-19}$), was identical to the motif detected by our transcriptome meta-analysis. Taken together these analyses demonstrate that the *Ago2*-HITS-CLIP datasets captured miRNA 3'UTR targeting events.

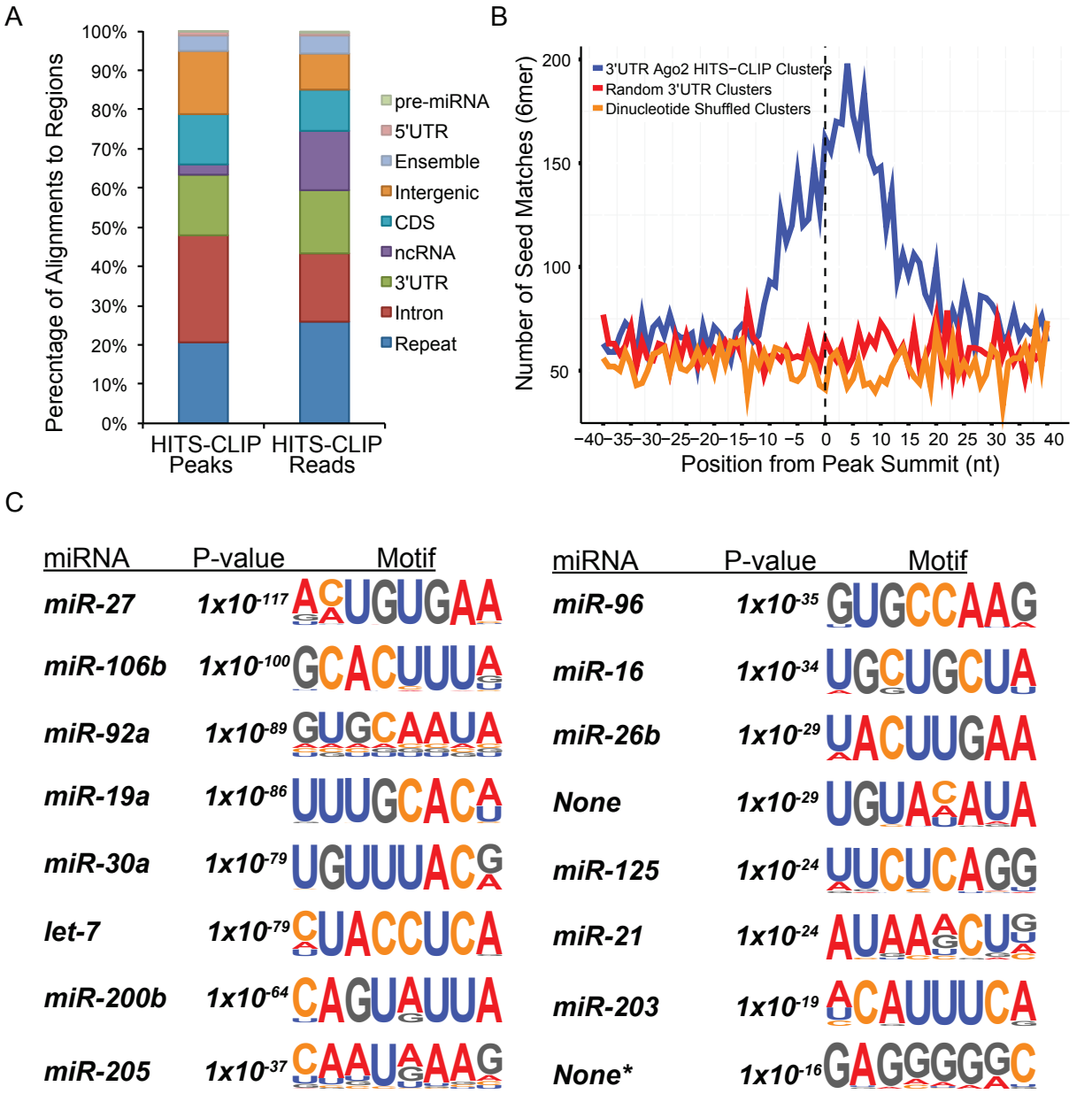

Figure 26. Ago2 HITS-CLIP 3'UTR peaks are enriched in keratinocyte miRNA seed matches, including miR-203. (A) Proportion of peaks and reads aligned to various genomic regions, excluding miRNA alignments (B) Position of miRNA seed matches for miRNAs highly expressed in total epidermal samples. The peak summit represents nucleotide position 0 (C) De novo motif searching identifies most enriched 8mer motifs in 3'UTR peaks. * = Motif similar to the G-rich motif identified in Ago2-HITS-CLIP datasets from Embryonic Stem Cells (Leung et al., 2011).

In order to define miRNA targets from the CLIP datasets it is necessary to predict which miRNA seed is likely responsible for the observed *Ago2* binding. There are many proposed methods for performing this prediction, which essentially have the same caveats and concerns for computation miRNA target predictions from 3'UTR sequences alone (Chi et al., 2009). In order to capture the largest network of targets for each miRNA, I choose to use an approach that maximized the sensitivity, with the caveat of potential decreased specificity. Because examining expression data for *miR-203* could be used to validate the miRNA target predictions, the danger of a high-false positive rate is less of a concern for this approach. To predict miRNA-targeting events, I searched for perfect 6mer seed matches corresponding to miRNAs highly expressed in keratinocytes within the HITS-CLIP clusters, including *miR-203* (Appendix Table 8). For *miR-203* total of 113 unique mRNAs were detected to have *miR-203*-mediated Ago2 binding sites (117 total sites identified). The low number of *miR-203* seed matches captured relative to other highly expressed *miRNAs* was an unexpected finding (See Discussion).

I next examined the expression of these targets in the *miR-203* expression and rank sum datasets. As shown in Figure 27A and B, targets predicted by HITS-CLIP were likely to be downregulated upon *miR-203* overexpression, and trended toward upregulation in the miR-203 KO datasets. Analysis of the ranked expression correlation to *miR-203* demonstrated that HITS-CLIP predicted targets for *miR-203* were more highly ranked than non-targeted transcripts, and additionally more highly ranked than predictions based solely on the presence of a 6,7 or 8mer seed match (Figure 27C).

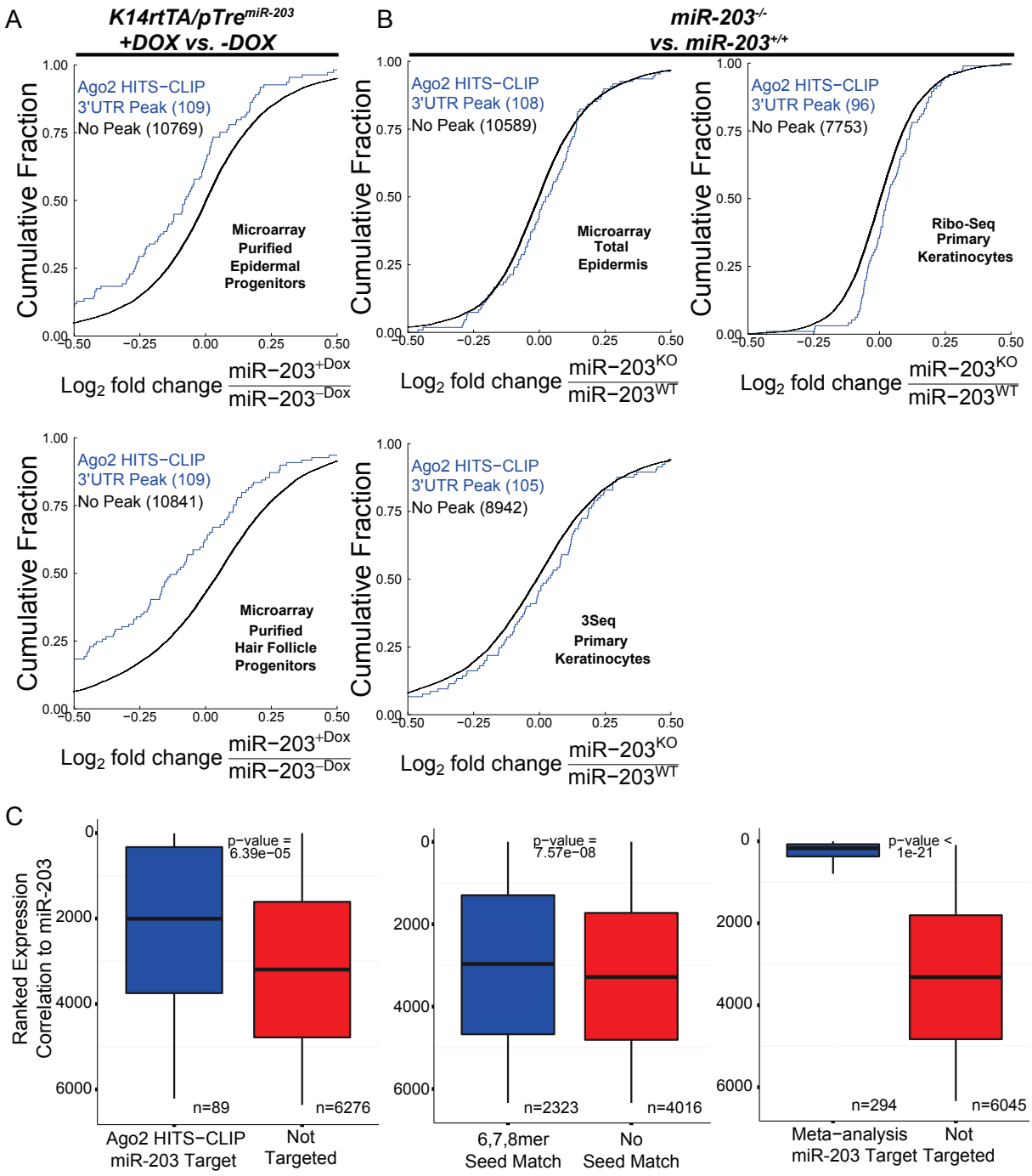

Figure 27. Predicted miR-203 targets based on HITS-CLIP are regulated by miR-203. (A) Cumulative distributions of *miR-203* targets or not targeted transcripts based on HITS-CLIP in *miR-203* overexpression datasets ($p < 0.05$ for both datasets). (B) Cumulative distributions of *miR-203* targets of not targeted transcripts based on HITS-CLIP in *miR-203* knockout datasets ((p-value = <0.05 for Ribo-Seq dataset, otherwise p-value =.19 and .16 for microarray and 3seq respectively). (C) Ranked analysis of *miR-*

203 targets detected by HITS-CLIP, based on 6,7,8mer seed only, or through meta-analysis (p value displayed on plots).

Together, these HITS-CLIP data independently miR-203 targets that acts via its seed sequence for mRNA target repression.

By combining the targets detected by our differential expression datasets and by HITS-CLIP I was able to identify a list of extremely high-confidence targets for *miR-203*. Within this final list of 21 regulated transcripts I found a number of regulators in the *Ras* signaling pathway and important genes involved in regulation of cell division including *Hbegf*, *Ccnd1*, *Snai2*, *Met,* and *Pola1* in this list (Figure 28A,B). Importantly, this analysis detects *Snai2* and *Cav1,* which were previously validated by independent groups as *bona fide miR*-203 targets (Cheng, 2014; Zhang et al., 2011b). This collection of *miR-203* targets suggests that miR-203 targets the Ras/MAPK signaling pathway and critical genes important for cell division to suppress cell proliferation.

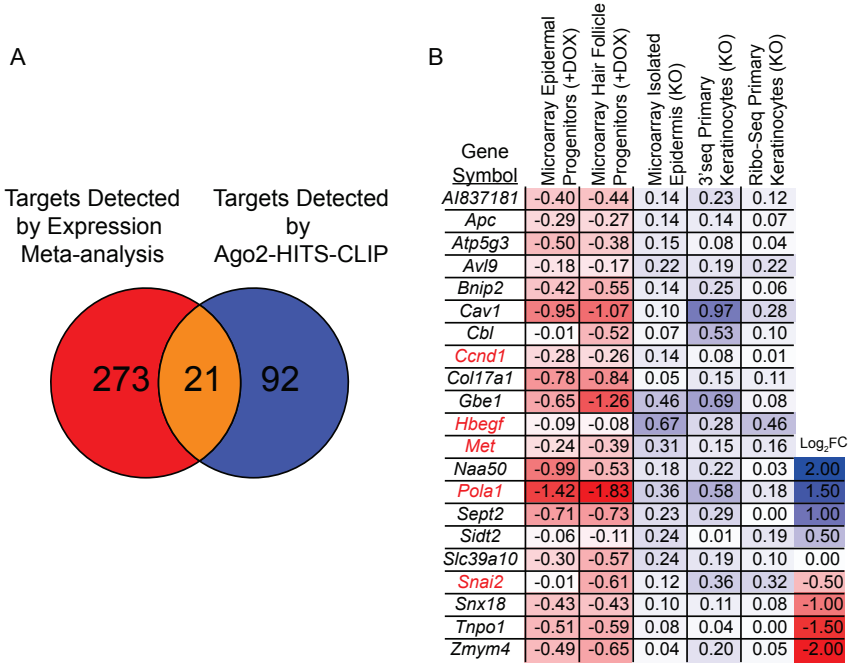

Figure28. miR-203 targets detected in both Ago2-HITS-CLIP and Expression Meta-analysis. (A) Venn-diagram illustrating the overlap between genes detected by Meta-

analysis and *Ago2*-HITS-CLIP. (B) Log_2 fold changes for expression datasets for 21 genes detected in both datasets. Red genes are genes of particular interest mentioned in the results section.

miR-203 directly targets Pola1 and Hbegf:

The genome-wide analyses identified a number of novel targets of *miR-203*. Given the finding that the loss of *miR-203* sensitized mice to oncogenic *HRas* driven tumorigenesis *in vivo* and expansion of *Ras* transformed keratinocytes *in vitro*, I was interested in providing insight into the underlying mechanism. Overall, *miR-203* targets identified by the meta-analysis were mildly upregulated in $HRas^{G12V}$ transformed keratinocytes, compared to non-targeted transcripts, consistent with the down-regulation of *miR-203* in these cells (Figure 29A). Among these targets, I was intrigued by the observation that multiple regulators of the Ras signaling pathway and critical factors for DNA replication and cell cycle progression were among our high confidence targets. To begin to validate the high-confidence set of *miR-203* targets, I selected *Pola1* and *Hbegf* for further study. *Pola1* is the catalytic subunit of the DNA-polymerase-alpha holoenzyme, which is required in initiation of DNA replication during S-phase (Lehman and Kaguni, 1989). *Hbegf* is an EGF-like ligand that activates MAPK signaling through activation of EGF-receptors, ErbB1 and ErbB4. In keratinocytes, *Hbegf* is mitogenic and promotes keratinocyte migration (Stoll et al., 2012). In an epithelial cancer cell line, *Hbegf* acts as an oncogene promoting cell proliferation (Miyamoto et al., 2004). Additionally, *Hbegf* is activated by oncogenic *ras* in keratinocytes and is thought to contribute to keratinocyte initiation during tumorigenesis (Dlugosz et al., 1997) (Figure 5).

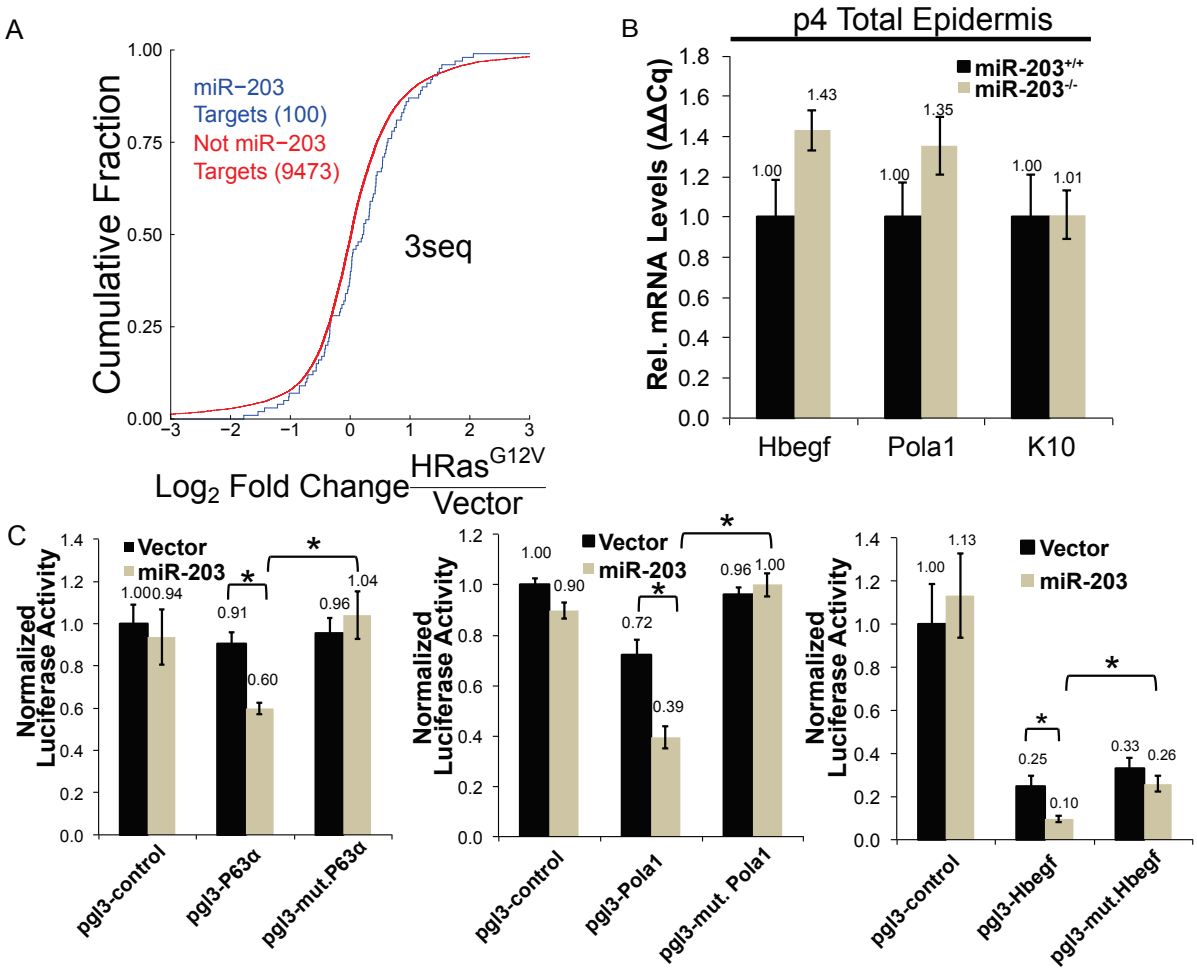

Figure 29. miR-203 directly targets Pola1 and Hbegf. (A) Cumulative distributions of *miR-203* targets or not targeted transcripts based on expression meta-analysis in *Ras* overexpression 3seq datasets ($p < 0.05$). (B) qPCR on total epidermal samples, n=8 *miR-203*$^{+/+}$ and n=10 *miR-203*$^{-/-}$ samples. Error bars represent S.E.M from qPCR reactions performed in technical duplicate on biological replicate samples. (C) 3'UTR luciferase assays performed in keratinocytes. For mutant 3'UTRs all seed matches for *miR-203* in each construct were mutated to reverse complement sequences (n=3 and 2 seed matches for Pola1 and Hbegf respectively). * = $p < 0.05$, student t-test two-way)

In *miR-203* null epidermis, both *Pola1* and *Hbegf* mRNAs were mildly elevated, consistent with the genome-wide expression analysis (Figure 29B). *Pola1* and *Hbegf* transcripts contain 3' UTR *miR-203* target sites (9-mer and 8-mer respectively) that are targeted by *miR-203*, based on HITS-CLIP. To validate these interactions I performed

3'UTR luciferase assays. As shown in Figure 29C, miR-203 targeted these binding sites, resulting in suppression of the reporter, which was relieved by mutation of the seed sequence sites. Lastly, I examined the protein levels of selected targets by western blot. *Pola1* protein levels were also elevated in *miR-203* null primary cells and further elevated in the presence of *HRas*^{G12V} and repressed by *miR-203* induction (Figure 30A,B).

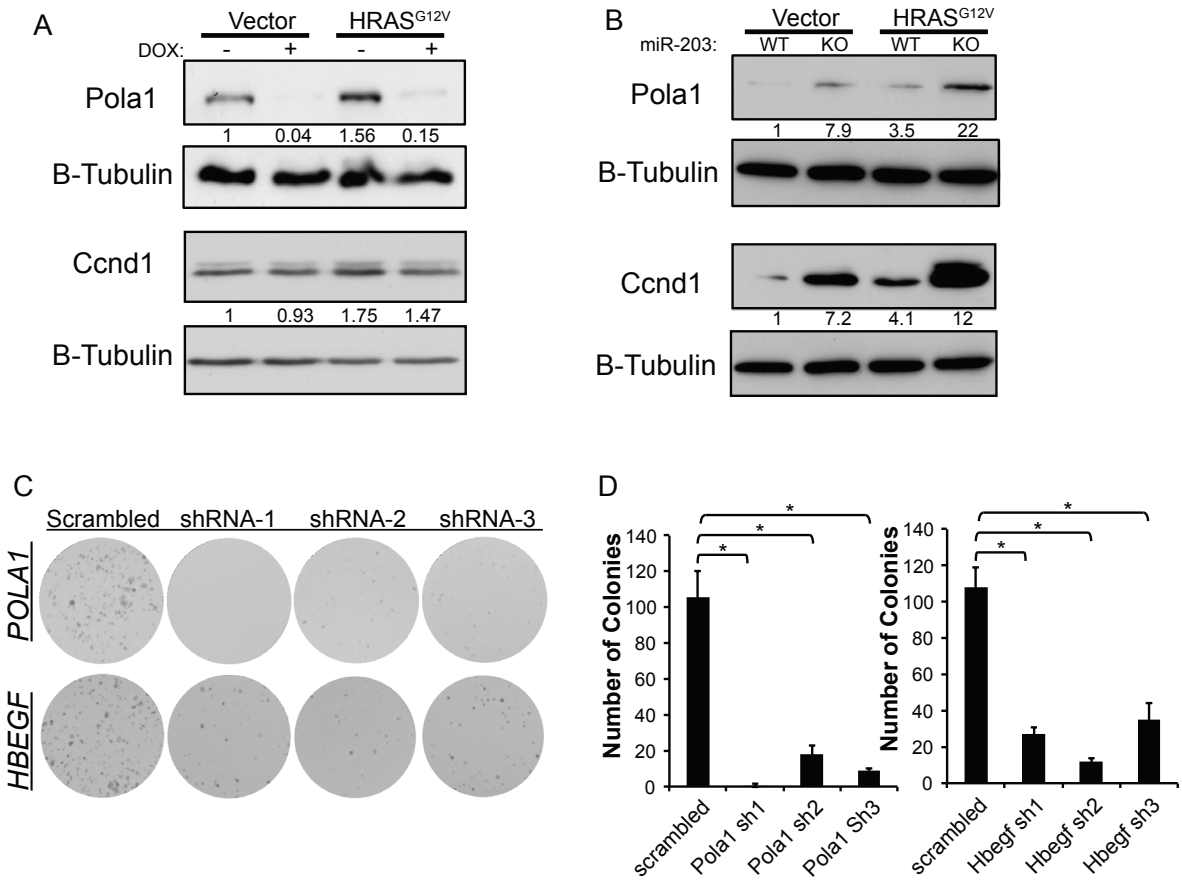

Figure 30. Pola1 and Hbegf are required for keratinocyte colony formation ability. (A) Western blot analysis of miR-203 overexpression lysates. Doxycyline was administered for 48hrs prior to harvest (B) Western blot analysis of miR-203 knockout lysates with or without HRas^{G12V}. (C) shRNA knockdown of *Hbegf* and *Pola1* in keratinocytes suppress colony formation ability. (D) Quantification of colony numbers in experiment C. Results are representative of n=3 independent experiments. Error bars represent standard deviations of mean colony numbers from triplicate wells.

I was unable to measure the protein level of *Hbegf* due to poor antibody performance. However, I observed that the expression of *Ccnd1*, an essential cell cycle regulator that is often induced or amplified by oncogenic *Ras* (Downward, 2003; Stransky et al., 2011), showed a strong negative correlation to *miR-203* (Figure 30A,B) although this target was not repressed by luciferase assay (data not shown). This suggested that loss of *miR-203* increases the levels of *Ccnd1* and contributes to the observed up-regulation of this critical gene, through mechanisms that could be secondary to *miR-203* binding. To assess the functional consequences of *Hbegf* and *Pola1* suppression on keratinocyte proliferation, I knocked down these targets using three independent shRNAs. Suppression of *Hbegf* and *Pola1* strongly suppressed the growth potential of keratinocytes (Figure 30C,D). Taken together these results validate *Hbegf* and *Pola1* as direct targets of *miR-203* and additionally demonstrate that these targets are critical for keratinocyte expansion.

DISCUSSION

A major challenge in understanding miRNA functions is to identify their high-confidence targets globally. To this end, I employed two independent but complementary approaches: transcriptome analysis with KO and inducible models and direct miRNA target capture by *Ago2* HITS-CLIP. The analyses present a comprehensive overview of the impact of *miR-203* upon keratinocyte gene expression and give insights into the targeting networks driving miR-203 function in regulating keratinocyte proliferation.

The approach presented here was able to capture many novel targets for *miR-203*, however it is also likely that the conservative nature of the methods employed

resulted in not identifying many true targets. Thus, it is likely that our identification of *miR-203* targets based on the transcriptome analysis was conservative. Additionally, because miRNA regulation can impact target gene expression on the order of 20-40%, it is expected that many targets will be difficult to detect with the small number of replicates traditionally used in genome-wide techniques. Furthermore, by relaxing the criteria for identifying *miR-203* targets to genes detected in either the meta-analysis or the HITS-CLIP data, reveals additional candidate targets with functions in tumorigenesis, including *p63*,*Src*, *Ralb*, *Lasp1*, and *Bmi1*, of which only *Ralb* hasn't been validated as a target in other systems (Lena et al., 2008; Mori, 2012; Wang et al., 2014; Wellner et al., 2009). For example *p63*, a well-established *miR-203* target, was not identified in the meta-analysis of differential gene expression. However, the recognition of the 3'UTR site of *p63* by *miR-203* was robustly detected by the HITS-CLIP and detected by western blot (Figure 24A and data not shown). Additionally *Src*, another target of *miR-203* that was identified in lung cancer cells, was also detectable by HITS-CLIP but not by the expression analysis (Wang et al., 2014).

In addition to identifying novel targets of *miR-203*, those transcripts that do not contain *miR-203* seed matches yet still are identified in the meta-analysis compromise a unique class of genes that either contain cryptic *miR-203* binding sites, or alternately are responsive to cellular changes driven by expression changes of actual *miR-203* targets. Further exploration of these transcripts is warranted and may provide insights into the mechanisms by which *miR-203* restricts tumorigenesis.

Interestingly the small number of targets identified by using *Ago2*-HITS-CLIP suggests that although *miR-203* is the most abundant miRNA in the skin, the high

abundance doesn't predict the regulatory capacity of the miRNA. However, this result may also be reflective of the low seed-pairing strength of the miR-203 seed, relative to other miRNAs, and the high seed target site abundance in the mouse transcriptome (Garcia et al., 2011). *miR-203's* seed is one of the most AU-rich seeds of all highly conserved miRNAs, which results in poor seed-pairing stability, but also inflates the number of possible targets in the transcriptome, due to the AU-rich nature of 3'UTRs. It therefore it is interesting to speculate that miR-203's abundant expression in keratinocytes may reflect the requirement for high levels of the miRNA to drive specific targeting over non-specific interactions.

Lastly, consistent with recent genome-wide studies on the impact of miRNA on mRNA levels and translation efficiency in mammals (Eichhorn et al., 2014; Guo et al., 2010), I found no evidence for changes in translational efficiency for the targets identified by either the meta-analysis or by Ago2-HITS-Clip (Figure 34). This result confirms the validity of using mRNA expression profiles as a tool to identify miRNA targets.

In summary, the results presented in this chapter demonstrate the utility of using multiple complementary approaches to identify miRNA targeting networks. Through the use of both gain of function and loss of function genome-wide profiling, I was able to identify transcripts whose expression is negatively correlated to miR-203 in different keratinocyte lineages. Additionally, by complementing the expression data with evidence for direct RISC association, a set of high-confidence miR-203 targets was identified, of which a subset have functions in the *Ras/Mapk* pathway. *Pola1* and *Hbegf* were validated by independent 3'UTR assays as being *miR-203* targets, and were

shown to be critical for keratinocyte expansion in culture. Taken together these results provide insights into the mechanism by which *miR-203* restricts keratinocyte expansion and likely identified *miR*-203 targets that additionally are regulated in other mammalian tissues.

CHAPTER 6

SUMMARY OF FINDINGS AND FUTURE DIRECTIONS

Oncogenic *Ras* has been extensively studied for decades, however, our understanding of the molecular mechanisms by which *Ras* drives tumorigenesis are continually evolving and being clarified. The discovery of the miRNA pathway as a new mechanism of post-transcriptional regulation has fueled research into the possibility that miRNAs may fill key gaps in our understanding about the mechanisms of Ras-driven tumorigenesis.

In this thesis I describe the identification and characterization of a tumor-suppressive miRNA antagonized by oncogenic *Ras* signaling in the skin. First, I demonstrate that activation of *Ras* in keratinocytes profoundly alters the transcriptome, while perturbing the expression of the most abundant miRNA in keratinocytes, *miR-203*. I then describe the generation and phenotypic analysis of a *miR-203* conditional knockout mouse model. Using this mouse model, I determined that *miR-203* was required during early embryonic development to maintain proper epidermal development. By next subjecting this mouse model to tumorigenic stress, I demonstrated that loss of miR-203 sensitized mice to skin tumorigenesis, further supporting a tumor suppressor role for miR-203 postulated by others and supported by studies in human cancers. Finally, by integrating multiple genome-wide datasets and implementing Ago2-HITS-CLIP, I was able to identify novel miRNA targets for miR-203 in keratinocytes. This approach faithfully recovered known targets and additionally identified a subset of targets with known functions in the *Ras/MAPK* pathway and in cell

division. In the next sections, I will place these results into the context of the literature and provide suggestions for future research endeavors motivated by my findings.

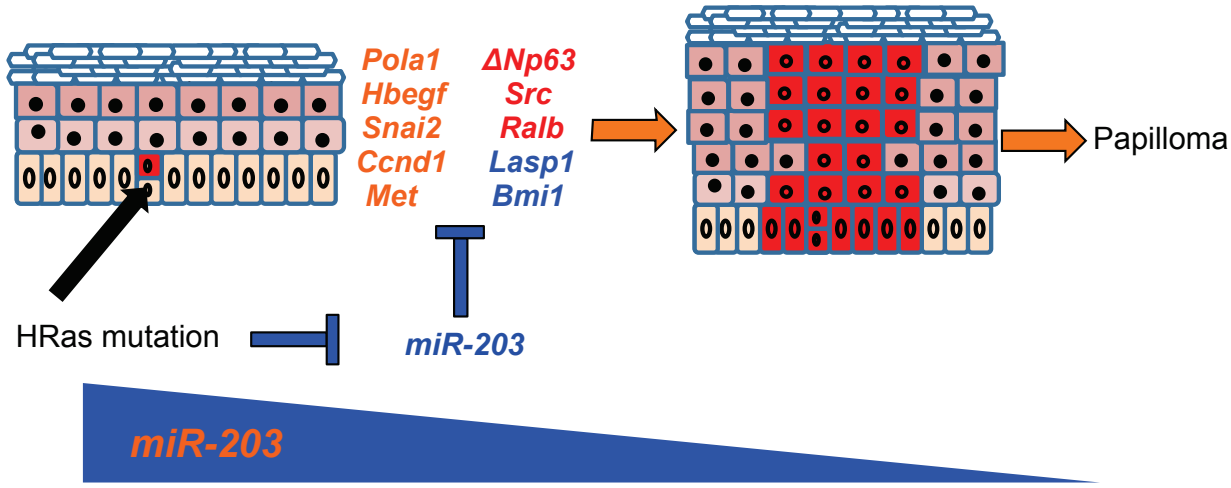

Figure 31. Summary of proposed functions for miR-203 in the regulation of skin tumorigenesis. *Selected miR-203* target genes identified by both *Ago2*-HITS-CLIP are indicated in orange, targets only found in HITS-CLIP in red, and those only found in the meta-analysis of the expression datasets in blue.

Genome-wide profiling of Oncogenic Ras initated keratinocytes:

By using a primary cell model to identify transcripts deregulated by oncogenic *Ras* I attempted to gain insights into the regulation of miRNA networks, as well as the dyanmics of 3'UTR usage driven by oncogenic RAS. The identification of these networks was also aimed at uncovering new insights into the tumorigenic initiated state that occurs *in* vivo upon *HRas* mutation. I discovered that only a handful of miRNAs are significantly regulated by Ras, including *miR-203, miR-205, miR-21*, and the *miR-23/24/27* cluster miRNAs. From these candidate miRNAs, I further investigated the expression of *miR-203* in mouse and human SCC tumors and demonstrated that *miR-203* is suppressed at early stages of SCC tumorigenesis.

Two important limitations of the approach taken in this thesis are worth discussing. First, the use of primary keratinocytes, while a tractable and accessible model for keratinocytes suffers from a problem of cellular heterogeneity. Within a keratinocyte primary culture, keratinocytes exist that span a continuum of differentiation states, which may lead to studying phenotypes and molecular events only occurring in a subpopulation of cells. Additionally, contaminating cell types, such as melanocytes can limit the faithful assignment of networks identified by genome-wide assays to the correct cell-type. Secondly, the activation of *Ras* in every cell in a cell culture does not model the initiated state established by oncogenic *Ras in vivo*, which begins with a single initiated keratinocyte. Oncogenic *Ras* can act through cell non-autonomous mechanism to modulate growth factor signaling of surrounding cells (Denning et al., 1996). Additionally, the normal surrounding cells likely influence the phenotype of the initiated keratinocyte. The clonal expansion of the initiated keratinocyte upon TPA treatment occurs in a stochastic manner in which some clones go on to form papillomas and others are rapidly lost to differentiation (Driessens et al., 2012). Identifying the cellular and molecular mechanisms that regulate these states would provide great insights into how *Ras* mutations drive skin tumorigenesis.

The use of flow-cytometry methods combined with transgenic mouse models expressing lineage specific markers would greatly aid obtaining relevant *in vivo* datasets to compliment the datasets generated in this thesis. A very compelling follow-up experiment could be focused on identifying the transcriptomic effects of oncogenic *Ras* on specific stem-cell lineages in the skin. The cellular origin of DMBA/TPA tumors can be both short-lived epidermal progenitors, long-lived hair follicle stem cells, and

differentiated suprabasal keratinocytes (Lapouge et al., 2011; White et al., 2011). While all of these cells are competent for tumorigenesis, the hair follicle stem cell are more prone to malignant tumorigenesis than epidermal counterparts, and the suprabasal cells are only capable of establishing benign tumors. By profiling the short-term effects of oncogenic Ras on these *in vivo* lineages, many additional insights are likely to be discovered about the nature of the initiated tumorigenic state established by oncogenic Ras.

Nevertheless, the datasets described in this thesis provide an important contribution to the field as not only the first published miRNA and mRNA-Seq dataset to dissect the impact of *Ras* on the primary keratinocyte transcriptome, but also by providing a wealth of potential novel target genes downstream of *Ras* that may contribute to instructing its cellular functions.

Generation of a miR-203 conditional mouse model to study its functions in skin development

In Chapter three, I described the generation of a *miR-203* knockout mouse. In this Chapter I used this conditional knockout mouse model to study *miR-203's* role in epidermal development. My findings demonstrate that *miR-203* is dispensable for epidermal homeostasis in the postnatal mouse, yet uncovered an early function for *miR-203* in restricting epidermal expansion during development.

Many researchers in the *miR-203* field will see these results as largely confirmatory. The previous studies done with antagomiR injections to inhibit *miR-203*, demonstrated a role for *miR-203* in restricting keratinocyte proliferation (Yi et al., 2008), albeit with a much more dramatic phenotype than the phenotype described in this

thesis. However, it is important to clarify that although the phenotype we observe is consistent with previous studies and hypothesized functions, the results presented in this thesis provide a more nuanced view of *miR-203's* role in regulation of epidermal proliferation. First, *miR-203* loss only impacted early epidermal development, whereas *miR-203* was not required for during adult homeostasis. Secondly, in culture *miR-203* loss of function results in defects in controlling keratinocyte expansion, suggesting that in highly proliferative conditions, such as cell culture, *miR-203's* function becomes more prominent than during normal homeostasis. These results are reminiscent of observations made with *p21*, *p27*, and *p53* knockouts (Guinea-Viniegra et al., 2012; Missero et al., 1996). Finally, no defects in other tissue and organs systems have been found to date, suggesting that the findings present here in the analysis of *miR-203's* function in the skin may be applicable to other tissues as well.

With this mouse model in hand, there are many additional avenues to explore. My work did not specifically focus on other more subtle processes that *miR-203* could control. For example, *miR-203* is expressed in the companion layer of the hair follicle, a region thought to function as a niche for hair follicle stem cells (Hsu et al., 2011; Jackson et al., 2013). One could speculate that hair follicle cycling and stem cell dynamics of the HFSCs could be perturbed by loss of *miR-203*, a process that I did not explore in depth. Another important line of experiments would be assessing the function of *miR-203* in wound healing. It is known that miR-203's expression is dynamic in healing wounds, and lost in the leading edge keratinocytes that migrate to repair the wound (Viticchie et al., 2012) (unpublished observations K.R.). Also *miR-203* has been associated with EMT processes, suggesting that the re-epithelization of a wound may

be perturbed without *miR-203* (Taube et al., 2013). Additionally, such studies could be complemented with functional studies of a miRNA biogenesis factor knockout (e.g. *Dicer* or *Dgcr8)*, and quantitative expression profiling to determine other miRNAs involved in this process.

Analysis of the function of miR-203 in skin tumorigenesis :

Motivated by the findings in Chapter 2 that *miR-203* was strongly suppressed by oncogenic *Ras* and reduced in SCC tumors, I was motivated to study *miR-203's* role in skin carcinogenesis. In Chapter Four, I demonstrated that *miR-203* loss of function sensitized mice to skin chemical carcinogenesis. Furthermore, I provided evidence that *miR-203* impacted tumor initiation, not later processes such as tumor promotion or conversion to malignancy.

miR-203 has been hypothesized to be a tumor suppressor for many years (Lena et al., 2008; Yi et al., 2008). Because *miR-203* is commonly found downregulated in human cancers, much of the experimental evidence for *miR-203* as a tumor suppressor has come from gain of function overexpression experiments. These approaches have demonstrated strong tumor suppression by *miR-203* in many cancer cell lines (Benaich et al., 2014; Wellner et al., 2009). However, the observation that *miR-203* function is reduced in human cancers begs the question of how important loss of *miR-203* is to tumor development. The results that I've presented using a mouse model of *miR-203* knock out demonstrate that loss of *miR-203* does not cause spontaneous tumorigenesis in mice (up to 18 months old, data not shown). On this basis alone the tumor suppressive properties of *miR-203* are mild in comparison with those of loss of *p53* for example (Lyle et al., 2014). *miR-203* loss therefore is not sufficient to initiate

tumorigenesis, instead my data argues that the downregulation of *miR-203* is required for oncogenic Ras to promote tumorigenesis. This finding is nicely complemented with studies of *miR-203* function in later stages of tumorigenesis, when *miR-203* is further reduced in expression, which show that endogenous *miR-203* can suppress metastasis in xenograft models (Benaich et al., 2014).

Moving forward, this conditional mouse model will serve as a resource to address miR-203s role in additional cancers. *miR-203* has been reported to be a tumor suppressor in both prostate and mammary tissue, yet a mouse model to test this hypothesis and study it mechanistically has not be utilized (Taube et al., 2013; Viticchiè et al., 2011). Additionally, as these cancers can be initiated without the use of oncogenic Ras, the study of these cancers may provide further insights into *miR-203s* role in tumorigenesis driven by other oncogenic pathways.

Identification of miR-203 targets via genome-wide expression profiling and Ago2-HITS-CLIP:

In Chapter Five, I sought to identify novel targets of *miR-203* to provide insights into its function in skin tumorigenesis and development. By using both genome-wide profiling techniques and *Ago2*-HITS-CLIP, I identified a group of high-confidence targets with known functions in the *Ras/Mapk* pathways and cell division.

The approach taken to identify *miR-203* targets was mainly driven by the very minor perturbations to the transcriptome observed in single profiling datasets. Using a single dataset would produce a low quality target dataset therefore it was unlikely that I would identify new insights about *miR-203* targets. Secondly, the minor perturbations initially observed prompted me to perform *Ago2*-HITS-CLIP, which would allow the

identification of direct *miR-203* targets, without relying on expression profiling. The genomics approach taken in this thesis would not likely be required for other miRNAs whose loss of function phenotype is more strong, and whose targeted transcript display strong regulation by the miRNA (e.g. *miR-205)* (Wang et al., 2013a).

With the development of the bioinformatics and experimental protocols for conducting Ago2-*HITS-CLIP,* many new exciting future research directions can be explored. Recently, a method of differential HITS-CLIP was developed that compares *Ago* binding profiles between wild-type and miRNA null samples (Loeb et al., 2012). By identifying those binding sites lost upon ablation of a miRNA, the direct targets of a miRNA can be identified without relying on computational identification of seed-sequence matches. This method requires a large number of replicates (n=12 samples per genotype), but would be ideally suitable to identify the targets of many miRNAs in the skin, for which knockout models have been generated. Additionally, by applying HITS-CLIP to different cellular states, such as the *Ras*-initiated keratinocyte, the regulatory targets of many miRNAs can be inferred, which would greatly aid the computational identification of miRNA targets based on expression profiling.

Summary

In this thesis I have investigated the miRNA-based mechanisms by which oncogenic *Ras* drives skin cancer in a mouse model. I performed genome-wide profiling experiments to define the mRNA and miRNA landscape regulated by oncogenic *Ras.* From these datasets I identified *miR-203* as strongly suppressed by oncogenic *Ras.* I characterized a conditional *miR-203* knockout mouse model and demonstrate that loss of *miR-203* perturbs epidermal embryonic development and sensitizes skin to chemical

carcinogenesis. In order to identify novel mechanisms by which *miR-203* restricts tumorigenesis, I utilized genome-wide expression profiling and *Ago2*-HITS-CLIP to identify high confidence *miR-203* targets. From these studies I identified novel *miR-203* targets, a subset of which that are involved in regulation of *Ras/MAPK* signaling and cell division. These findings establish a tumor suppressive function for *miR-203* that operates in murine skin.

REFERENCES

Abel, E.L., Angel, J.M., Kiguchi, K., and DiGiovanni, J. (2009). Multi-stage chemical carcinogenesis in mouse skin: Fundamentals and applications. Nat. Protoc. *4*, 1350–1362.

Ahmed, M.I., Alam, M., Emelianov, V.U., Poterlowicz, K., Patel, A., Sharov, A.A., Mardaryev, A.N., and Botchkareva, N.V. (2014). MicroRNA-214 controls skin and hair follicle development by modulating the activity of the Wnt pathway. J. Cell Biol. *207*, 549–567.

Alam, M., and Ratner, D. (2001). Cutaneous squamous-cell carcinoma. N. Engl. J. Med. *344*, 975–983.

Alexa, A., and Rahnenfuhrer, J. (2010). topGO: Enrichment analysis for Gene Ontology. R Package *2.18.0*.

Alexa, A., Rahnenfuhrer, J., and Lengauer, T. (2006). Improved scoring of functional groups from gene expression data by decorrelating GO graph structure. Bioinformatics *22*, 1600–1607.

Alexiou, P., Maragkakis, M., Papadopoulos, G.L., Reczko, M., and Hatzigeorgiou, A.G. (2009). Lost in translation: an assessment and perspective for computational microRNA target identification. Bioinformatics *25*, 3049–3055.

Altschul, S.F., Madden, T.L., Schäffer, A.A., Zhang, J., Zhang, Z., Miller, W., and Lipman, D.J. (1997). Gapped BLAST and PSI-BLAST: a new generation of protein database search programs. Nucleic Acids Res. *25*, 3389–3402.

Alvarez-Saavedra, E., and Horvitz, H.R. (2010). Many families of C. elegans microRNAs are not essential for development or viability. Curr. Biol. CB *20*, 367–373.

Amelio, I., Lena, A.M., Viticchiè, G., Shalom-Feuerstein, R., Terrinoni, A., Dinsdale, D., Russo, G., Fortunato, C., Bonanno, E., Spagnoli, L.G., et al. (2012). miR-24 triggers epidermal differentiation by controlling actin adhesion and cell migration. J. Cell Biol. *199*, 347–363.

Amelio, I., Lena, A.M., Bonanno, E., Melino, G., and Candi, E. (2013). miR-24 affects hair follicle morphogenesis targeting Tcf-3. Cell Death Dis. *4*, e922.

Anders, S., Reyes, A., and Huber, W. (2012). Detecting differential usage of exons from RNA-seq data. Genome Res. *22*, 2008–2017.

Andl, T., Murchison, E.P., Liu, F., Zhang, Y., Yunta-Gonzalez, M., Tobias, J.W., Andl, C.D., Seykora, J.T., Hannon, G.J., and Millar, S.E. (2006). The miRNA-processing

enzyme dicer is essential for the morphogenesis and maintenance of hair follicles. Curr. Biol. *16*, 1041–1049.

Bader, A.G., and Lammers, P. (2011). The therapeutic potential of microRNAs. Innov. Pharm. Technol. 52–55.

Bailleul, B., Surani, M.A., White, S., Barton, S.C., Brown, K., Blessing, M., Jorcano, J., and Balmain, A. (1990). Skin hyperkeratosis and papilloma formation in transgenic mice expressing a ras oncogene from a suprabasal keratin promoter. Cell *62*, 697–708.

Balmain, A. (2014). Milestones in Skin Carcinogenesis: The Biology of Multistage Carcinogenesis. J. Invest. Dermatol.

Bartel, D.P. (2009). MicroRNAs: target recognition and regulatory functions. Cell *136*, 215–233.

Bazzini, A.A., Lee, M.T., and Giraldez, A.J. (2012). Ribosome profiling shows that miR-430 reduces translation before causing mRNA decay in zebrafish. Science *336*, 233–237.

Bejarano, F., Bortolamiol-Becet, D., Dai, Q., Sun, K., Saj, A., Chou, Y.-T., Raleigh, D.R., Kim, K., Ni, J.-Q., Duan, H., et al. (2012). A genome-wide transgenic resource for conditional expression of Drosophila microRNAs. Development *139*, 2821–2831.

Benaich, N., Woodhouse, S., Goldie, S.J., Mishra, A., Quist, S.R., and Watt, F.M. (2014). Rewiring of an Epithelial Differentiation Factor, miR-203, to Inhibit Human Squamous Cell Carcinoma Metastasis. Cell Rep. *9*, 104–117.

Berezikov, E. (2011). Evolution of microRNA diversity and regulation in animals. Nat. Rev. Genet. *12*, 846–860.

Bernstein, E., Caudy, A.A., Hammond, S.M., and Hannon, G.J. (2001). Role for a bidentate ribonuclease in the initiation step of RNA interference. Nature *409*, 363–366.

Bild, A.H., Yao, G., Chang, J.T., Wang, Q., Potti, A., Chasse, D., Joshi, M.-B., Harpole, D., Lancaster, J.M., Berchuck, A., et al. (2006). Oncogenic pathway signatures in human cancers as a guide to targeted therapies. Nature *439*, 353–357.

Blanpain, C., and Fuchs, E. (2006). Epidermal stem cells of the skin. Annu. Rev. Cell Dev. Biol. *22*, 339.

Blanpain, C., and Fuchs, E. (2009). Epidermal homeostasis: a balancing act of stem cells in the skin. Nat. Rev. Mol. Cell Biol. *10*, 207–217.

Boiko, A.D., Porteous, S., Razorenova, O.V., Krivokrysenko, V.I., Williams, B.R., and Gudkov, A.V. (2006). A systematic search for downstream mediators of tumor suppressor function of p53 reveals a major role of BTG2 in suppression of Ras-induced transformation. Genes Dev. *20*, 236–252.

Bornachea, O., Santos, M., Martínez-Cruz, A.B., García-Escudero, R., Dueñas, M., Costa, C., Segrelles, C., Lorz, C., Buitrago, A., Saiz-Ladera, C., et al. (2012). EMT and induction of miR-21 mediate metastasis development in Trp53-deficient tumours. Sci. Rep. *2*.

Boumahdi, S., Driessens, G., Lapouge, G., Rorive, S., Nassar, D., Le Mercier, M., Delatte, B., Caauwe, A., Lenglez, S., Nkusi, E., et al. (2014). SOX2 controls tumour initiation and cancer stem-cell functions in squamous-cell carcinoma. Nature *511*, 246–250.

Bourcier, C. (2006). p44 Mitogen-Activated Protein Kinase (Extracellular Signal-Regulated Kinase 1)-Dependent Signaling Contributes to Epithelial Skin Carcinogenesis. Cancer Res. *66*, 2700–2707.

Brown, K., Quintanilla, M., Ramsden, M., Kerr, I.B., Young, S., and Balmain, A. (1986). v-ras genes from harvey and BALB murine sarcoma viruses can act as initiators of two-stage mouse skin carcinogenesis. Cell *46*, 447–456.

Brown, K., Buchmann, A., and Balmain, A. (1990). Carcinogen-induced mutations in the mouse c-Ha-ras gene provide evidence of multiple pathways for tumor progression. Proc. Natl. Acad. Sci. *87*, 538–542.

Bueno, M.J., Pérez de Castro, I., Gómez de Cedrón, M., Santos, J., Calin, G.A., Cigudosa, J.C., Croce, C.M., Fernández-Piqueras, J., and Malumbres, M. (2008). Genetic and Epigenetic Silencing of MicroRNA-203 Enhances ABL1 and BCR-ABL1 Oncogene Expression. Cancer Cell *13*, 496–506.

Byrne, C., Tainsky, M., and Fuchs, E. (1994). Programming gene expression in developing epidermis. Development *120*, 2369–2383.

Calin, G.A., Dumitru, C.D., Shimizu, M., Bichi, R., Zupo, S., Noch, E., Aldler, H., Rattan, S., Keating, M., Rai, K., et al. (2002). Frequent deletions and down-regulation of micro-RNA genes miR15 and miR16 at 13q14 in chronic lymphocytic leukemia. Proc. Natl. Acad. Sci. *99*, 15524–15529.

Calin, G.A., Sevignani, C., Dumitru, C.D., Hyslop, T., Noch, E., Yendamuri, S., Shimizu, M., Rattan, S., Bullrich, F., Negrini, M., et al. (2004). Human microRNA genes are frequently located at fragile sites and genomic regions involved in cancers. Proc. Natl. Acad. Sci. U. S. A. *101*, 2999–3004.

Chekulaeva, M., Mathys, H., Zipprich, J.T., Attig, J., Colic, M., Parker, R., and Filipowicz, W. (2011). miRNA repression involves GW182-mediated recruitment of CCR4–NOT through conserved W-containing motifs. Nat. Struct. Mol. Biol. *18*, 1218–1226.

Cheng, N. (2014). miR‐203 inhibits tumor cell migration and invasion via caveolin‐1 in pancreatic cancer cells. Oncol. Lett.

Cheng, C., Kilkenny, A.E., Roop, D., and Yuspa, S.H. (1990). The v-ras oncogene inhibits the expression of differentiation markers and facilitates expression of cytokeratins 8 and 18 in mouse keratinocytes. Mol. Carcinog. *3*, 363–373.

Chhabra, R., Dubey, R., and Saini, N. (2010). Cooperative and individualistic functions of the microRNAs in the miR-23a~ 27a~ 24-2 cluster and its implication in human diseases. Mol. Cancer *9*, 232.

Chi, S.W., Zang, J.B., Mele, A., and Darnell, R.B. (2009). Argonaute HITS-CLIP decodes microRNA-mRNA interaction maps. Nature *460*, 479–486.

Chi, S.W., Hannon, G.J., and Darnell, R.B. (2012). An alternative mode of microRNA target recognition. Nat. Struct. Mol. Biol. *19*, 321–327.

Christophe Cataisson, and Yuspa, S.H. (2011). Interacting Signaling Pathways in Mouse Skin Tumor Initiation and Progression. Signal. Pathw. Squamous Cancer 149–164.

Cimmino, A., Calin, G.A., Fabbri, M., Iorio, M.V., Ferracin, M., Shimizu, M., Wojcik, S.E., Aqeilan, R.I., Zupo, S., Dono, M., et al. (2005). miR-15 and miR-16 induce apoptosis by targeting BCL2. Proc. Natl. Acad. Sci. U. S. A. *102*, 13944–13949.

Clayton, E., Doupé, D.P., Klein, A.M., Winton, D.J., Simons, B.D., and Jones, P.H. (2007). A single type of progenitor cell maintains normal epidermis. Nature *446*, 185–189.

Cotsarelis, G., Sun, T.-T., and Lavker, R.M. (1990). Label-retaining cells reside in the bulge area of pilosebaceous unit: implications for follicular stem cells, hair cycle, and skin carcinogenesis. Cell *61*, 1329–1337.

Darido, C., Georgy, S.R., Wilanowski, T., Dworkin, S., Auden, A., Zhao, Q., Rank, G., Srivastava, S., Finlay, M.J., Papenfuss, A.T., et al. (2011). Targeting of the tumor suppressor GRHL3 by a miR-21-dependent proto-oncogenic network results in PTEN loss and tumorigenesis. Cancer Cell *20*, 635–648.

Denning, M.F., Dlugosz, A.A., Threadgill, D.W., Magnuson, T., and Yuspa, S.H. (1996). Activation of the epidermal growth factor receptor signal transduction pathway stimulates tyrosine phosphorylation of protein kinase C delta. J. Biol. Chem. *271*, 5325–5331.

Der, C.J., Krontiris, T.G., and Cooper, G.M. (1982). Transforming genes of human bladder and lung carcinoma cell lines are homologous to the ras genes of Harvey and Kirsten sarcoma viruses. Proc. Natl. Acad. Sci. *79*, 3637–3640.

Ding, X.C., and Grobhans, H. (2009). Repression of C. elegans microRNA targets at the initiation level of translation requires GW182 proteins. EMBO J. *28*, 213–222.

Ding, X., Park, S.I., McCauley, L.K., and Wang, C.-Y. (2013). Signaling between transforming growth factor β (TGF-β) and transcription factor SNAI2 represses expression of microRNA miR-203 to promote epithelial-mesenchymal transition and tumor metastasis. J. Biol. Chem. *288*, 10241–10253.

Djuranovic, S., Nahvi, A., and Green, R. (2012). miRNA-mediated gene silencing by translational repression followed by mRNA deadenylation and decay. Science *336*, 237–240.

Dlugosz, A.A., Hansen, L., Cheng, C., Alexander, N., Denning, M.F., Threadgill, D.W., Magnuson, T., Coffey Jr, R.J., and Yuspa, S.H. (1997). Targeted disruption of the epidermal growth factor receptor impairs growth of squamous papillomas expressing the v-rasHa oncogene but does not block in vitro keratinocyte responses to oncogenic ras. Cancer Res. *57*, 3180–3188.

Downward, J. (2003). Targeting RAS signalling pathways in cancer therapy. Nat. Rev. Cancer *3*, 11–22.

Driessens, G., Beck, B., Caauwe, A., Simons, B.D., and Blanpain, C. (2012). Defining the mode of tumour growth by clonal analysis. Nature *488*, 527–530.

Durchdewald, M., Guinea-Viniegra, J., Haag, D., Riehl, A., Lichter, P., Hahn, M., Wagner, E.F., Angel, P., and Hess, J. (2008). Podoplanin Is a Novel Fos Target Gene in Skin Carcinogenesis. Cancer Res. *68*, 6877–6883.

Van Duuren, B.L., Sivak, A., Katz, C., Seidman, I., and Melchionne, S. (1975). The Effect of Aging and Interval between Primary and Secondary Treatment in Two-Stage Carcinogenesis on Mouse Skin. Cancer Res. *35*, 502–505.

Ebert, M.S., and Sharp, P.A. (2012). Roles for microRNAs in conferring robustness to biological processes. Cell *149*, 515–524.

Ehrenreiter, K., Kern, F., Velamoor, V., Meissl, K., Galabova-Kovacs, G., Sibilia, M., and Baccarini, M. (2009). Raf-1 Addiction in Ras-Induced Skin Carcinogenesis. Cancer Cell *16*, 149–160.

Eichhorn, S.W., Guo, H., McGeary, S.E., Rodriguez-Mias, R.A., Shin, C., Baek, D., Hsu, S.-H., Ghoshal, K., Villén, J., and Bartel, D.P. (2014). mRNA destabilization is the dominant effect of mammalian microRNAs by the time substantial repression ensues. Mol. Cell *56*, 104–115.

Eisen, M.B., Spellman, P.T., Brown, P.O., and Botstein, D. (1998). Cluster analysis and display of genome-wide expression patterns. Proc. Natl. Acad. Sci. *95*, 14863–14868.

Frezzetti, D., De Menna, M., Zoppoli, P., Guerra, C., Ferraro, A., Bello, A.M., De Luca, P., Calabrese, C., Fusco, A., and Ceccarelli, M. (2010). Upregulation of miR-21 by Ras in vivo and its role in tumor growth. Oncogene *30*, 275–286.

Furuta, M., Kozaki, K., Tanaka, S., Arii, S., Imoto, I., and Inazawa, J. (2010). miR-124 and miR-203 are epigenetically silenced tumor-suppressive microRNAs in hepatocellular carcinoma. Carcinogenesis *31*, 766–776.

Garcia, D.M., Baek, D., Shin, C., Bell, G.W., Grimson, A., and Bartel, D.P. (2011). Weak seed-pairing stability and high target-site abundance decrease the proficiency of lsy-6 and other microRNAs. Nat Struct Mol Biol *18*, 1139–1146.

Garofalo, M., Romano, G., Leva, G.D., Nuovo, G., Jeon, Y.-J., Ngankeu, A., Sun, J., Lovat, F., Alder, H., Condorelli, G., et al. (2012). EGFR and MET receptor tyrosine kinase-altered microRNA expression induces tumorigenesis and gefitinib resistance in lung cancers. Nat. Med. *18*, 74–82.

Greenberg, J.R. (1979). Ultraviolet light-induced crosslinking of mRNA to proteins. Nucleic Acids Res. *6*, 715–732.

Grimson, A., Farh, K.K.-H., Johnston, W.K., Garrett-Engele, P., Lim, L.P., and Bartel, D.P. (2007). MicroRNA Targeting Specificity in Mammals: Determinants beyond Seed Pairing. Mol. Cell *27*, 91–105.

Gu, S., Jin, L., Zhang, F., Sarnow, P., and Kay, M.A. (2009). Biological basis for restriction of microRNA targets to the 3′ untranslated region in mammalian mRNAs. Nat. Struct. 38 Mol. Biol. *16*, 144–150.

Guinea-Viniegra, J., Zenz, R., Scheuch, H., Jiménez, M., Bakiri, L., Petzelbauer, P., and Wagner, E.F. (2012). Differentiation-induced skin cancer suppression by FOS, p53, and TACE/ADAM17. J. Clin. Invest. *122*, 2898–2910.

Guo, H., Ingolia, N.T., Weissman, J.S., and Bartel, D.P. (2010). Mammalian microRNAs predominantly act to decrease target mRNA levels. Nature *466*, 835–840.

Guo, S., Bai, H., Megyola, C.M., Halene, S., Krause, D.S., Scadden, D.T., and Lu, J. (2012). Complex oncogene dependence in microRNA-125a-induced myeloproliferative neoplasms. Proc. Natl. Acad. Sci. *109*, 16636–16641.

Guy, G.P., Machlin, S.R., Ekwueme, D.U., and Yabroff, K.R. (2015). Prevalence and Costs of Skin Cancer Treatment in the U.S., 2002−2006 and 2007−2011. Am. J. Prev. Med. *48*, 183–187.

Guzmán, C., Bagga, M., Kaur, A., Westermarck, J., and Abankwa, D. (2014). ColonyArea: An ImageJ Plugin to Automatically Quantify Colony Formation in Clonogenic Assays. PLoS ONE *9*, e92444.

Ha, M., and Kim, V.N. (2014). Regulation of microRNA biogenesis. Nat. Rev. Mol. Cell Biol. *15*, 509–524.

Halfar, K., Rommel, C., Stocker, H., and Hafen, E. (2001). Ras controls growth, survival and differentiation in the Drosophila eye by different thresholds of MAP kinase activity. Development *128*, 1687–1696.

He, L., Thomson, J.M., Hemann, M.T., Hernando-Monge, E., Mu, D., Goodson, S., Powers, S., Cordon-Cardo, C., Lowe, S.W., Hannon, G.J., et al. (2005). A microRNA polycistron as a potential human oncogene. Nature *435*, 828–833.

He, L., He, X., Lim, L.P., de Stanchina, E., Xuan, Z., Liang, Y., Xue, W., Zender, L., Magnus, J., Ridzon, D., et al. (2007). A microRNA component of the p53 tumour suppressor network. Nature *447*, 1130–1134.

Heinz, S., Benner, C., Spann, N., Bertolino, E., Lin, Y.C., Laslo, P., Cheng, J.X., Murre, C., Singh, H., and Glass, C.K. (2010). Simple Combinations of Lineage-Determining Transcription Factors Prime cis-Regulatory Elements Required for Macrophage and B Cell Identities. Mol. Cell *38*, 576–589.

Hockensmith, J.W., Kubasek, W.L., Vorachek, W.R., and von Hippel, P.H. (1986). Laser cross-linking of nucleic acids to proteins. Methodology and first applications to the phage T4 DNA replication system. J. Biol. Chem. *261*, 3512–3518.

Hsu, Y.-C., Pasolli, H.A., and Fuchs, E. (2011). Dynamics between Stem Cells, Niche, and Progeny in the Hair Follicle. Cell *144*, 92–105.

Huang, D.W., Sherman, B.T., and Lempicki, R.A. (2008). Systematic and integrative analysis of large gene lists using DAVID bioinformatics resources. Nat. Protoc. *4*, 44–57.

Huelsken, J., Vogel, R., Erdmann, B., Cotsarelis, G., and Birchmeier, W. (2001). β-Catenin controls hair follicle morphogenesis and stem cell differentiation in the skin. Cell *105*, 533–545.

Huse, J.T., Brennan, C., Hambardzumyan, D., Wee, B., Pena, J., Rouhanifard, S.H., Sohn-Lee, C., le Sage, C., Agami, R., Tuschl, T., et al. (2009). The PTEN-regulating microRNA miR-26a is amplified in high-grade glioma and facilitates gliomagenesis in vivo. Genes Dev. *23*, 1327–1337.

Hutvagner, G., and Simard, M.J. (2008). Argonaute proteins: key players in RNA silencing. Nat. Rev. Mol. Cell Biol. *9*, 22–32.

Ise, K., Nakamura, K., Nakao, K., Shimizu, S., Harada, H., Ichise, T., Miyoshi, J., Gondo, Y., Ishikawa, T., Aiba, A., et al. (2000). Targeted deletion of the H-ras gene decreases tumor formation in mouse skin carcinogenesis. Oncogene *19*, 2951–2956.

Jackson, S.J., Zhang, Z., Feng, D., Flagg, M., O'Loughlin, E., Wang, D., Stokes, N., Fuchs, E., and Yi, R. (2013). Rapid and widespread suppression of self-renewal by microRNA-203 during epidermal differentiation. Development *140*, 1882–1891.

Jiang, Z., Yu, N., Kuang, P., Chen, M., Shao, F., Martin, G., Chui, D.H.K., Cardoso, W.V., Ai, X., and Lü, J. (2012). Trinucleotide Repeat Containing 6a (Tnrc6a)-mediated MicroRNA Function Is Required for Development of Yolk Sac Endoderm. J. Biol. Chem. *287*, 5979–5987.

Johnson, S.M., Grosshans, H., Shingara, J., Byrom, M., Jarvis, R., Cheng, A., Labourier, E., Reinert, K.L., Brown, D., and Slack, F.J. (2005). RAS Is Regulated by the let-7 MicroRNA Family. Cell *120*, 635–647.

Jones-Rhoades, M.W., and Bartel, D.P. (2004). Computational identification of plant microRNAs and their targets, including a stress-induced miRNA. Mol. Cell *14*, 787–799.

Karlsson, R., Pedersen, E.D., Wang, Z., and Brakebusch, C. (2009). Rho GTPase function in tumorigenesis. Biochim. Biophys. Acta BBA - Rev. Cancer *1796*, 91–98.

Karnoub, A.E., and Weinberg, R.A. (2008). Ras oncogenes: split personalities. Nat. Rev. Mol. Cell Biol. *9*, 517–531.

Kemp, C. (2005). Multistep skin cancer in mice as a model to study the evolution of cancer cells. Semin. Cancer Biol. *15*, 460–473.

Kent, O.A., Chivukula, R.R., Mullendore, M., Wentzel, E.A., Feldmann, G., Lee, K.H., Liu, S., Leach, S.D., Maitra, A., and Mendell, J.T. (2010). Repression of the miR-143/145 cluster by oncogenic Ras initiates a tumor-promoting feed-forward pathway. Genes Dev. *24*, 2754–2759.

Kim, V.N. (2005). MicroRNA biogenesis: coordinated cropping and dicing. Nat. Rev. Mol. Cell Biol. *6*, 376–385.

Koster, M.I. (2010). p63 in Skin Development and Ectodermal Dysplasias. J. Invest. Dermatol. *130*, 2352–2358.

Koster, M.I., and Roop, D.R. (2007). Mechanisms regulating epithelial stratification. Annu Rev Cell Dev Biol *23*, 93–113.

Kozaki, K., Imoto, I., Mogi, S., Omura, K., and Inazawa, J. (2008). Exploration of Tumor-Suppressive MicroRNAs Silenced by DNA Hypermethylation in Oral Cancer. Cancer Res. *68*, 2094–2105.

Kretzschmar, K., Cottle, D.L., Donati, G., Chiang, M.-F., Quist, S.R., Gollnick, H.P., Natsuga, K., Lin, K.-I., and Watt, F.M. (2014). BLIMP1 Is Required for Postnatal Epidermal Homeostasis but Does Not Define a Sebaceous Gland Progenitor under Steady-State Conditions. Stem Cell Rep. *3*, 620–633.

Kumar, M.S., Pester, R.E., Chen, C.Y., Lane, K., Chin, C., Lu, J., Kirsch, D.G., Golub, T.R., and Jacks, T. (2009). Dicer1 functions as a haploinsufficient tumor suppressor. Genes Dev. *23*, 2700–2704.

Lai, E.C. (2002). Micro RNAs are complementary to 3′ UTR sequence motifs that mediate negative post-transcriptional regulation. Nat. Genet. *30*, 363–364.

Landgraf, P., Rusu, M., Sheridan, R., Sewer, A., Iovino, N., Aravin, A., Pfeffer, S., Rice, A., Kamphorst, A.O., and Landthaler, M. (2007). A mammalian microRNA expression atlas based on small RNA library sequencing. Cell *129*, 1401–1414.

Lapouge, G., Youssef, K.K., Vokaer, B., Achouri, Y., Michaux, C., Sotiropoulou, P.A., and Blanpain, C. (2011). Identifying the cellular origin of squamous skin tumors. Proc. Natl. Acad. Sci. *108*, 7431–7436.

Lawrence, M.S., Sougnez, C., Lichtenstein, L., Cibulskis, K., Lander, E., Gabriel, S.B., Getz, G., Ally, A., Balasundaram, M., Birol, I., et al. (2015). Comprehensive genomic characterization of head and neck squamous cell carcinomas. Nature *517*, 576–582.

Le, M.T.N., Teh, C., Shyh-Chang, N., Xie, H., Zhou, B., Korzh, V., Lodish, H.F., and Lim, B. (2009). MicroRNA-125b is a novel negative regulator of p53. Genes Dev. *23*, 862–876.

Lechler, T., and Fuchs, E. (2005). Asymmetric cell divisions promote stratification and differentiation of mammalian skin. Nature *437*, 275–280.

Lee, R.C., Feinbaum, R.L., and Ambros, V. (1993). The C. elegans heterochronic gene lin-4 encodes small RNAs with antisense complementarity to lin-14. Cell *75*, 843–854.

Lee, Y., Ahn, C., Han, J., Choi, H., Kim, J., Yim, J., Lee, J., Provost, P., R\a admark, O., Kim, S., et al. (2003). The nuclear RNase III Drosha initiates microRNA processing. Nature *425*, 415–419.

Lee, Y., Kim, M., Han, J., Yeom, K.-H., Lee, S., Baek, S.H., and Kim, V.N. (2004). MicroRNA genes are transcribed by RNA polymerase II. EMBO J. *23*, 4051–4060.

Lehman, I.R., and Kaguni, L.S. (1989). DNA polymerase alpha. J. Biol. Chem. *264*, 4265–4268.

Lena, A.M., Shalom-Feuerstein, R., di Val Cervo, P.R., Aberdam, D., Knight, R.A., Melino, G., and Candi, E. (2008). miR-203 represses “stemness” by repressing ΔNp63. Cell Death Differ. *15*, 1187–1195.

Leung, A.K.L., Young, A.G., Bhutkar, A., Zheng, G.X., Bosson, A.D., Nielsen, C.B., and Sharp, P.A. (2011). Genome-wide identification of Ago2 binding sites from mouse embryonic stem cells with and without mature microRNAs. Nat. Struct. Mol. Biol. *18*, 237–244.

Lewis, B.P., Shih, I. -hun., Jones-Rhoades, M.W., Bartel, D.P., and Burge, C.B. (2003). Prediction of mammalian microRNA targets. Cell *115*, 787–798.

Li, J., Chen, Y., Zhao, J., Kong, F., and Zhang, Y. (2011). miR-203 reverses chemoresistance in p53-mutated colon cancer cells through downregulation of Akt2 expression. Cancer Lett. *304*, 52–59.

Li, P., He, Q., Luo, C., and Qian, L. (2015). Differentially Expressed miRNAs in Acute Wound Healing of the Skin: A Pilot Study. Medicine (Baltimore) *94*, e458.

Li, Y., Choi, P.S., Casey, S.C., Dill, D.L., and Felsher, D.W. (2014). MYC through miR-17-92 Suppresses Specific Target Genes to Maintain Survival, Autonomous Proliferation, and a Neoplastic State. Cancer Cell *26*, 262–272.

Lianoglou, S., Garg, V., Yang, J.L., Leslie, C.S., and Mayr, C. (2013). Ubiquitously transcribed genes use alternative polyadenylation to achieve tissue-specific expression. Genes Dev. *27*, 2380–2396.

Licatalosi, D.D., Mele, A., Fak, J.J., Ule, J., Kayikci, M., Chi, S.W., Clark, T.A., Schweitzer, A.C., Blume, J.E., and Wang, X. (2008). HITS-CLIP yields genome-wide insights into brain alternative RNA processing. Nature *456*, 464–469.

Lichti, U., Anders, J., and Yuspa, S.H. (2008). Isolation and short-term culture of primary keratinocytes, hair follicle populations and dermal cells from newborn mice and keratinocytes from adult mice for in vitro analysis and for grafting to immunodeficient mice. Nat. Protoc. *3*, 799–810.

Lim, L.P., Glasner, M.E., Yekta, S., Burge, C.B., and Bartel, D.P. (2003). Vertebrate microRNA genes. Science *299*, 1540–1540.

Liu, A.-X., Rane, N., Liu, J.-P., and Prendergast, G.C. (2001). RhoB Is Dispensable for Mouse Development, but It Modifies Susceptibility to Tumor Formation as Well as Cell Adhesion and Growth Factor Signaling in Transformed Cells. Mol. Cell. Biol. *21*, 6906–6912.

Liu, J., Carmell, M.A., Rivas, F.V., Marsden, C.G., Thomson, J.M., Song, J.-J., Hammond, S.M., Joshua-Tor, L., and Hannon, G.J. (2004). Argonaute2 Is the Catalytic Engine of Mammalian RNAi. Science *305*, 1437–1441.

Loeb, G.B., Khan, A.A., Canner, D., Hiatt, J.B., Shendure, J., Darnell, R.B., Leslie, C.S., and Rudensky, A.Y. (2012). Transcriptome-wide miR-155 binding map reveals widespread noncanonical microRNA targeting. Mol. Cell *48*, 760–770.

Lu, J., Getz, G., Miska, E.A., Alvarez-Saavedra, E., Lamb, J., Peck, D., Sweet-Cordero, A., Ebert, B.L., Mak, R.H., Ferrando, A.A., et al. (2005). MicroRNA expression profiles classify human cancers. Nature *435*, 834–838.

Lyle, S., Hoover, K., Colpan, C., Zhu, Z., Matijasevic, Z., and Jones, S.N. (2014). Dicer Cooperates with p53 to Suppress DNA Damage and Skin Carcinogenesis in Mice. PLoS ONE *9*, e100920.

Malliri, A., Van Der Kammen, R.A., Clark, K., Van Der Valk, M., Michiels, F., and Collard, J.G. (2002). Mice deficient in the Rac activator Tiam1 are resistant to Ras-induced skin tumours. Nature *417*, 867–871.

Mardaryev, A.N., Ahmed, M.I., Vlahov, N.V., Fessing, M.Y., Gill, J.H., Sharov, A.A., and Botchkareva, N.V. (2010). Micro-RNA-31 controls hair cycle-associated changes in gene expression programs of the skin and hair follicle. FASEB J. *24*, 3869–3881.

Martin, M. (2011). Cutadapt removes adapter sequences from high-throughput sequencing reads. EMBnet J. *17*, pp – 10.

Mayr, C., and Bartel, D.P. (2009). Widespread Shortening of 3′UTRs by Alternative Cleavage and Polyadenylation Activates Oncogenes in Cancer Cells. Cell *138*, 673–684.

McKenna, D.J., McDade, S.S., Patel, D., and McCance, D.J. (2010). MicroRNA 203 Expression in Keratinocytes Is Dependent on Regulation of P53 Levels by E6. J. Virol. *84*, 10644–10652.

Medina, P.P., Nolde, M., and Slack, F.J. (2010). OncomiR addiction in an in vivo model of microRNA-21-induced pre-B-cell lymphoma. Nature *467*, 86–90.

Mehrel, T., Hohl, D., Rothnagel, J.A., Longley, M.A., Bundman, D., Cheng, C., Lichti, U., Bisher, M.E., Steven, A.C., Steinert, P.M., et al. (1990). Identification of a major keratinocyte cell envelope protein, loricrin. Cell *61*, 1103–1112.

Meister, G., Landthaler, M., Patkaniowska, A., Dorsett, Y., Teng, G., and Tuschl, T. (2004). Human Argonaute2 mediates RNA cleavage targeted by miRNAs and siRNAs. Mol. Cell *15*, 185–197.

Melar-New, M., and Laimins, L.A. (2010). Human papillomaviruses modulate expression of microRNA 203 upon epithelial differentiation to control levels of p63 proteins. J. Virol. *84*, 5212–5221.

Melendez-Colon, V.J., Luch, A., Seidel, A., and Baird, W.M. (1999). Cancer initiation by polycyclic aromatic hydrocarbons results from formation of stable DNA adducts rather than apurinic sites. Carcinogenesis *20*, 1885–1891.

Menacho-Márquez, M., García-Escudero, R., Ojeda, V., Abad, A., Delgado, P., Costa, C., Ruiz, S., Alarcón, B., Paramio, J.M., and Bustelo, X.R. (2013). The Rho Exchange Factors Vav2 and Vav3 Favor Skin Tumor Initiation and Promotion by Engaging Extracellular Signaling Loops. PLoS Biol. *11*, e1001615.

Mendell, J.T., and Olson, E.N. (2012). MicroRNAs in stress signaling and human disease. Cell *148*, 1172–1187.

Miska, E.A., Alvarez-Saavedra, E., Abbott, A.L., Lau, N.C., Hellman, A.B., McGonagle, S.M., Bartel, D.P., Ambros, V.R., and Horvitz, H.R. (2007). Most Caenorhabditis

elegans microRNAs are individually not essential for development or viability. PLoS Genet. *3*, e215.

Missero, C., Di Cunto, F., Kiyokawa, H., Koff, A., and Dotto, G.P. (1996). The absence of p21Cip1/WAF1 alters keratinocyte growth and differentiation and promotes ras-tumor progression. Genes Dev. *10*, 3065–3075.

Miyamoto, S., Hirata, M., Yamazaki, A., Kageyama, T., Hasuwa, H., Mizushima, H., Tanaka, Y., Yagi, H., Sonoda, K., Kai, M., et al. (2004). Heparin-binding EGF-like growth factor is a promising target for ovarian cancer therapy. Cancer Res. *64*, 5720–5727.

Moes, M., Le Béchec, A., Crespo, I., Laurini, C., Halavatyi, A., Vetter, G., del Sol, A., and Friederich, E. (2012). A Novel Network Integrating a miRNA-203/SNAI1 Feedback Loop which Regulates Epithelial to Mesenchymal Transition. PloS One *7*, e35440.

Moore, M.J., Zhang, C., Gantman, E.C., Mele, A., Darnell, J.C., and Darnell, R.B. (2014). Mapping Argonaute and conventional RNA-binding protein interactions with RNA at single-nucleotide resolution using HITS-CLIP and CIMS analysis. Nat. Protoc. *9*, 263–293.

Mori, M. (2012). miR-203 inhibits the migration and invasion of esophageal squamous cell carcinoma by regulating LASP1. Int. J. Oncol.

Mortensen, R.D., Serra, M., Steitz, J.A., and Vasudevan, S. (2011). Posttranscriptional activation of gene expression in Xenopus laevis oocytes by microRNA–protein complexes (microRNPs). Proc. Natl. Acad. Sci. *108*, 8281–8286.

Mudhasani, R., Zhu, Z., Hutvagner, G., Eischen, C.M., Lyle, S., Hall, L.L., Lawrence, J.B., Imbalzano, A.N., and Jones, S.N. (2008). Loss of miRNA biogenesis induces p19Arf-p53 signaling and senescence in primary cells. J. Cell Biol. *181*, 1055–1063.

Nissan, X., Denis, J.A., Saidani, M., Lemaitre, G., Peschanski, M., and Baldeschi, C. (2011). miR-203 modulates epithelial differentiation of human embryonic stem cells towards epidermal stratification. Dev. Biol. *356*, 506–515.

Owens, D.M. (2003). Suprabasal 6 4 integrin expression in epidermis results in enhanced tumourigenesis and disruption of TGF signalling. J. Cell Sci. *116*, 3783–3791.

Pálmer, H.G., Martinez, D., Carmeliet, G., and Watt, F.M. (2008). The vitamin D receptor is required for mouse hair cycle progression but not for maintenance of the epidermal stem cell compartment. J. Invest. Dermatol. *128*, 2113–2117.

Parada, L.F., Tabin, C.J., Shih, C., and Weinberg, R.A. (1982). Human EJ bladder carcinoma oncogene is homologue of Harvey sarcoma virus ras gene. Nature *297*, 474–478.

Paranjape, T., Heneghan, H., Lindner, R., Keane, F.K., Hoffman, A., Hollestelle, A., Dorairaj, J., Geyda, K., Pelletier, C., Nallur, S., et al. (2011). A 3′-untranslated region KRAS variant and triple-negative breast cancer: a case-control and genetic analysis. Lancet Oncol. *12*, 377–386.

París, R., Henry, R.E., Stephens, S.J., McBryde, M., and Espinosa, J.M. (2008). Multiple p53-independent gene silencing mechanisms define the cellular response to p53 activation. Cell Cycle *7*, 2427–2433.

Parsons, J.T., Horwitz, A.R., and Schwartz, M.A. (2010). Cell adhesion: integrating cytoskeletal dynamics and cellular tension. Nat. Rev. Mol. Cell Biol. *11*, 633–643.

Pastar, I., Khan, A.A., Stojadinovic, O., Lebrun, E.A., Medina, M.C., Brem, H., Kirsner, R.S., Jimenez, J.J., Leslie, C., and Tomic-Canic, M. (2012). Induction of Specific MicroRNAs Inhibits Cutaneous Wound Healing. J. Biol. Chem. *287*, 29324–29335.

Porter, R.M., Leitgeb, S., Melton, D.W., Swensson, O., Eady, R.A., and Magin, T.M. (1996). Gene targeting at the mouse cytokeratin 10 locus: severe skin fragility and changes of cytokeratin expression in the epidermis. J. Cell Biol. *132*, 925–936.

Prior, I.A., Lewis, P.D., and Mattos, C. (2012). A Comprehensive Survey of Ras Mutations in Cancer. Cancer Res. *72*, 2457–2467.

Pylayeva-Gupta, Y., Grabocka, E., and Bar-Sagi, D. (2011). RAS oncogenes: weaving a tumorigenic web. Nat. Rev. Cancer *11*, 761–774.

Quintanilla, M., Brown, K., Ramsden, M., and Balmain, A. (1986). Carcinogen-specific mutation and amplification of Ha-ras during mouse skin carcinogenesis. Nature *322*, 78–80.

Riemondy, K., Hoefert, J.E., and Yi, R. (2014). Not miR-ly micromanagers: the functions and regulatory networks of microRNAs in mammalian skin. Wiley Interdiscip. Rev. RNA.

Robinson, M.D., McCarthy, D.J., and Smyth, G.K. (2010). edgeR: a Bioconductor package for differential expression analysis of digital gene expression data. Bioinformatics *26*, 139–140.

Robles, A.I., Rodriguez-Puebla, M.L., Glick, A.B., Trempus, C., Hansen, L., Sicinski, P., Tennant, R.W., Weinberg, R.A., Yuspa, S.H., and Conti, C.J. (1998). Reduced skin tumor development in cyclin D1-deficient mice highlights the oncogenic ras pathway in vivo. Genes Dev. *12*, 2469–2474.

Roop, D.R., Lowy, D.R., Tambourin, P.E., Strickland, J., Harper, J.R., Balaschak, M., Spangler, E.F., and Yuspa, S.H. (1986). An activated Harvey ras oncogene produces benign tumours on mouse epidermal tissue. Nature *323*, 822–824.

Saldanha, A.J. (2004). Java Treeview--extensible visualization of microarray data. Bioinformatics *20*, 3246–3248.

Sandberg, R., Neilson, J.R., Sarma, A., Sharp, P.A., and Burge, C.B. (2008). Proliferating Cells Express mRNAs with Shortened 3' Untranslated Regions and Fewer MicroRNA Target Sites. Science *320*, 1643–1647.

Santos, E., Tronick, S.R., Aaronson, S.A., Pulciani, S., and Barbacid, M. (1982). T24 human bladder carcinoma oncogene is an activated form of the normal human homologue of BALB- and Harvey-MSV transforming genes. Nature *298*, 343–347.

Schnall-Levin, M., Rissland, O.S., Johnston, W.K., Perrimon, N., Bartel, D.P., and Berger, B. (2011). Unusually effective microRNA targeting within repeat-rich coding regions of mammalian mRNAs. Genome Res. *21*, 1395–1403.

Schneider, M.R., Schmidt-Ullrich, R., and Paus, R. (2009). The hair follicle as a dynamic miniorgan. Curr. Biol. *19*, R132–R142.

Schober, M., and Fuchs, E. (2011). Tumor-initiating stem cells of squamous cell carcinomas and their control by TGF- and integrin/focal adhesion kinase (FAK) signaling. Proc. Natl. Acad. Sci. *108*, 10544–10549.

Scholl, F.A., Dumesic, P.A., Barragan, D.I., Harada, K., Charron, J., and Khavari, P.A. (2009). Selective Role for Mek1 but not Mek2 in the Induction of Epidermal Neoplasia. Cancer Res. *69*, 3772–3778.

Schwamborn, J.C., Berezikov, E., and Knoblich, J.A. (2009). The TRIM-NHL Protein TRIM32 Activates MicroRNAs and Prevents Self-Renewal in Mouse Neural Progenitors. Cell *136*, 913–925.

Schwarz, D.S., Hutvágner, G., Du, T., Xu, Z., Aronin, N., and Zamore, P.D. (2003). Asymmetry in the assembly of the RNAi enzyme complex. Cell *115*, 199–208.

Sennett, R., and Rendl, M. (2012). Mesenchymal–epithelial interactions during hair follicle morphogenesis and cycling. In Seminars in Cell & Developmental Biology, (Elsevier), pp. 917–927.

Shin, C., Nam, J.-W., Farh, K.K.-H., Chiang, H.R., Shkumatava, A., and Bartel, D.P. (2010). Expanding the MicroRNA Targeting Code: Functional Sites with Centered Pairing. Mol. Cell *38*, 789–802.

Sodhi, A., Montaner, S., Miyazaki, H., and Gutkind, J.S. (2001). MAPK and Akt Act Cooperatively but Independently on Hypoxia Inducible Factor-1α in rasV12 Upregulation of VEGF. Biochem. Biophys. Res. Commun. *287*, 292–300.

Sonkoly, E., Wei, T., Janson, P.C., Sääf, A., Lundeberg, L., Tengvall-Linder, M., Norstedt, G., Alenius, H., Homey, B., and Scheynius, A. (2007). MicroRNAs: novel regulators involved in the pathogenesis of psoriasis? PLoS One *2*, e610.

Sonkoly, E., Wei, T., Loriè, E.P., Suzuki, H., Kato, M., Törmä, H., St\a ahle, M., and Pivarcsi, A. (2010). Protein kinase C-dependent upregulation of miR-203 induces the differentiation of human keratinocytes. J. Invest. Dermatol. *130*, 124–134.

Stoll, S.W., Rittié, L., Johnson, J.L., and Elder, J.T. (2012). Heparin-binding EGF-like growth factor promotes epithelial-mesenchymal transition in human keratinocytes. J. Invest. Dermatol. *132*, 2148–2157.

Stransky, N., Egloff, A.M., Tward, A.D., Kostic, A.D., Cibulskis, K., Sivachenko, A., Kryukov, G.V., Lawrence, M.S., Sougnez, C., McKenna, A., et al. (2011). The Mutational Landscape of Head and Neck Squamous Cell Carcinoma. Science *333*, 1157–1160.

Subramanian, A., Tamayo, P., Mootha, V.K., Mukherjee, S., Ebert, B.L., Gillette, M.A., Paulovich, A., Pomeroy, S.L., Golub, T.R., Lander, E.S., et al. (2005). Gene set enrichment analysis: a knowledge-based approach for interpreting genome-wide expression profiles. Proc. Natl. Acad. Sci. U. S. A. *102*, 15545–15550.

Subtelny, A.O., Eichhorn, S.W., Chen, G.R., Sive, H., and Bartel, D.P. (2014). Poly(A)-tail profiling reveals an embryonic switch in translational control. Nature *advance online publication*.

Sun, K., and Lai, E.C. (2013). Adult-specific functions of animal microRNAs. Nat. Rev. Genet. *14*, 535–548.

Sun, F., Fu, H., Liu, Q., Tie, Y., Zhu, J., Xing, R., Sun, Z., and Zheng, X. (2008). Downregulation of CCND1 and CDK6 by miR-34a induces cell cycle arrest. FEBS Lett. *582*, 1564–1568.

Talotta, F., Cimmino, A., Matarazzo, M.R., Casalino, L., De Vita, G., D'Esposito, M., Di Lauro, R., and Verde, P. (2009). An autoregulatory loop mediated by miR-21 and PDCD4 controls the AP-1 activity in RAS transformation. Oncogene *28*, 73–84.

Taube, J.H., Malouf, G.G., Lu, E., Sphyris, N., Vijay, V., Ramachandran, P.P., Ueno, K.R., Gaur, S., Nicoloso, M.S., and Rossi, S. (2013). Epigenetic silencing of microRNA-203 is required for EMT and cancer stem cell properties. Sci. Rep. *3*.

Teta, M., Choi, Y.S., Okegbe, T., Wong, G., Tam, O.H., Chong, M.M.W., Seykora, J.T., Nagy, A., Littman, D.R., Andl, T., et al. (2012). Inducible deletion of epidermal Dicer and Drosha reveals multiple functions for miRNAs in postnatal skin. Dev. Camb. Engl. *139*, 1405–1416.

The Australian National Endometrial Cancer Study Group, The Hunter Community Study, Studies of Epidemiology and Risk Factors in Cancer Heredity, Moir-Meyer, G.L., Pearson, J.F., Lose, F., Scott, R.J., McEvoy, M., Attia, J., Holliday, E.G., et al. (2015). Rare germline copy number deletions of likely functional importance are implicated in endometrial cancer predisposition. Hum. Genet. *134*, 269–278.

Thiagalingam, A., De Bustros, A., Borges, M., Jasti, R., Compton, D., Diamond, L., Mabry, M., Ball, D.W., Baylin, S.B., and Nelkin, B.D. (1996). RREB-1, a novel zinc finger protein, is involved in the differentiation response to Ras in human medullary thyroid carcinomas. Mol. Cell. Biol. *16*, 5335–5345.

Trang, P., Wiggins, J.F., Daige, C.L., Cho, C., Omotola, M., Brown, D., Weidhaas, J.B., Bader, A.G., and Slack, F.J. (2011). Systemic Delivery of Tumor Suppressor microRNA Mimics Using a Neutral Lipid Emulsion Inhibits Lung Tumors in Mice. Mol. Ther. *19*, 1116–1122.

Tritschler, F., Huntzinger, E., and Izaurralde, E. (2010). Role of GW182 proteins and PABPC1 in the miRNA pathway: a sense of déjà vu. Nat Rev Mol Cell Biol *11*, 379–384.

Ulitsky, I., Shkumatava, A., Jan, C.H., Subtelny, A.O., Koppstein, D., Bell, G.W., Sive, H., and Bartel, D.P. (2012). Extensive alternative polyadenylation during zebrafish development. Genome Res. *22*, 2054–2066.

Viticchiè, G., Lena, A.M., Latina, A., Formosa, A., Gregersen, L.H., Lund, A.H., Bernardini, S., Mauriello, A., Miano, R., and Spagnoli, L.G. (2011). MiR-203 controls proliferation, migration and invasive potential of prostate cancer cell lines. Cell Cycle *10*, 1121–1131.

Viticchie, G., Lena, A.M., Cianfarani, F., Odorisio, T., Annicchiarico-Petruzzelli, M., Melino, G., and Candi, E. (2012). MicroRNA-203 contributes to skin re-epithelialization. Cell Death Dis *3*, e435.

Volinia, S., Calin, G.A., Liu, C.-G., Ambs, S., Cimmino, A., Petrocca, F., Visone, R., Iorio, M., Roldo, C., Ferracin, M., et al. (2006). A microRNA expression signature of human solid tumors defines cancer gene targets. Proc. Natl. Acad. Sci. U. S. A. *103*, 2257–2261.

Volinia, S., Galasso, M., Costinean, S., Tagliavini, L., Gamberoni, G., Drusco, A., Marchesini, J., Mascellani, N., Sana, M.E., Abu Jarour, R., et al. (2010). Reprogramming of miRNA networks in cancer and leukemia. Genome Res. *20*, 589–599.

Wang, D., Zhang, Z., O'Loughlin, E., Lee, T., Houel, S., O'Carroll, D., Tarakhovsky, A., Ahn, N.G., and Yi, R. (2012). Quantitative functions of Argonaute proteins in mammalian development. Genes Dev. *26*, 693–704.

Wang, D., Zhang, Z., O'Loughlin, E., Wang, L., Fan, X., Lai, E.C., and Yi, R. (2013a). MicroRNA-205 controls neonatal expansion of skin stem cells by modulating the PI(3)K pathway. Nat. Cell Biol. *15*, 1153–1163.

Wang, L., Dowell, R.D., and Yi, R. (2013b). Genome-wide maps of polyadenylation reveal dynamic mRNA 3'-end formation in mammalian cell lineages. RNA *19*, 413–425.

Wang, N., Liang, H., Zhou, Y., Wang, C., Zhang, S., Pan, Y., Wang, Y., Yan, X., Zhang, J., Zhang, C.-Y., et al. (2014). miR-203 Suppresses the Proliferation and Migration and Promotes the Apoptosis of Lung Cancer Cells by Targeting SRC. PLoS ONE *9*, e105570.

Wang, Z., Tollervey, J., Briese, M., Turner, D., and Ule, J. (2009). CLIP: Construction of cDNA libraries for high-throughput sequencing from RNAs cross-linked to proteins in vivo. Methods *48*, 287–293.

Wang, Z., Pedersen, E., Basse, A., Lefever, T., Peyrollier, K., Kapoor, S., Mei, Q., Karlsson, R., Chrostek-Grashoff, A., and Brakebusch, C. (2010). Rac1 is crucial for Ras-dependent skin tumor formation by controlling Pak1-Mek-Erk hyperactivation and hyperproliferation in vivo. Oncogene *29*, 3362–3373.

Wellner, U., Schubert, J., Burk, U.C., Schmalhofer, O., Zhu, F., Sonntag, A., Waldvogel, B., Vannier, C., Darling, D., Hausen, A. zur, et al. (2009). The EMT-activator ZEB1 promotes tumorigenicity by repressing stemness-inhibiting microRNAs. Nat. Cell Biol. *11*, 1487–1495.

White, A.C., Tran, K., Khuu, J., Dang, C., Cui, Y., Binder, S.W., and Lowry, W.E. (2011). Defining the origins of Ras/p53-mediated squamous cell carcinoma. Proc. Natl. Acad. Sci. *108*, 7425–7430.

White, R.A., Neiman, J.M., Reddi, A., Han, G., Birlea, S., Mitra, D., Dionne, L., Fernandez, P., Murao, K., Bian, L., et al. (2013). Epithelial stem cell mutations that promote squamous cell carcinoma metastasis. J. Clin. Invest. *123*, 4390–4404.

Wickham, H. (2009). ggplot2: elegant graphics for data analysis (Springer New York).

Witkos, T.M., Koscianska, E., and Krzyzosiak, W.J. (2011). Practical aspects of microRNA target prediction. Curr. Mol. Med. *11*, 93.

Wong, C.E., Yu, J.S., Quigley, D.A., To, M.D., Jen, K.-Y., Huang, P.Y., Del Rosario, R., and Balmain, A. (2013). Inflammation and Hras signaling control epithelial-mesenchymal transition during skin tumor progression. Genes Dev. *27*, 670–682.

Xie, M., Li, M., Vilborg, A., Lee, N., Shu, M.-D., Yartseva, V., Šestan, N., and Steitz, J.A. (2013). Mammalian 5′-Capped MicroRNA Precursors that Generate a Single MicroRNA. Cell *155*, 1568–1580.

Yamagiwa, K., and Ichikawa, K. (1977). Experimental study of the pathogenesis of carcinoma. CA. Cancer J. Clin. *27*, 174–181.

Yeom, K.-H., Lee, Y., Han, J., Suh, M.R., and Kim, V.N. (2006). Characterization of DGCR8/Pasha, the essential cofactor for Drosha in primary miRNA processing. Nucleic Acids Res. *34*, 4622–4629.

Yi, R. (2003). Exportin-5 mediates the nuclear export of pre-microRNAs and short hairpin RNAs. Genes Dev. *17*, 3011–3016.

Yi, R., and Fuchs, E. (2011). MicroRNAs and their roles in mammalian stem cells. J. Cell Sci. *124*, 1775–1783.

Yi, R., O'Carroll, D., Pasolli, H.A., Zhang, Z., Dietrich, F.S., Tarakhovsky, A., and Fuchs, E. (2006). Morphogenesis in skin is governed by discrete sets of differentially expressed microRNAs. Nat Genet *38*, 356–362.

Yi, R., Poy, M.N., Stoffel, M., and Fuchs, E. (2008). A skin microRNA promotes differentiation by repressing "stemness." Nature *452*, 225–229.

Yi, R., Pasolli, H.A., Landthaler, M., Hafner, M., Ojo, T., Sheridan, R., Sander, C., O'Carroll, D., Stoffel, M., and Tuschl, T. (2009). DGCR8-dependent microRNA biogenesis is essential for skin development. Proc. Natl. Acad. Sci. *106*, 498–502.

Zekri, L., Huntzinger, E., Heimstadt, S., and Izaurralde, E. (2009). The Silencing Domain of GW182 Interacts with PABPC1 To Promote Translational Repression and Degradation of MicroRNA Targets and Is Required for Target Release. Mol. Cell. Biol. *29*, 6220–6231.

Zhang, F., Yang, Z., Cao, M., Xu, Y., Li, J., Chen, X., Gao, Z., Xin, J., Zhou, S., Zhou, Z., et al. (2014a). MiR-203 suppresses tumor growth and invasion and down-regulates MiR-21 expression through repressing Ran in esophageal cancer. Cancer Lett. *342*, 121–129.

Zhang, L., Stokes, N., Polak, L., and Fuchs, E. (2011a). Specific microRNAs are preferentially expressed by skin stem cells to balance self-renewal and early lineage commitment. Cell Stem Cell *8*, 294–308.

Zhang, L., Ge, Y., and Fuchs, E. (2014b). *miR-125b* can enhance skin tumor initiation and promote malignant progression by repressing differentiation and prolonging cell survival. Genes Dev. *28*, 2532–2546.

Zhang, Z., Zhang, B., Li, W., Fu, L., Fu, L., Zhu, Z., and Dong, J.-T. (2011b). Epigenetic Silencing of miR-203 Upregulates SNAI2 and Contributes to the Invasiveness of Malignant Breast Cancer Cells. Genes Cancer *2*, 782–791.

Zhang, Z., Lee, J.E., Riemondy, K., Anderson, E.M., and Yi, R. (2013). High-efficiency RNA cloning enables accurate quantification of miRNA expression by deep sequencing. Genome Biol. *14*, R109.

APPENDICES

Oligo name	Sequence	Usage
P7T20V	CTTGGCACCCGAGAATTCCATTTTTTTTTTTTTTTTTTV	3Seq Reverse Transcription
5'Adaptor	GTTCAGAGTTCTACAGTCCGACGAT	3Seq Adaptor Ligation
5'AdaptorRV	(P)TCGTCGGACTGTAGAACTCTGAAC	3Seq Adaptor Ligation
RP1	AATGATACGGCGACCACCGAGATCTACACGTTCAGAGTTCTACAGTCCGA	3Seq and small Rna-Seq library PCR
RT Primer	GCCTTGGCACCCGAGAATTCCA	small RNA-Seq RTand PCR
5' adaptor miR-seq	GUUCAGAGUUCUACAGUCCGACGAUCNN	small RNA-Seq linker (Note RNA)
3' Adaptor miR-seq	NNTGGAATTCTCGGGTGCCAAGG	small RNA-Seq linker (5' preadenylated)
miR-203priF	CTCCGGGCTGTGCAGAACT	qPCR
miR-203priR	CGGGTCTAGTGGTCCTAAACATT	qPCR
K10F	GGAGGGTAAAATCAAGGAGTGGTA	qPCR
K10R	TCAATCTGCAGCAGCACGTT	qPCR
Pola1F	GTA CAC CCA GCT GTG CTT TTA CCG	qPCR
PolaR	AAC TGC TCT GCT ATG TTC TTG ACT T	qPCR
HbegfF	CGGGGAGTGCAGATACCTG	qPCR
HbegfR	TTCTCCACTGGTAGAGTCAGC	qPCR
Pola1_3'UTR_F	atattctagAAGTCCTGAGAGAGCCGGGAAG	3'UTR cloning
Pola1_3'UTR_R	atatctcgAGATAAGTATTTAAGGCTGCCATATT	3'UTR cloning
Hbegf_3'UTR_F	atattctagaGGCTACTTCTGAGACAGTGGTTCG	3'UTR cloning
Hbegf_3'UTR_R	atatagaattcTTGTAACAGTTCAGACATGGCACT	3'UTR cloning
Pola1mut33	CTAGtaaagtTCAGTTCTTCAGAATAGTGTC	3'UTR cloning Mutations
Pola1mut35	GAAGAACTGAactttaCTAGCAAGCACTGGATCCTGTCA	3'UTR cloning Mutations
Pola1mut23	CTTTGTCCTttgtaaagtCAAAATTTATGGTGAGGTTGTAGTAAG	3'UTR cloning Mutations
Pola1mut25	actttacaaAGGACAAAGTATTTAAAATGTGC	3'UTR cloning Mutations
Pola1mut13	taaagtGTGCTGTCTTTCATATAAGTGGTG	3'UTR cloning Mutations
Pola1mut15	TGAAAGACAGCACactttaCAGCCATGCTTGTAGCCAGTAGC	3'UTR cloning Mutations
Hbegfmut15	GTCTAGGCACTactttaATTATTGTTAGATTGTTAA	3'UTR cloning Mutations
Hbegfmut13	TAATtaaagtAGTGCCTAGACTGTTACTTTGGC	3'UTR cloning Mutations
Hbegfmut25	TCTTCactttacaAGACAGACAATAAATTACTACCG	3'UTR cloning Mutations
Hbegfmut23	TGTCTtgtaaagtGAAGATGTCCCTGGAGCAGA	3'UTR cloning Mutations
HaRasmut5	AAGCCTGTTGTTTTGCAGGA	HRas Q61L mutation
HaRasmut3	GGTGGCTCACCTGTACTGATG	HRas Q61L mutation

Table 1. Oligonucleotides used in this study

	miR-203$^{+/+}$ Vector		miR-203$^{-/-}$ Vector		miR-203$^{+/+}$ HRAS^{G12V}		miR-203$^{-/-}$ HRAS^{G12V}	
	rep. 1	rep. 2	rep. 1	rep. 2	rep. 1	rep. 2	rep. 1	rep. 2
Raw Reads	21,353,639	21,014,713	20,805,674	20,253,567	18,460,461	17,041,451	18,264,934	17,133,047
Reads Uniquely Mapped	17,914,434	17,447,436	18,348,508	16,608,243	15,832,338	14,320,434	14,802,086	14,464,448
Unique Alignment Percentage	83.89%	83.80%	88.19%	82.00%	85.76%	84.03%	81.04%	84.42%
Unique Alignments Annotated to 3'UTRs	13,184,882	12,949,894	13,352,259	12,539,847	10,989,882	10,132,233	9,720,835	10,691,157

Table 2. Mapping Statistics for 3'Seq libraries

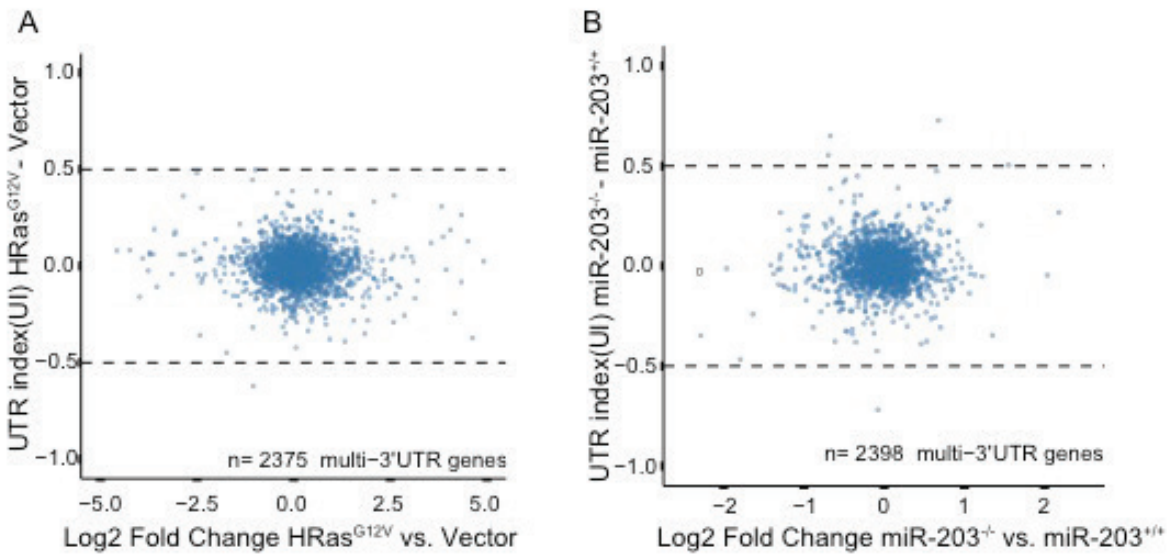

Figure 32. HRas^{G12V} expression or miR-203 ablation in keratinocytes does not strongly perturb 3'UTR usage dynamics. (A) The UTR index (UI represents the ratio of mapped reads to a single 3'UTR isoform to all mapped reads from all 3'UTR isoforms for a gene was calculated. The difference in UI between samples indicates 3'UTR isoforms that are changed usage irrespective of overall transcript expression level changes. Shown in A are results from comparing HRas^{G12V} expressing keratinocyte to vector control (B) Comparison between miR-203$^{-/-}$ and miR-203$^{+/+}$ samples.

	Vector		HRAS^{G12V}		Total Epidermis P4	
	rep. 1	rep. 2	rep. 1	rep. 2	miR-203$^{+/+}$	miR-203$^{-/-}$
Raw Reads	772,307	5,440,980	7,356,089	7,846,395	2,789,021	3,968,317
Reads Remaining after Trimming	713,808	5,047,466	6,920,037	7,074,027	2,066,472	3,233,833
Reads Aligned to miRNA	73,169	508,760	1,007,172	731,030	1,210,218	1,813,062

Table 3. Mapping statistics for small-RNA-Seq libraries.

Primary Antibody	Usage	Dilutions	Cat. Number	Company
K5	IF	1:2000	Sig-3475	Covance
Brdu	IF	1:100	ab6326	Abcam
K1	IF	1:200	n/a	Gift From E. Fuchs
Loricrin	IF	1:200	n/a	Gift From E. Fuchs
p63	IF	1:100	4892	Cell Signaling
Ki67	IF	1:100	ab15580	Abcam
Pola1	WB	1:1000 in 5% BSA	A302-851A	Bethyl
B-tubulin	WB	1:5000 in 5% BSA	2146	Cell Signaling
Ccnd1	WB	1:1000 in 5% BSA	2978	Cell Signaling
Ago2	CLIP	3ug /ml of lysate	Clone 2D4	Wako
HRas	WB	1:2500 in 5% BSA	SC-520	Santa Cruz

Table 4. Antibody information and usage recommendations.

	miR-203$^{+/+}$		miR-203$^{-/-}$	
	rep. 1	rep. 2	rep. 1	rep. 2
Raw Reads	17,486,318	22,770,301	14,733,775	20,762,514
Reads Remaining after Trimming	16,945,919	21,995,669	14,154,906	20,169,723
Reads Mapped to rRNA	2,615,233	5,357,438	3,295,184	2,809,327
Reads Mapped to tRNA	2,453,229	2,586,723	1,150,757	3,646,802
Reads Mapped to ncRNA	1,550,534	2,202,004	1,496,549	2,126,097
Reads Uniquely Mapped to CDS	4,396,226	6,839,613	4,998,762	5,469,180
Unique CDS Alignment Percentage	25.14%	30.04%	33.93%	26.34%

Table 5. Mapping statistics for the Ribosome Profiling libraries.

	Primary Keratinocytes			
	rep. 1	rep. 2	rep. 3	rep. 4
Raw Reads	18,629,300	35,977,426	31,838,598	31,628,093
Reads Aligned to miRNA	930,455	2,788,847	4,279,814	2,282,176
Non-miRNA reads without sequence duplicates	794,971	1,181,332	825,478	821,509
Reads uniquely aligned to genome	317,710	479,380	287,440	329,308
Combined Reads uniquely aligned to 3'UTRs	228,109			
Combined 3'UTR Peaks	6,770			

Table 6. Mapping statistics for the Ago2-HITS-CLIP experiments

Name	shRNA number	sequence	Targeted region
Scrambled	SHC002	CCTAAGGTTAAGTCGCCCTCGCTCGAGCGAGGGCGACTTAACCTTAGG	NA
Hbegf shRNA 1	TRCN0000335387	CCGGCCCATGCCTCAGGAAATACAACTCGAGTTGTATTTCCTGAGGCATGGGTTTTTG	CDS
Hbegf shRNA 2	TRCN0000089220	CCGGGAGGAGGTTATGACTTGGAAACTCGAGTTTCCAAGTCATAACCTCCTCTTTTTG	CDS
Hbegf shRNA 3	TRCN0000089221	CCGGCCCATGCCTCAGGAAATACAACTCGAGTTGTATTTCCTGAGGCATGGGTTTTTG	CDS
Pola1 shRNA 1	TRCN0000071229	CCGGGCCAATCAGTTGGTGTAAATTCTCGAGAATTTACACCAACTGATTGGCTTTTTG	CDS
Pola1 shRNA 2	TRCN0000071230	CCGGCCAGTTTGTATCGTTGCAGTACTCGAGTACTGCAACGATACAAACTGGTTTTTG	CDS
Pola1 shRNA 3	TRCN0000071231	CCGGCGTCAGGATGATGACTGGATTCTCGAGAATCCAGTCATCATCCTGACGTTTTTG	CDS

Table 7. shRNA constructs used in this study.

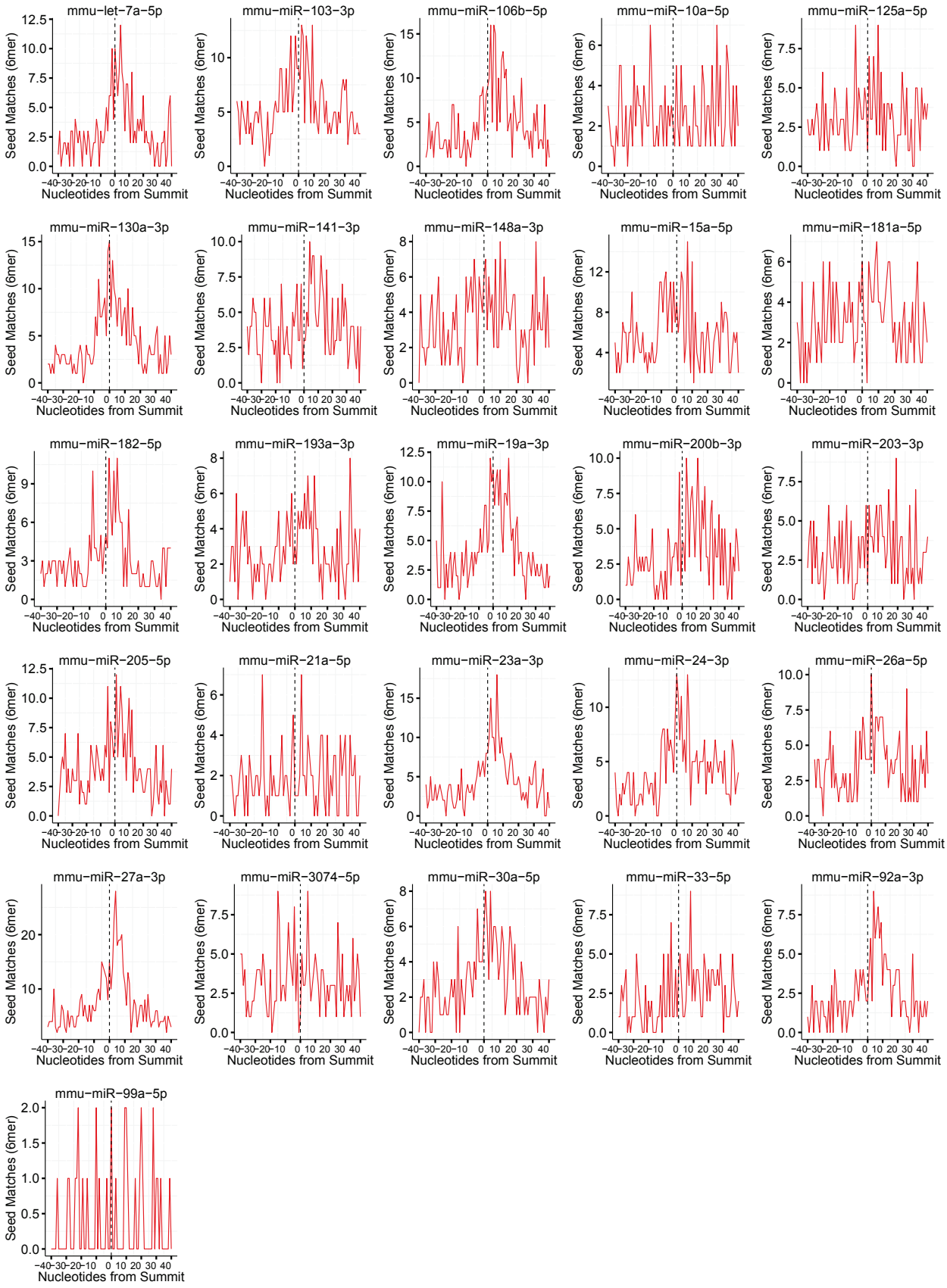
mmu−let−7a−5p
mmu−miR−103−3p
mmu−miR−106b−5p
mmu−miR−10a−5p
mmu−miR−125a−5p
mmu−miR−130a−3p
mmu−miR−141−3p
mmu−miR−148a−3p
mmu−miR−15a−5p
mmu−miR−181a−5p
mmu−miR−182−5p
mmu−miR−193a−3p
mmu−miR−19a−3p
mmu−miR−200b−3p
mmu−miR−203−3p
mmu−miR−205−5p
mmu−miR−21a−5p
mmu−miR−23a−3p
mmu−miR−24−3p
mmu−miR−26a−5p
mmu−miR−27a−3p
mmu−miR−3074−5p
mmu−miR−30a−5p
mmu−miR−33−5p
mmu−miR−92a−3p
mmu−miR−99a−5p
Seed Matches (6mer)
Nucleotides from Summit

Figure 33. miRNA seed distribution surrounding Ago2 HITS-CLIP 3'UTR peak summits for highly expressed microRNA in epidermis.

6mer or 7mer or 8mer		7mer or 8mer		8mer	
3'UTR binding sites	miRNA Family	3'UTR binding sites	miRNA Family	3'UTR binding sites	miRNA Family
392	*miR-27a-3p*	152	*miR-106b-5p*	55	*miR-106b-5p*
260	*miR-103-3p*	152	*miR-27a-3p*	37	*miR-30a-5p*
257	*miR-15a-5p*	140	*miR-15a-5p*	31	*miR-19a-3p*
233	*miR-130a-3p*	139	*miR-19a-3p*	28	*miR-27a-3p*
231	*miR-23a-3p*	132	*miR-23a-3p*	27	*miR-125a-5p*
230	*miR-19a-3p*	99	*miR-130a-3p*	26	*miR-24-3p*
225	*miR-106b-5p*	99	*miR-30a-5p*	25	*miR-15a-5p*
206	*miR-24-3p*	98	*miR-24-3p*	21	*miR-429-3p*
189	*miR-205-5p*	87	*let-7a-5p*	20	*miR-23a-3p*
163	*let-7a-5p*	79	*miR-200b-3p*	19	*miR-203-3p*
155	*miR-26a-5p*	77	*miR-92a-3p*	19	*miR-92a-3p*
152	*miR-182-5p*	75	*miR-148a-3p*	18	*let-7a-5p*
150	*miR-141-3p*	66	*miR-182-5p*	18	*miR-205-5p*
145	*miR-200b-3p*	65	*miR-125a-5p*	17	*miR-130a-3p*
141	*miR-30a-5p*	65	*miR-141-3p*	17	*miR-182-5p*
139	*miR-148a-3p*	47	*miR-205-5p*	16	*miR-26a-5p*
131	*miR-125a-5p*	47	*miR-26a-5p*	15	*miR-141-3p*
124	*miR-181a-5p*	46	*miR-103-3p*	13	*miR-103-3p*
121	*miR-193a-3p*	46	*miR-203-3p*	12	*miR-181a-5p*
121	*miR-92a-3p*	43	*miR-181a-5p*	10	*miR-3074-5p*
117	*miR-203-3p*	35	*miR-96-5p*	9	*miR-148a-3p*
115	*miR-3074-5p*	28	*miR-193a-3p*	9	*miR-96-5p*
84	*miR-33-5p*	28	*miR-3074-5p*	8	*miR-200b-3p*
82	*miR-10a-5p*	27	*miR-21a-5p*	7	*miR-193a-3p*
66	*miR-21a-5p*	15	*miR-33-5p*	5	*miR-21a-5p*
19	*miR-99a-5p*	11	*miR-10a-5p*	3	*miR-10a-5p*
		6	*miR-99a-5p*	3	*miR-33-5p*

Table 8. The number of 3'UTR binding sites for miRNAs highly expressed in keratinocytes. The miRNA familes accounting for 90% of all miRNAs expressed in epidermis were used for seed searching.

6mer or 7mer or 8mer		7mer or 8mer		8mer	
3'UTR transcripts	miRNA Family	3'UTR transcripts	miRNA Family	3'UTR transcripts	miRNA Family
378	*miR-27a-3p*	149	*miR-106b-5p*	55	*miR-106b-5p*
252	*miR-103-3p*	149	*miR-27a-3p*	37	*miR-30a-5p*
247	*miR-15a-5p*	138	*miR-19a-3p*	31	*miR-19a-3p*
228	*miR-130a-3p*	137	*miR-15a-5p*	27	*miR-125a-5p*
228	*miR-23a-3p*	132	*miR-23a-3p*	27	*miR-27a-3p*
226	*miR-19a-3p*	98	*miR-130a-3p*	26	*miR-24-3p*
220	*miR-106b-5p*	98	*miR-24-3p*	25	*miR-15a-5p*
200	*miR-24-3p*	97	*miR-30a-5p*	21	*miR-429-3p*
184	*miR-205-5p*	87	*let-7a-5p*	20	*miR-23a-3p*
162	*let-7a-5p*	79	*miR-200b-3p*	19	*miR-203-3p*
155	*miR-26a-5p*	77	*miR-92a-3p*	19	*miR-92a-3p*
149	*miR-182-5p*	75	*miR-148a-3p*	18	*let-7a-5p*
148	*miR-141-3p*	66	*miR-182-5p*	18	*miR-205-5p*
143	*miR-200b-3p*	65	*miR-125a-5p*	17	*miR-130a-3p*
138	*miR-148a-3p*	65	*miR-141-3p*	17	*miR-182-5p*
134	*miR-30a-5p*	47	*miR-205-5p*	16	*miR-26a-5p*
128	*miR-125a-5p*	47	*miR-26a-5p*	15	*miR-141-3p*
124	*miR-181a-5p*	46	*miR-103-3p*	13	*miR-103-3p*
121	*miR-92a-3p*	46	*miR-203-3p*	12	*miR-181a-5p*
119	*miR-193a-3p*	43	*miR-181a-5p*	10	*miR-3074-5p*
116	*miR-203-3p*	35	*miR-96-5p*	9	*miR-148a-3p*
115	*miR-3074-5p*	28	*miR-193a-3p*	9	*miR-96-5p*
84	*miR-33-5p*	28	*miR-3074-5p*	8	*miR-200b-3p*
82	*miR-10a-5p*	27	*miR-21a-5p*	7	*miR-193a-3p*
66	*miR-21a-5p*	15	*miR-33-5p*	5	*miR-21a-5p*
19	*miR-99a-5p*	11	*miR-10a-5p*	3	*miR-10a-5p*
		6	*miR-99a-5p*	3	*miR-33-5p*

Table 9. The number of unique 3'UTRs targeted by miRNAs highly expressed in keratinocytes. The miRNA familes accounting for 90% of all miRNAs expressed in epidermis were used for seed searching.

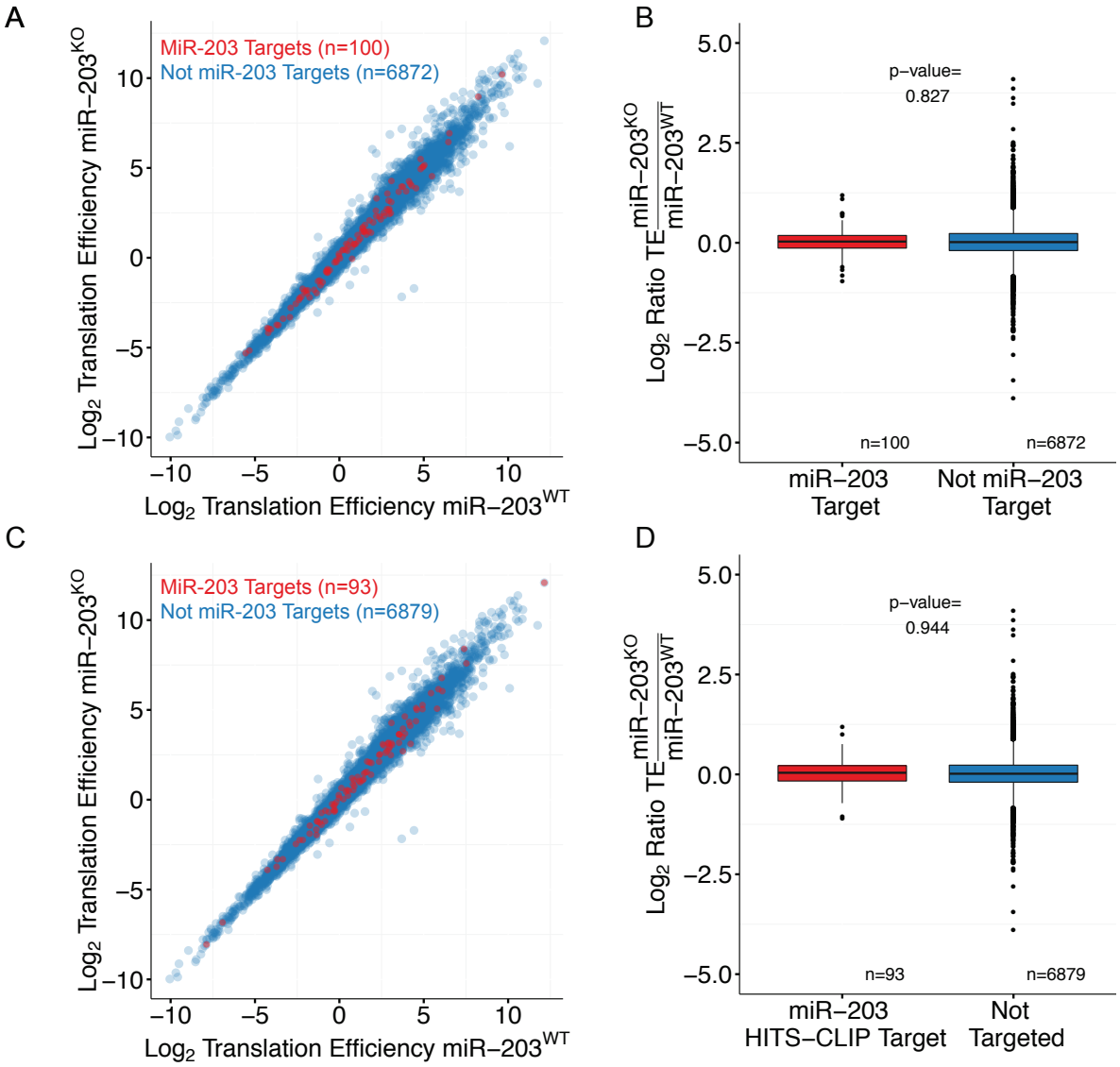

Figure 34. miR-203 targets do not display translation efficiency changes upon miR-203 ablation.(A) Comparison of translation efficiency for miR-203targets (red) and non-targeted transcripts (blue) identified by expression meta-analysis. (B) Quantification of the change in translation efficiency in miR-203ko samples for miR-203 targets identified by expression meta-analysis. (C) Comparison of translation efficiency for miR-203 targets identified by Ago2-HITS-CLIP (red) and non-targeted transcripts (blue). (D) Quantification of the change in translation efficiency in miR-203ko samples for miR-203 targets based on Ago2-HITS-CLIP.

Sh3bgrl	-0.83	-1.67	0.42	0.91	0.57		*Arl6ip6*	-0.38	-0.29	0.18	0.25	0.14
Vopp1	-0.74	-1.34	0.51	0.38	0.37		*Met*	-0.24	-0.39	0.31	0.15	0.16
Pola1	-1.42	-1.83	0.36	0.58	0.18		*Zdhhc16*	-0.34	-0.62	0.23	0.25	0.06
Rapgef1	-0.29	-1.29	0.49	0.87	0.60		*Nsdhl*	-0.47	-0.45	0.31	0.01	0.18
Lasp1	-1.13	-1.31	0.28	0.33	0.22		*Klhl22*	-0.06	-0.38	0.20	0.53	0.21
Rap1b	-0.43	-0.55	0.43	0.44	0.31		*AI837181*	-0.40	-0.44	0.14	0.23	0.12
Tax1bp3	-0.57	-0.79	0.27	0.38	0.23		*Vapb*	-0.21	-0.72	0.33	0.10	0.13
Cav1	-0.95	-1.07	0.10	0.97	0.28		*Tcof1*	-0.54	-0.37	0.21	0.38	0.04
Gbe1	-0.65	-1.26	0.46	0.69	0.08		*Elf2*	-0.12	-0.32	0.14	0.76	0.18
Ndufb2	-0.67	-0.91	0.29	0.24	0.20		*Snapc3*	-0.58	-0.24	0.37	0.25	0.05
Lnx2	-0.42	-0.29	0.45	0.75	0.25	Log2FC	*Naa50*	-0.99	-0.53	0.18	0.22	0.03
Pgam5	-0.39	-0.79	0.47	0.22	0.31	2.00	*Prps2*	-0.46	-1.32	0.01	0.33	0.12
Slc12a4	-0.64	-0.66	0.38	0.33	0.13	1.50	*Lgals8*	-0.21	-0.37	0.25	0.16	0.16
Sh3pxd2b	-0.99	-0.43	0.31	0.59	0.12	1.00	*Tada1*	-0.47	-0.10	0.08	0.53	0.20
Yars2	-0.61	-0.60	0.48	0.32	0.11	0.50	*Col17a1*	-0.78	-0.84	0.05	0.15	0.11
Ctps2	-0.84	-0.69	0.09	0.44	0.26	0.00	*Fam193a*	-0.64	0.00	0.40	0.15	0.24
Ppap2c	-0.42	-0.38	0.33	0.25	0.37	-0.50	*Igf2bp2*	-0.16	-0.40	0.36	0.10	0.18
Prmt6	-0.54	-0.19	0.58	0.60	0.15	-1.00	*Zfp281*	-0.37	-0.42	0.16	0.07	0.19
Dhx36	-0.24	-0.58	0.22	0.51	0.22	-1.50	*Bnip2*	-0.42	-0.55	0.14	0.25	0.06
Tprkb	-0.24	-0.42	0.42	0.74	0.15	-2.00	*Hbegf*	-0.09	-0.08	0.67	0.28	0.46
Gpr180	-0.70	-0.64	0.39	0.05	0.37		*Pdcl3*	-0.26	-0.39	0.11	0.45	0.10
Smtnl2	-0.19	-0.57	0.20	0.62	0.27		*Snai2*	-0.01	-0.61	0.12	0.36	0.32
Dennd6a	-1.17	-0.97	0.29	0.09	0.14		*Atp6v1c1*	-0.57	-0.57	0.57	0.09	0.01
Trim27	-0.45	-0.86	0.48	0.26	0.07		*Lpp*	-0.43	-0.55	0.01	0.37	0.12
Itgb6	-0.57	-0.91	0.40	0.20	0.08		*Chchd6*	-0.15	-0.44	0.07	0.25	0.57
Dlg5	-0.41	-0.38	0.46	0.37	0.10		*Dcun1d1*	-0.15	-0.29	0.22	0.18	0.19
Col7a1	-0.48	-0.90	0.14	0.39	0.11		*Mcoln1*	-0.22	-0.56	0.01	0.32	0.23
Wdr77	-0.39	-0.66	0.29	0.18	0.15		*Bri3*	-0.10	-0.06	0.39	0.42	0.21
Pinx1	-0.73	-0.30	0.25	0.22	0.17		*Lama3*	-0.55	-0.34	0.12	0.23	0.07
D1Ertd622e	-1.01	-0.20	0.29	0.16	0.36		*Tiprl*	-0.51	-0.60	0.28	0.01	0.08
Rbm26	-0.15	-0.39	0.44	0.45	0.16		*Vps29*	-0.19	-0.35	0.22	0.19	0.11
Pxn	-0.44	-0.80	0.16	0.15	0.26		*Xpnpep3*	-0.25	-0.50	0.44	0.09	0.07
Xrn2	-0.35	-1.31	0.30	1.05	0.02		*Myo19*	-0.07	-0.09	0.25	0.46	0.27
Sec24d	-0.66	-0.81	0.47	0.21	0.04		*Cnot11*	-0.19	-0.07	0.33	0.23	0.20
Lmo1	-0.28	-0.27	0.22	0.26	0.88		*Ssbp3*	-0.46	-0.25	0.22	0.10	0.11
Bpnt1	-1.13	-0.51	0.34	0.06	0.13		*Fscn1*	-0.19	-0.47	0.16	0.43	0.05
Golph3	-0.41	-0.28	0.34	0.37	0.10		*Avl9*	-0.18	-0.17	0.22	0.19	0.22
Cryzl1	-0.27	-0.21	0.21	0.49	0.22		*Ptp4a1*	-0.60	-0.55	0.04	0.28	0.06
Alg6	-0.29	-0.07	0.42	0.37	0.38		*Eif1b*	-0.24	-0.23	0.09	0.19	0.37
Scrn3	-0.49	-0.50	0.16	0.45	0.08		*Fancb*	-0.08	-0.23	0.12	0.96	0.17
Foxk2	-0.46	-0.58	0.47	0.14	0.07		*Mtrr*	-0.30	-0.11	0.25	0.26	0.10
Tubgcp3	-0.72	-0.50	0.12	0.41	0.08		*Dym*	-0.24	0.00	0.28	0.27	0.22
Bcam	-0.30	-0.86	0.25	0.17	0.10		*Pon2*	-0.26	-0.45	0.22	0.27	0.03
Ahcyl2	-0.35	-0.31	0.09	0.55	0.19		*Rab34*	-0.28	-0.25	0.34	0.07	0.13
Atf2	-0.89	-0.78	0.20	0.33	0.01		*Mex3c*	-0.70	-0.14	0.04	0.55	0.10
Chek2	-0.28	-0.36	0.13	0.40	0.16		*Trim26*	-0.24	-0.28	0.11	0.39	0.10
Fam118b	-0.19	-0.57	0.42	0.47	0.04		*Slc12a2*	-0.34	-0.12	0.20	0.14	0.17
Sept2	-0.71	-0.73	0.23	0.29	0.00		*Tes*	-0.31	-0.12	0.23	0.41	0.06
Bmi1	-0.57	-0.56	0.16	0.84	0.01		*Phc3*	-0.18	-0.19	0.13	0.20	0.36
Slc39a10	-0.30	-0.57	0.24	0.19	0.10		*Abcb6*	-0.11	-0.23	0.11	0.24	0.44
Vasp	-0.38	-0.52	0.23	0.17	0.10		*Ciz1*	-0.45	-0.14	0.17	0.52	0.04
Ythdf3	-0.73	-0.62	0.13	0.05	0.20		*Ajuba*	-0.26	-0.43	0.35	0.18	0.02

Table 10. miR-203 targets detected by Meta-Analysis. Red Indicates the presence of a 6,7 or 8mer miR-203 seed match. Table continues onto next two pages.

Chst14	-0.63	-0.31	0.22	0.34	0.05
Pold3	-0.41	-0.51	0.46	0.07	0.01
BC017158	-0.29	-0.30	0.20	0.28	0.03
Orc4	-0.49	-0.07	0.25	0.36	0.05
Tmem18	-0.10	-0.16	0.08	0.57	0.31
Yeats2	-0.04	-0.33	0.15	0.52	0.11
Nradd	-0.07	-0.20	0.06	0.83	0.27
Tbc1d8b	-0.32	-0.34	0.05	0.77	0.05
Zmym4	-0.49	-0.65	0.04	0.20	0.05
Sra1	-0.46	-0.28	0.20	0.06	0.10
Serhl	-0.13	-0.25	0.10	0.27	0.17
Snx18	-0.43	-0.43	0.10	0.11	0.08
Hint2	-0.18	-0.11	0.21	0.34	0.10
Capns2	-0.11	-0.16	0.17	0.23	0.17
Dnm1l	-0.40	-0.44	0.07	0.03	0.18
Apopt1	-0.08	-0.18	0.12	0.34	0.19
Ssbp2	-0.08	-0.16	0.19	0.15	0.43
Ccng1	-0.46	-0.52	0.05	0.29	0.02
Mthfd1	-0.40	-0.37	0.04	0.78	0.01
Pwp1	-0.56	-0.45	0.06	0.19	0.04
Tbc1d1	-0.63	-0.28	0.23	0.09	0.03
Mmachc	-0.04	-0.38	0.18	0.37	0.08
Tspan3	-0.28	-0.25	0.03	0.22	0.16
Afap1l2	-0.13	-0.12	0.36	0.16	0.11
Med15	-0.27	-0.22	0.15	0.14	0.11
Trappc6a	-0.31	-0.02	0.12	0.31	0.14
Higd2a	-0.19	-0.20	0.22	0.11	0.13
Acadsb	-0.22	-0.10	0.14	0.73	0.06
Atp5g3	-0.50	-0.38	0.15	0.08	0.04
Swi5	-0.07	-0.80	0.09	0.15	0.14
Nxt2	-0.19	-0.41	0.07	0.12	0.16
Hscb	-0.25	-0.17	0.20	0.16	0.08
Fat1	-0.10	-0.41	0.24	0.05	0.13
Lxn	-0.32	-0.51	0.07	0.10	0.09
Cbl	-0.01	-0.52	0.07	0.53	0.10
Rfc3	-0.40	-0.36	0.29	0.05	0.03
Hif1a	-0.46	-0.28	0.08	0.29	0.01
Prkcdbp	-0.08	-0.31	0.07	0.17	0.25
Ltbp1	-0.21	-0.10	0.22	0.06	0.20
Pias2	-0.27	-0.13	0.28	0.19	0.04
Sec61b	-0.14	-0.17	0.07	0.30	0.14
Apc	-0.29	-0.27	0.14	0.14	0.07
Mrps22	-0.24	-0.27	0.08	0.39	0.04
Zfp532	-0.30	-0.05	0.16	0.26	0.09
Gusb	-0.18	-0.41	0.04	0.08	0.22
Pttg1ip	-0.22	-0.62	0.18	0.03	0.06
Ehd2	-0.19	-0.49	1.12	0.02	0.02
Slc7a6	-0.20	-0.26	0.07	0.16	0.12
Pcbp2	-0.40	-0.17	0.08	0.08	0.14
Dmd	-0.19	-0.32	0.27	0.12	0.03
Tnks	-0.24	-0.26	0.21	0.22	0.00
Fubp1	-0.35	-0.13	0.07	0.28	0.06
Nufip2	-0.34	-0.51	0.16	0.05	0.02

Krtcap2	-0.10	-0.23	0.20	0.16	0.10
Efr3a	-0.39	-0.23	0.30	0.08	0.00
Pus3	-0.32	-0.03	0.17	0.02	0.29
Psmf1	-0.44	-0.35	0.02	0.06	0.12
Gins1	-0.62	-0.24	0.13	0.03	0.07
Slc2a1	-0.25	-0.12	0.05	0.32	0.10
Commd6	-0.08	-0.06	0.18	0.31	0.12
Nit2	-0.49	-0.35	0.08	0.07	0.06
Zcchc17	-0.05	-0.28	0.12	0.07	0.30
Alg10b	-0.13	-0.37	0.10	0.06	0.15
Cog5	-0.20	-0.13	0.11	0.14	0.13
Tmem242	-0.10	-0.33	0.29	0.02	0.11
Mzt1	-0.28	-0.14	0.24	0.14	0.03
Snrpg	-0.40	-0.17	0.17	0.08	0.06
Dpm1	-0.14	-0.45	0.24	0.08	0.03
Ckmt1	-0.14	-0.35	0.05	0.45	0.04
Higd1a	-0.25	-0.05	0.15	0.50	0.02
Cyb5r1	-0.05	-0.35	0.16	0.20	0.06
Ikzf5	-0.10	-0.15	0.03	0.63	0.10
Ube2d2a	-0.25	-0.28	0.08	0.08	0.10
Dscr3	-0.01	-0.32	0.26	0.02	0.15
Tnpo1	-0.51	-0.59	0.08	0.04	0.00
Pcsk6	-0.19	-0.18	0.06	0.05	0.30
Clic1	-0.22	-0.56	0.03	0.05	0.10
Smpd4	-0.29	-0.13	0.10	0.13	0.08
Rbpj	-0.03	-0.42	0.06	0.12	0.16
Pcbd2	-0.16	-0.12	0.12	0.03	0.23
Hif1an	-0.11	-0.31	0.06	0.18	0.09
Smim8	-0.16	-0.19	0.14	0.10	0.08
Snrpb2	-0.18	-0.12	0.05	0.27	0.10
Mb21d2	-0.36	-0.01	0.03	0.15	0.19
Mtss1	-0.09	-0.07	0.02	0.27	0.42
Psmg2	-0.18	-0.06	0.01	0.71	0.11
Srbd1	-0.02	-0.15	0.08	0.31	0.13
Ppp2cb	-0.14	-0.12	0.11	0.13	0.12
Dyrk1a	-0.02	-0.11	0.17	0.07	0.24
Alg14	-0.24	-0.01	0.09	0.12	0.15
Grhl2	-0.02	-0.15	0.12	0.33	0.09
Uba3	-0.18	-0.21	0.09	0.16	0.06
Dctd	-0.28	-0.40	0.03	0.02	0.10
Gosr2	-0.17	-0.18	0.04	0.33	0.05
Net1	-0.13	-0.09	0.22	0.05	0.12
Gna13	-0.24	-0.10	0.01	0.50	0.06
Ccnd1	-0.28	-0.26	0.14	0.08	0.01
Nudt1	-0.15	-0.54	0.06	0.16	0.01
Laptm4a	-0.11	-0.17	0.17	0.02	0.14
Nme4	-0.24	-0.02	0.30	0.10	0.05
Sidt2	-0.06	-0.11	0.24	0.01	0.19
Surf4	-0.11	-0.21	0.18	0.08	0.06
Capn1	-0.22	-0.09	0.14	0.05	0.11
Fbxo11	-0.07	-0.11	0.09	0.18	0.12
Naa60	-0.09	-0.07	0.12	0.13	0.14
Rbmxl1	-0.27	-0.26	0.23	0.02	0.01

Zfp503	-0.24	-0.07	0.09	0.33	0.10
Zc3h7b	0.00	-0.22	0.24	0.16	0.04
Cry1	-0.09	-0.17	0.13	0.03	0.16
Dpy19l3	-0.09	-0.81	0.02	0.14	0.06
Adora2b	-0.09	0.00	0.26	0.08	0.12
Tnrc6a	-0.18	-0.03	0.20	0.27	0.01
Tpp2	-0.15	-0.21	0.03	0.13	0.11
Sec13	-0.14	-0.08	0.02	0.64	0.07
Grhpr	-0.13	-0.37	0.13	0.01	0.08
Jag2	-0.07	-0.05	0.14	0.07	0.20
Usp32	-0.14	-0.06	0.05	0.07	0.34
Specc1	-0.16	-0.09	0.32	0.05	0.04
Srprb	-0.17	-0.24	0.16	0.05	0.04
Srpk2	0.00	-0.43	0.00	0.16	0.12
Bub3	-0.20	-0.06	0.13	0.27	0.01
Rasa1	-0.02	-0.05	0.05	0.40	0.13
Zfand3	-0.10	-0.08	0.03	0.12	0.27
Nae1	-0.02	-0.17	0.09	0.42	0.04
Pafah1b2	-0.33	-0.11	0.16	0.02	0.03
Nudt21	-0.12	-0.01	0.04	0.20	0.16
Tmx2	-0.18	-0.04	0.01	0.30	0.10
Ndufa8	-0.21	-0.13	0.03	0.12	0.09
Cd9	-0.02	-0.02	0.10	0.20	0.15
Tex261	-0.01	-0.28	0.03	0.03	0.35
Maged1	-0.29	-0.11	0.08	0.03	0.07
Rab24	-0.13	-0.07	0.09	0.05	0.14
Itpk1	-0.01	-0.10	0.15	0.15	0.09
Lima1	-0.05	-0.37	0.02	0.20	0.05
Trim28	-0.30	-0.11	0.13	0.02	0.03
Mapk8	-0.22	-0.02	0.02	0.16	0.10
Nln	-0.10	-0.04	0.06	0.21	0.09
Pagr1a	-0.12	-0.19	0.11	0.02	0.08
Rchy1	-0.07	-0.03	0.16	0.01	0.17
Tmem126a	-0.04	-0.21	0.03	0.05	0.17
Tsn	-0.03	-0.21	0.18	0.07	0.04
Mob1a	-0.04	-0.08	0.02	0.34	0.08
Cdk2	-0.29	-0.04	0.09	0.11	0.01
Ercc4	-0.06	-0.29	0.07	0.10	0.03
Mfap3	-0.12	-0.02	0.08	0.20	0.05
Rnf38	-0.10	-0.05	0.02	0.03	0.42
Sf3b5	-0.15	-0.11	0.02	0.11	0.07
Cinp	-0.01	-0.11	0.13	0.14	0.05
Akr1b3	-0.04	-0.15	0.00	0.24	0.07
Cox7a2l	0.00	-0.11	0.08	0.22	0.05
Taf1d	-0.14	-0.24	0.08	0.06	0.01
Nfu1	-0.22	-0.04	0.03	0.10	0.06
Snrpc	-0.09	-0.20	0.11	0.03	0.04
Ndufab1	-0.06	-0.03	0.04	0.43	0.02
Srpk1	-0.19	0.00	0.01	0.15	0.08
Cr1l	-0.01	-0.13	0.09	0.01	0.11
Snx9	-0.01	-0.12	0.18	0.03	0.05
Fth1	-0.14	-0.02	0.16	0.11	0.00
Mapk6	-0.08	-0.11	0.12	0.10	0.01

Slc38a2	-0.06	-0.07	0.05	0.07	0.11
Mmadhc	-0.03	-0.08	0.02	0.21	0.08
Tsc2	-0.15	-0.01	0.06	0.11	0.06
Park7	-0.11	-0.06	0.10	0.12	0.01
Ndufc1	-0.11	-0.09	0.06	0.06	0.06
Rpap2	-0.04	-0.10	0.07	0.06	0.08
Ddx46	-0.41	-0.05	0.02	0.06	0.01
Eif3e	-0.07	-0.02	0.03	0.16	0.08
Srsf5	-0.05	-0.18	0.06	0.04	0.07
Slc29a3	-0.06	-0.03	0.02	0.07	0.16
Dda1	-0.05	-0.10	0.01	0.09	0.11
Coro1b	-0.10	-0.09	0.00	0.10	0.08
Oat	-0.10	-0.25	0.02	0.01	0.06
Vprbp	-0.13	-0.08	0.02	0.01	0.10
Gsk3b	-0.04	-0.04	0.05	0.03	0.12
Baz1a	-0.12	-0.04	0.15	0.00	0.03
Mdh1	-0.13	-0.02	0.06	0.04	0.05
Oaz1	-0.15	-0.02	0.04	0.14	0.01
Cnbp	-0.06	-0.05	0.01	0.24	0.02
Lsm2	-0.05	-0.09	0.06	0.05	0.05
Psma1	-0.06	-0.05	0.01	0.14	0.05
Mtpn	-0.05	-0.14	0.00	0.02	0.07
Hsd17b12	-0.09	-0.01	0.05	0.06	0.05
Plscr3	-0.03	-0.08	0.03	0.02	0.10
Glrx3	-0.04	-0.16	0.03	0.07	0.01
Rcn1	-0.01	-0.01	0.03	0.18	0.02
Btf3l4	0.00	-0.03	0.08	0.08	0.02
Mtmr2	-0.05	-0.11	0.04	0.02	0.02
Gjb4	-0.06	0.00	0.02	0.07	0.04
Fxyd3	-0.07	-0.01	0.02	0.07	0.01
Coro1c	-0.04	-0.09	0.02	0.02	0.03